People's Democratic Republic of Algeria

Ministry of Higher Education and Scientific Research

Mohamed Boudiaf University of M'sila

Faculty of Technology

الجمهورية الجزائرية الديمقراطية الشعبية

وزارة التعليم العالي والبحث العلمي

جامعة المسيلة

كلية التكنولوجيا

END OF STUDY MEMORY

Submission submitted for receipt From the Academic Master's degree

In Mechanical Engineering

OPTION : MATERIALS ENGINEERING

Presented by :

Belabbas Fadila and Seghiri Sena

Entitled

STUDY OF THE EFFECT OF COMPRESSIVE FORCES ON THE MECHANICAL PROPERTIES OF A CERAMIC BY SPECKLE PHOTOGRAPHY

In front of the jury composed of:

name and surname	Grade	Quality
Farsi Chouki	MCA	President
Zemmamouche Redouane	MCB	Supervisor
Zeggane Hauari	MCB	examiner

Academic year: 2020 /2021

N° d'ordre : GM/2020/2021

Acknowledgments

We thank God for all the courage he has given us to carry out this work well and to the end. Of course, words will never be enough to recognize to God all the goods he has filled us with.

We express our sincere gratitude toMr.REDOUANE.ZEMMAMOUCHE our coach who has supervised us during the whole process of elaboration of this work and whose availability, know-how and support have never failed us.

A big thank you to all our families especially our parents, our wives and my children for their constant support.

Finally, a big thank you to all our colleagues in Materials Engineering.

TABLE OF CONTENTS

LIST OF FIGURES

CHAPITRE I

LIST OF TABLES

CHAPITRE I

LIST OF FIGURES

CHAPITRE II

LIST OF TABLES

CHAPITRE III

LIST OF FIGURES

CHAPITRE III

Résume

L’objectif principal de cette recherche est d’étudier les propriétés mécaniques de la céramique, d’où nous avons pris comme exemple d’étude le kaolin (KT2). Nous avons utilisé une nouvelle techniques optique appelé photographie de speckle pour exploiter qualitativement le comportement à la compression des céramiques. Cette méthode nous à permet aussi de visualiser les champs de déformations des céramiques sous compressions sur toutes la surface de l’échantillon et les défauts probable lors de la fabrication.

Abstract

The main objective of this research is to study the mechanical properties of ceramics, from which we took kaolin (KT2) as an example. We used a new optical technique called speckle photography to qualitatively exploit the compressive behaviour of ceramics. This method also allows us to visualize the deformation fields of the ceramic under compression on all the surface of the sample and the probable defects during manufacture.

ملخص

ان الهدف الاساسي من هذا البحث هو دراسة الخصائص الميكانيكية للخزف ولقد اخذنا الكاولين كمثال حيث قمنا باستخدام احدى التقنيات المسمات (speckle photography) التي بدورها تمكننا من معرفة الأخطاء المتواجدة في القطعة كاملة داخليا ودراستها بشكل متقن ودقيق وتقوم هذه التقنية على مبدأ شرح مختصر speckle ، والذي قمنا بإجراءها في مخابر جامعة مسيلة .

لذا أولا من أجل دراستنا المخبرية قمنا بتشكيل مادة الكاولين إلى قطع إسطوانية للقيام بإختبار الضغط عليها المتابع بالمراقبة بإستخدام تقنية speckle وذلك بإستخدام مجموعة من الخطوات المتمثلة تدريجيا في الطحن الغربلة القولبة بالضغط الطهو والتمليس .في النهاية لوحظ إختلاف في النتائج المتحصل عليها وذلك مبدئيا نتج من إختلاف ضغط.قولبة العينات عند تشكيلها فقد أظهرت دراستنا التالي القطع المشكلة تحت ضغط صغير أدى إلى تخليف مشاكل داخلية في القطعة وسهل إنكسارها عند تعرضها لضغط خارجي وكل مازادت القوة الضاغطة المشكلة للعينات نقصت الاخطاء الداخلية وزادت مقاومة العينات تدريجيا للقوى الخارجية لذا بشكل عام إستنتجنا نظريا وتجريبيا ان التقنية المستخدمة في التصنيع تحدد مقدار صلابة وجودة المواد المصنعة في النهاية.

GENERALE INTRODUCTION

Generale Introduction :

General introduction :

Ceramics have been used since time immemorial in many craft industries, and over time there has been much interest. With these materials for availability, expansion and accessibility, their study and use have expanded considerably, their products have broken into various industrial fields, among other uses are thermal bricks, cement, glass, etc.

The use of ceramics is no longer limited to traditional purposes such as cooking pots and thermal bricks, but has become key materials in many modern technological industries, owing to the fact that these materials are used in many applications for ease of manufacture and are of good mechanical and resistive properties, and because of their low thermal dilation factors used in electrical products such as circuit parts, filters and fuel controls in motor vehicles, Etc .

The main objective of this research is to study the mechanical properties of ceramics using a new method or so-called non-destructive experiments;

The research was divided into three main chapters, where we tried to capture the most important properties of ceramic materials.

In chapter II we speak about Speckle photography that is a technique that makes it easy for measure in-plane displacements using simple optical systems. The general procedure is to illuminate the object with a single laser beam and make a photographic recording on a single photographic plate of the object before and after displacement. Illuminated by a laser, there are two primary geometries where speckles are observed. The first is called an “objective speckle” and the second called “subjective speckles.The objective of the correlation algorithm is to determine the deformation and the degree of primary decorrelation between two states of the object from a pair of associated digital image data.

In chapter III we take the kaolin KT2 from its raw state as clay and we made a group of samples from it through many steps that were as follows: (crushing, sifting, pressure forming, cooking, and polishing). Then we take the final samples and study them using the speckle photograpie technique when subjected to pressure, which allows us to read the movement of its molecules over the entire surface of the samples.

Chapter I

GENERAL ABOUT CERAMICS

I.1.Generalities around ceramics

I.1.1. Definition of ceramic material

The term ceramics is derived from the Greek word "**keramos"**, meaning "clay" or "pottery clay."(1) Defined as solid materials formed through thermoregulation and sometimes heat and pressure. Ceramics include inorganic and non-metallic substances. A somewhat simpler definition provided by "**kingery"** is where ceramics are defined as solid material consisting mainly of non-metallic and inorganic substances obtained by roasting.

I.2. Structure and microstructure of ceramics

I.2.1. Ceramic structure

A ceramic, like a metal, has an atomic-scale structure; its crystalline structure (if crystallized) or its amorphous structure (if glassy). It owns also a larger scale structure: the shape and body of the grains or phases, the size and density of the pores it contains (most ceramics are porous).

A crucial distinction must be made at the outset, that is the distinction between the ceramics that are predominantly ionic and those with character mostly covalent in their atomic bonds.

- **Ionic ceramics**

Are typically compounds of a metal and a non-metallic, sodium chloride NaCl, magnesium oxide MgO, alumina Al2O3, zirconia ZrO_2.

Examples:

Cubic zirconia (ZrO_2):

Zirconia is an increasingly widespread industrial ceramic. Its structure crystallography consists of a Zirconium CFC stack, with O^{2-} ions in tetrahedral sites. As there are 2 tetrahedral sites per network atom, the formula of zirconia is ZrO_2.

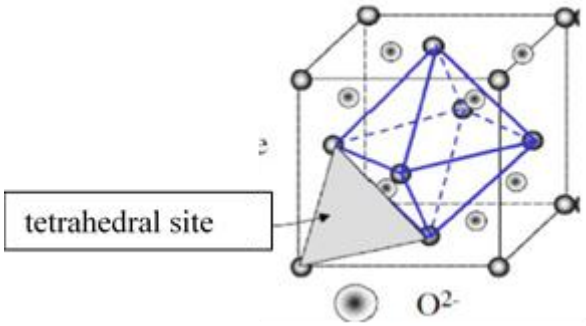

Figure.I.1: Schematic of the **ZrO_2** structure.

Alumina (Al_2O_3):

Alumina is a structural ceramic used in cutting tools and grinding wheels and is also used in the composition of bricks and pottery. Its crystallographic structure consists of an HC stack of oxygen ions with Al^{3+} ions located in octahedral sites. The HC structure has one octahedral site and two tetrahedral sites (such as CFC). The Al^{3+} ions are surrounded by 6 ions O^{2-}, but for the crystal to be electroneutral, the number of Al ions corresponds to the filling of two-thirds of the sites, so one site on three empty mansions.

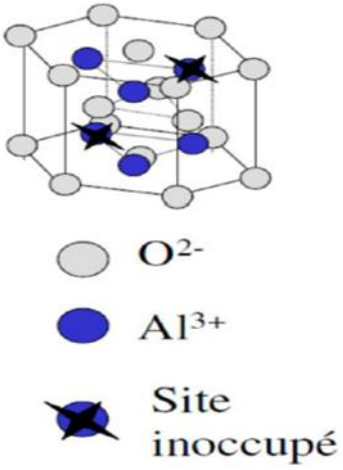

Figure.I.2: Schematic of the **Al_2O_3** structure.

- **covalent ceramics**

For covalent ceramics, these are compounds of two non-metals (such as silica Si), or, on occasion, simply pure elements such as diamond C, silica SiO2. An atom of a ceramic of this type binds by sharing electrons with its neighbours to produce a fixed number of directional bonds [1].

Examples:

Silicon carbide (SiC):

Silicon carbide (SiC) has a diamond-like structure; one out of every two carbon atoms is replaced by silicon. After diamonds, silicon carbides are one of the hardest substances. Generally used for high-pressure parts such as high-temperature bearings or engine parts.

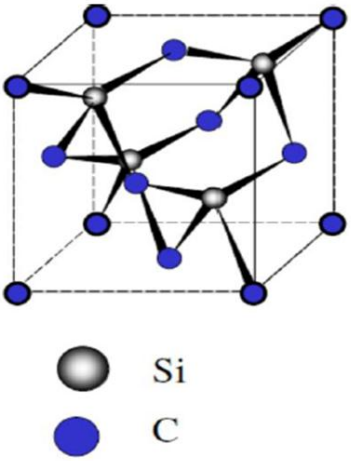

Figure.I.3: Schematic of the **SiC** structure.

I.2.2. Silica and silicates

The Earth's crust is essentially composed of silicates. Among all the raw materials used by man, silica and its compounds are the most widespread, abundant and cheap. A silicon atom binds strongly to four oxygen atoms to form a very stable tetrahedral pattern **SiO_4.**

The **SiO_4** tetrahedrons (corresponding to the monomer) can bind together either directly or through a bond with a metal ion (M). When silica is combined with metal oxides such as **MgO**, **CaO** or **Al_2O_3**, three cases of figures can occur, depending on the **MO/SiO_2** ratio:

a. Greater than 2:

The resulting silicate is composed of SiO_4 monomers isolated and connected by metal oxide (MO) molecules (olivine, the main constituent material of the upper layers of the earth's crust mantle, is a silicate of this type).

Figure.I.4: SiO_4 monomers.

b. Slightly less than 2:

Silica dimers form with 1 oxygen atom common to the 2 monomers (Oxygen Bridge). This is the first step towards polymerization of the monomer to produce chains, leaflets and networks.

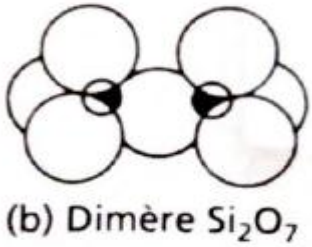

Figure.I.5: Dimer Si_2O_7.

c. Less than 2:

The degree of polymerization increases, with the formation of long chains of tetrahedrons -Si-O-Si-O-. Two oxygens of each tetrahedron are shared. The others form ion bonds between chains, associated with MOs. These last bonds are weaker than the bonds -Si-O-Si- which constitute the skeleton, so that these silicates are fibrous; asbestos, for example, has this type of structure.

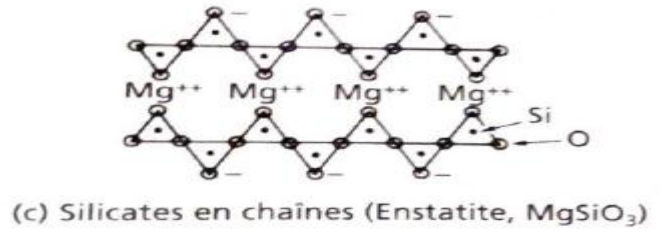

Figure.I.6: Double chain structure (MgSiO3).

In the third case, if 3 oxygens of each tetrahedron are shared, leaf structures are formed. This is the basic structure of clays, talc and micas, etc.). The additional M attaches preferentially to one side of the sheet, that of the first available oxygen atom. The sheets are strongly polarized, that is to say they have negative charges on one side and positive on the other. This causes strong interactions with water (strongly polar), leading to the formation of water between the sheets and making the clays plastic. Leaflets can easily slide one over the other, lubricated by water layers. The laminated silicates are very resistant in the plane of their leaves, but cleave or easily split between two leaves.

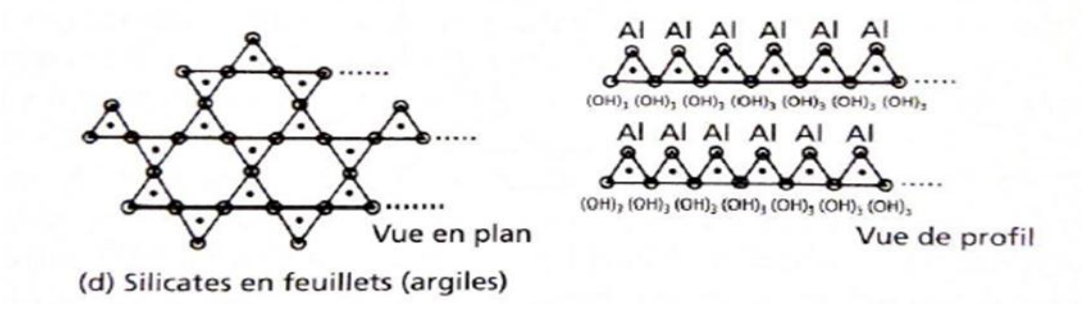

Figure.I.7: Silicate structure.

I.3.The microstructure of ceramics

Crystalline ceramics form polycrystalline microstructures, very similar to those of metal alloys. Each grain is a monocrystal more or less perfect next to its neighbours by a grain seal. The structure of grain joints in ceramics is more complex than that of metals: ions of the same sign must always be avoided and the imperatives of valence must be respected as far as possible in the joint, just as they are in grains. Many ceramics are not completely dense. A fraction of porosity of 20% is commonly found in their microstructure (Figure 1.2). Micro-cracks are more harmful, although much more difficult to detect, they are produced by the manufacturing process, or initiated by differences in coefficient of expansion or modulus of elasticity between grains or phases [1].

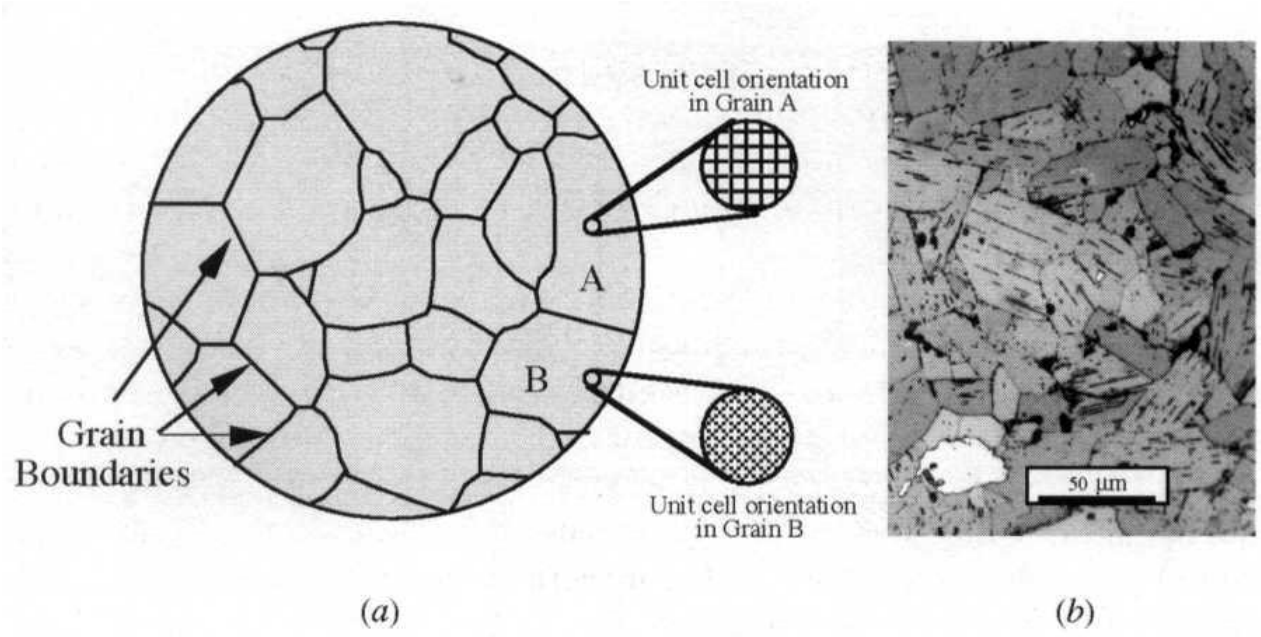

Figure.I.8**:** *(a)* Schematic of a polycrystalline sample. A polycrystal is made up of many grains separated from one another by regions of disorder known as grain boundaries. (*b*) Typical microstructure as seen through an optical microscope.

I.4. Ceramic classification

I.4.1. Traditional ceramics

They're silicate compounds, obtained by mixing clouds or clay with water to give an easy-to-shape den paste that becomes solid and immobile after thermally treated.

Figure.I.9**:** Exemple des céramiques traditionnelles.

I.4.1.1.Plastic raw materials

a. Clays

The raw material of traditional ceramics is clay. This term is used to describe a group of grains of less than 2 μm in size, rich in phyllosilicates (hydrated aluminosilicates of lamellar structure) and capable of forming a colloidal suspension in water. Among the phyllosilicates present in the clays, we can distinguish alumina silicates, such as kaolinite and halloysite, products containing alkali or alkaline-earths in their crystalline network, such as micas (muscovite and illite) and smectites. Mixed with a certain amount of water, the clay powder forms a plastic paste, malleable and cohesive, similar to that used by the potter on his turn. This plasticity is due to the wafer shape of phyllosilicate grains and their strong affinity for liquid water. Ceramists usually classify clays according to their plasticity (fitness for shaping) and their cooking behaviour. [2]

- Red clays are mainly used in the manufacture of terracotta products. Their high iron content (several % mass equivalents Fe_2O_3) is the origin of the red-brown colour of the shards after cooking.
- Stiff plastic clays are distinguished by the high plasticity of the pastes formed with water and the appearance of an abundant viscous flow (sanding phenomenon) during cooking.
- Refractory clays are predominantly kaolinite.
- Products called ball clay are plastic clays with a marked refractory character.[2]

The clay, by the colloidal nature of its particles silicates, develops in the presence of water properties of plasticity that allows its shaping. It is formed by a mixture of silicate, known

as clay minerals (kaolinite, montmorillonite), in addition, it contains fine constituents such as silica, limestone, organic materials.

Clays are more or less hydrated aluminosilicates and the majority of clay minerals belong to the group of phyllites silico-aluminates. They are organized in plane layers, made up of tetrahedral and octahedral structural units connected by their tops.

In clays, impurities are often found, in the form of metallic oxides (CaO, Fe_2O_3,' FeO, MgO, TiO_2, Na_2O, etc.), impurities that influence the colour of the final product.

b. The kaolin

The basic constituent of argi1es, used in the manufacture of porcelain; its chemical formula can be written $Al_2O_3.2SiO_2.2H_2O$ (Al_2 (Si_2O_5) (OH_4) (kaolinite). They usually arise from the alteration of granite rock feldspars. It has a leaf structure and is made up of flat grains from 1 to 5 μm in diameter and about 0.05μm thick. [2]

I.4.1.2. Non-plastic raw materials

Although easy to form, a clay-only paste would be too deformable to handle the preform. Moreover, the drying and cooking of such a preform would be accompanied by a significant contraction (withdrawal) which would make it difficult to control the shape and dimensions of the final piece. To limit these adverse effects, non-plastic products capable of forming an interconnected rigid skeleton must be present in the initial mineral mixture. More commonly, they are called degreasers, in the form of relatively large grains (> 10 μm). Non-plastic raw materials can be divided into two classes: fluxes and degreasers. [2]

a. Degreasers

These are mainly baked clay (chamotte), silica (quartz).

The role of degreasers is to:

- Decrease the plasticity of the dough;
- Reduce shrinkage and ease of product shaping

The siliceous sand (small quartz particles SiO_2) added to the clay forms a refractory compound that does not undergo any transformation during cooking, apart from allotropic crystallographic transformations. It changes the plasticity and behaviour of clays during drying and cooking.

The Chamottes are calcined clay compositions, resulting from high-temperature heat treatment of certain types of clay.

b. The fluxes

Sintering of silicate-rich mineral mixtures, such as those used to make traditional ceramics, involves the flow of a silica-rich viscous flow. For it to have a significant influence on the evolution of the microstructure (consolidation and densification), it must be able to

represent a significant density fraction and its viscosity must be less than about 107 Pa.s. To lower the sintering temperature, it is customary to introduce into the initial mixtures minerals, called fluxes, which are at the same time flow-forming and purveyors of fluidifying elements (alkali, alkaline-earth or certain transition elements). These fluxes can be alkaline-rich phyllosilicates (micas or smectites) or non-plastic minerals such as feldspar or chalk.The latter act as degreasers during shaping and as fluxes during sintering.

Example

The feldspars

Feldspars are hard rocks composed of silica, alumina and alkali. Feldspars are fluxes: during cooking, they form, with silica and kaolin, low-melting compounds, which become liquid, cementing kaolin and silica particles and thus reducing porosity. The most commonly used are:

Orthosis ($K_2O.Al_2O_3.6SiO_2$) (fusion: 1150)

Albite ($6SiO_2Al_2O_3Na_2O$) (fusion: 1100)

Anorthite ($2SiO_2.Al_2O_3.CaO$). (Fusion: 1532)

I.4.2. Technical ceramics

It is a non-metallic and inorganic material obtained at high temperatures. It is intended for industrial applications. There are several types of technical ceramics, including silicate, oxidic, and oxidative ceramics. They are mainly made of raw materials, together with aluminas, such as aluminum silicate, and oxide, mainly zirconium oxides. The other type of oxide is made of materials made from carbon, nitrogen and silicon compounds, such as silicon carbide or aluminum nitride.

I.4.2.1. Oxide-based ceramics

Ceramic oxides are characterized by a very high melting temperature, high chemical stability even at high temperature, obvious oxidation resistance, high hardness. All these properties are related to the strongly ionic nature of their binding.

Among the most commonly used oxides for thermomechanical applications are aluminium oxide commonly known as alumina, zirconium oxide (zirconia) and cordierite ($2MgO\ 2Al_2O_3\ 5SiO_2$). Their main properties are shown in (Table I.1).

I.4.2.2. Non-oxide ceramics

Non-oxide ceramics are characterized by high melting or decomposition temperatures, good chemical stability even at high temperatures, fairly good oxidation resistance, very high hardness and mechanical resistance. All these properties are related to the strongly covalent character of their interatomic bonds. From then on, these ceramics will be found as abrasives

and cutting tools thanks to their exceptional hardness and good toughness as well as structural elements at medium and high temperature in the corrosive environment because of their good mechanical strength.

The most commonly used non-oxides for thermomechanical applications include silicon, titanium, boron and tungsten carbides, diamond, titanium boride and silicon, boron and titanium nitrides.

I.5. Application of ceramics by pressing

In the most common practice, the cold powder is compressed to produce an object with sufficient cohesion to be handled and transported to the sintering furnace. A powder cannot be formed without consolidation. In cold compaction, consolidation takes place in a mould or dies under more or less pressure. It allows the realization of parts practically «at the final dimensions», which is one of the main interests of powder metallurgy. This step is followed by a sintering operation.

The science of sintering is not new, on the contrary, the technique of sintering is very old since it precedes the processes of classical metallurgy: the Egyptians already used it for the manufacture of instruments, 3,000 years before our era. However, they are only really developed in the 20th century. Indeed, since the appearance of the science of ceramics, we observe many innovations both in the field of processes and in the field of compositions which allows then new uses of ceramics.

I.6. Characteristics of powders

The granular nature of a pulverulent material is characterized by a certain number of physical parameters: total mass (m), total volume of powder (V), the volume of the solid part (V_s), the volume of voids (V_v), density of the dense material ($\rho_d = m/V_s$), the relative density related to the density of the dense material, etc. These parameters essentially qualify the state of the material concerning the porosity during the characteristic phases of the form.

Other parameters should also be considered to distinguish the precision of industrial powders. Indeed, the characterization hardness mechanics leads to define two broad classes of materials for powders:

- Ductile materials which are "soft" materials and which can be plastically deformed without breaking (for example, iron, copper, lead . . .)
- Fragile materials are hard and can break without significant plastic deformation carbides and ceramics.

The characterization of powders is also based on the analysis of the morphology of grains:

- grain size is measured by sieving or micrograph that provide the grain size of the mixture, the shape of the grains partly determines the behaviour of the powder for some phases of the formatting process. [3]

I.6.1.Sieving

Sieving is a very simple, cheap and reliable method. The method consists of passing the powder dry or wet through a tower made up of a sieve stack that is vibrated. There's no upper limit to the size of the grain it's characterizing. However, under 50 µm, dry sieving becomes difficult. However, with a powder in suspension, a lower limit of 5 µm can be reached although the method is not always easy to implement. If the particles are not spherical, the mesh of the sieve will not correspond to the actual diameter. For reasons of precision, precautions must be taken when cleaning and handling sieves with openings less than 250 µm. Sieving is often used with granulated powders prepared by atomization for dry pressing (50-500 µm). It is also particularly used for the classification of powders and the elimination of large agglomerates or unwanted fine particles.

I.7. Forming processes from powders

I.7.1. Uniaxial Compression

The compression phase has two goals which are densification by bonding and deformation of solid grains using external pressure and the production of tablets of the desired shape and size. The most commonly used compression is cold uniaxial. The compaction cycle is described in (Figure I.10). [3]

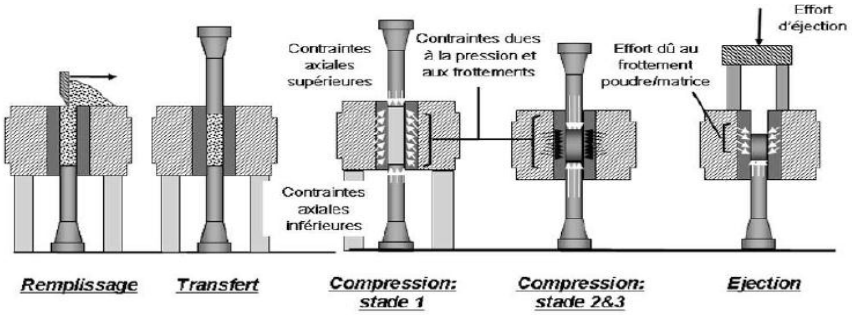

Figure.I.10: The different phases of obtaining the tablet.

After filling and following the transfer phase, the compression of the powder with the matching of the different punches (Fig I.10).

During the compression phase, the powder densifies under the action of three phenomena that allow the compression phase to be split into three stages ordered:

- Grain rearrangement results in particle displacements with possible fracturing or fragmentation.

- Local grain deformation results in surface crushing of grain due to increased compactness. This local grain deformation is visible on contact areas and causes the appearance of flat surfaces on the grains.
- The large-amplitude plastic deformation of each grain involved in the high compactness achieved by ductile metal powders.

I.7.2. Isostatic cold compression

The principle of this process is to immerse a flexible container filled with powder in a liquid, usually water, which is compressed to high pressure. The powder thus compacted by a uniform pressure in all directions. This brings us to a good uniformity of density. The cold is always followed by sintering to consolidate it. This process is distinguished by its ability to produce very slender parts such as bars. [3]

I.7.3. Hot Isostatic Compression

This process combines mechanical and thermal stresses, the principle of is to exert high isotropic pressure on a powder contained in a deformable matrix at a temperature close to the melting temperature of the powder. The combination of mechanical loading and heat input allows welding the grains under pressure. The parts obtained by this process have isotropic physical and mechanical properties with minimal porosity, especially for massive pieces.

I.8. Sintering of ceramics

The science of sintering is not new, on the contrary, the technique of sintering is very old since it precedes the processes of classical metallurgy: the Egyptians already used it for the manufacture of instruments, 3,000 years before our era. However, they are only really developed in the 20th century. Indeed, since the appearance of the science of ceramics, we observe many innovations both in the field of processes and in the field of compositions which allows then new uses of ceramics.

The sintering phenomenon – knowing that it is a very complex process and covering an important domain of existence – can be defined as “the method of heat treatment, with or without application of external pressures, whereby a system of individual particles or a porous body modifies some of its properties in the direction of evolution towards a state of maximum compactness, that is to say, towards a state of zero porosity».

Sintering thus allows, by the use of high-temperature furnaces, to consolidate the material after the steps of shaping and consolidating the paste which represents the different stages of elaboration of a ceramic. [3]

I.8.1.Definition of sintering

Sintering is the thermal consolidation of a pulverulent material without melting at least one of its constituents. This is one of the most delicate and often the most expensive operations when preparing ceramics. During the thermal cycle, the microstructure is set up, by transporting material between grains, in order to minimize the excess of interface energies, which is usually accompanied by a decrease in porosity. The latter manifests itself in a macroscopic way by a withdrawal with respect to the «raw» part.

Among the different Physico-chemical characteristics, porosity is usually chosen as a parameter for the description of the sintering process of the ceramic bodies because the geometric variations of the material can be interpreted by the variations in pore size and shape, which are related to the growth phenomena of crystalline phases.

For geometric variations to occur in the material during sintering several factors are important: the nature of the sintered material – single or mixed oxides, presence of liquid phase, inhibitors of crystal growth, etc., and sintering conditions-temperature, time, atmosphere, and pressure application. The extreme complexity of the sintering process and the difficulty of directly studying its mechanism make it necessary to base the description of phenomena on defined and particularly simple models.

Sintering is therefore the consolidation, under the effect of temperature, of a pulverulent agglomerate, à non-cohesive granular material (often called compact, whereas its porosity is 40%, therefore its compactness of 60%), the particles of the starting powder welding to each other to give à mechanically cohesive solid, usually a polycrystalpolycrystal.

The term sintering refers to four different phenomena that develop in parallel and often compete:

- consolidation: development of bridges that weld the particles together.
- densification: reduction of porosity, thus contraction of the whole part.
- granular magnification: magnification of grain particles.
- Physico-chemical reactions within the material being consolidated.

Sintering is only possible if atoms can diffuse to establish bridges that bind the articulations together. The transport of matter can be done in the vapour phase, within a liquid, by diffusion in a crystal, or by viscous flow of glass. Most of the mechanisms are thermally activated because the action of temperature is necessary to overcome the potential barrier between the initial state of higher energy and the final state of lower energy.

Even if thermodynamic conditions make sintering possible, it is necessary for the process to intervene, that its speed is sufficient. The transport of materials in a solid is very slow

compared to what it is in à liquid or a gas. This transport of matter can come from an overall movement, from the repetition of unit processes at the atomic scale, or the transformation of the vapour phase or into the liquid phase. The velocity is only significant if the temperature is high enough.

The movement of matter occurs from high-energy areas to lower-energy areas – essentially the sintering neck between the particles. Two cases must be distinguished, depending on the location of the material source:

- when the source of matter is the surface, the mechanism is nonidentifying, which means that the spheres take an ellipsoidal shape, without their centre getting closer. There is no macroscopic shrinkage and the porosity of the granular compact is not significantly reduced; the decay of the interfacial energy comes mainly from granular magnification.
- when the source of the material is inside the grains the mechanism is densifying: there is shrinkage and reduction of porosity.

There are six possible dissemination paths:

1: Surface diffusion

2: Diffusion in volume with the source of material the surface

3: Evaporation-condensation

4: Diffusion along grain joints

5: Diffusion in volume with grain joints as the source of material

6: Volume diffusion with defects such as dislocations as the source of material

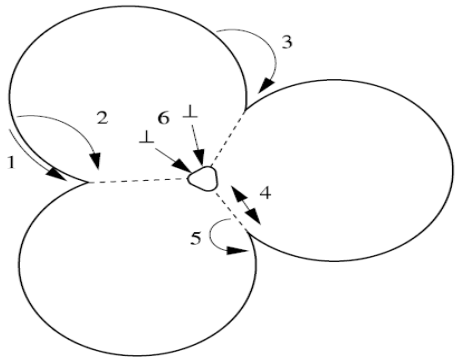

Figure.I.11: Matter transport during a solid phase sintering; mechanisms 1, 2 and 3 are nondensifying; mechanisms 4, 5 and 6 are densifying; ⊥ schematizes a dislocation [ASH 75]

Table I.1. Matter transport during a solid phase sintering [ASH 75]

Path	diffusion path	material source	Material well	result obtained
1	surface scattering	Surface	Sintering neck	grain coarsening
2	Volume release	Surface	Sintering neck	grain coarsening
3	Evaporation-Condensation	Surface	Sintering neck	grain coarsening
4	Diffusion along grain joints	grain boundaries	Sintering neck	Densifying sintering
5	Volume release	grain boundaries	Sintering neck	Densifying sintering
6	Volume release	Defects, such as dislocations	Sintering neck	Densifying sintering

I.8.1.1.Different forms of sintering

a) Solid-phase sintering

Solid-phase sintering consists of agglomerating powders at a temperature at which all the constituents remain in the solid state, by simultaneously applying pressure or charge. Solid-phase sintering is the case where no liquid phase has been identified. The microstructure of the material will evolve under the effect of a modification of the curvature of the pore/solid interface. To model particle sintering, particles were generally assimilated to spheres and looked at what was happening in the case of two or three spheres. Solid-phase sintering is developed in three successive stages:

-Initial stage: the particle system is assimilated to a set of spheres in contact, between which sintering bridges develop. Let X be the radius of the neck, R the radius of the particles, then the growth over time t of the ratio, for isothermal sintering, is of the form:

With B a characteristic parameter of the material and the exponents n and m vary according to the process involved.

-Intermediate stage: the system is schematized by stacking of polyhedral grains on their common faces, with pores forming a network of channels along the common three-grain edges, connected at the quadruple points.

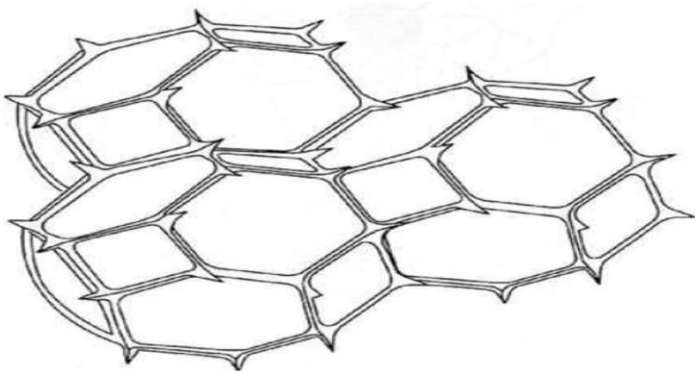

Figure.I.12**:** Diagram of the porosity in the form of inter-connected canals along the edges of à polyhedron with 14 faces, typical of the intermediate stage of sintering [GER 96]

- final stage: the porosity is closed, only the isolated pores remain, often located at the four-fold points between the grains but which can be trapped in the intragranular position.

In these morphological changes, a change of free energy occurs due to the decrease of the overall surface of the material by elimination of solid/gas interfaces.

Some of these mechanisms lead to densification (reduction of room size) and others do not.

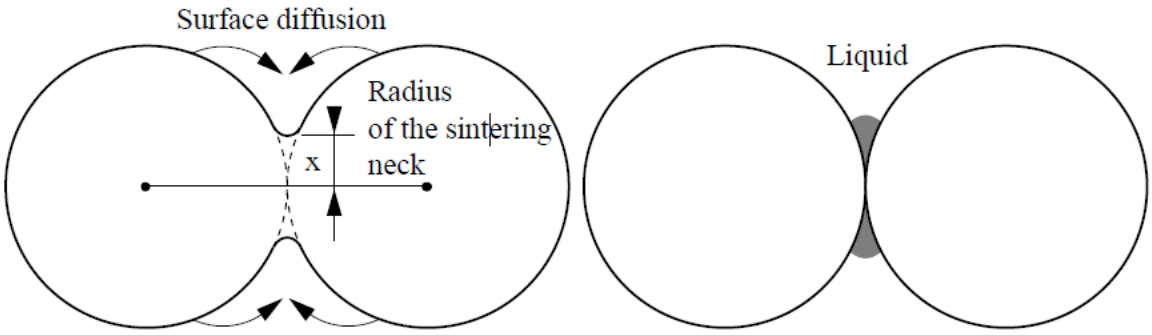

Figure.I.13**:**Frittege of two spheres without (A) and with (B) densification**.**

In the following figure, we have shown the six main mechanisms that can be involved, as well as the sources of material involved.

Most ceramics are multiphase materials with both crystallised and vitreous phases. But we can also observe millimetre crystal agglomerates with a very porous microstructure (refractory steel), or polycrystals with fine grains (10 µm) without glassy phases and with very low porosity (alumina or zirconia hip prostheses). In addition to the chemical nature of the compound, the properties are controlled by the microstructure of the material (size, grain shape, porosity rate and types, phase distribution). Jernot (1982) showed the essential role played in solid-phase sintering by the number of contacts between particles and powder, which effectively governs all sintering operations.

b) Liquid phase sintering

Liquid phase sintering implies that at least one of the constituents is liquid and bathes the solid phase during the operation. Involving diffusion phenomena leads to a weld between the different particles, recrystallization of the grains and the partial elimination of the porosity.

Various technical ceramics, most metals and cermets are also sintered in the presence of a liquid phase. Most ceramic products contain

Ambient temperature and in more or less considerable quantities, a glass phase essentially acts as a binder of different crystalline elements.

The main parameters are quantity of liquid phase, viscosity, wettability, respective solubilities.

Wettability is quantifiable:

$\gamma LV \cos\theta = \gamma SV - \gamma SL$

With γLV vapour liquid energy

γSV solid energy steam

γSL liquid-solid energy

Θ angle of contact

Within a granular solid that contains a liquid: $2\,\gamma SL \cos(\theta/2) = \gamma JG$, with γJG grain seal energy.

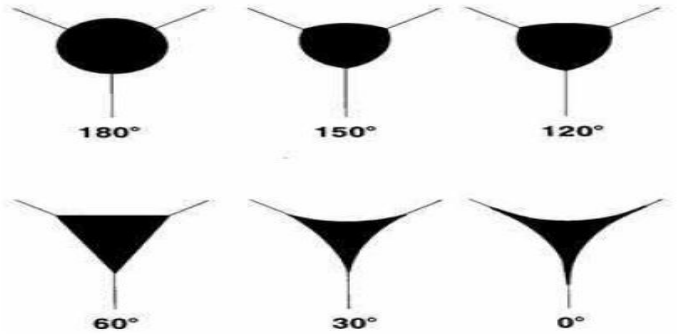

Figure.I.14**:** Penetration of the liquid between the grains depending on the value of Θ [GER 96].

The phenomena involved are:

- Particle rearrangement and viscous flow due to variations in surface tension leading to high densification;
- dissolution-reprecipitation: dissolution of the small crystals of the solid phase in the liquid phase and reprecipitation on the larger crystals;
- coalescence and particle growth: the liquid phase is eliminated by the formation of crystals or solid solution.

Two mechanisms limit growth: diffusion into the liquid and reactions to liquid/solid interfaces. The slowest will be decisive.

I.9. Ceramic Properties

I.9.1. Mechanical properties

Ceramics have high values for elasticity coefficients as a result of the strength of their chemical bond, which allows crystalline levels to slip in relation to each other as in metals, so they are described as pellets. [4]

Materials have mechanical properties in field industries and applications, and since most ceramics are fragile They are resistant to deformation as a result of the strength of their chemical bonds, which do not allow crystal levels to slip to each other compared to metals, so they are described as short materials. (The power to create deformation in the eye is greater than the power to break it)It is also attached to the undesirable characteristic of rapid refraction, and the scope for the doughnut of these substances at normal temperatures is absent compared to metals as shown in the article, as well as high hardness. For example, in carbidation up to 25 GPa and in diamonds 90 GPa, ceramics have weak hardness coefficient values that express the resistance of the material to the spread of cracks when the sample collapses as shown in (Table I.2).

Ceramics, like metals, have a well-defined Young module, that is to say, that the module remains constant during the application of a load (unlike the polymer whose elasticity is not linear). Moreover, ionic bonds and bonds covalent are very cohesive:

E Ceramics > E Metals > E Polymers

In addition, ceramics are made of light atoms (C, O, Si, Al) and have a crystalline structure often not compact:

ρ Metals> ρ Ceramics> ρ Polymers

The specific module of ceramics is therefore very favourable:

(E / ρ) Ceramics >> (E / ρ) Metals

This property makes ceramics a material of choice as a reinforcing charge in composites. [5]

Table.I.2.Young modules and densities of ceramics and metals

Material	E(GPa)	ρ(SD)	(E/ ρ) (GPa)
Steel	210	1.8	27
aluminium alloys	70	2.7	26
Alumina	390	3.9	100
Silica	69	2.6	27
Cement	45	2.4	19

I.9.1.1.Hardness

Ceramics have the highest hardness of any material. They are used as abrasives for cutting, grinding or polishing all materials, including glass.

H ceramics > H metal alloys > H pure metals >> H polymer

Table.I.3. Hardness of some materials [6]

Ceramic	H/E	metal alloys	H/E	pure metals	H/E
Diamond	$1,5.10^{-1}$	Brass	9.10^{-3}	Cu	$1.2.10^{-3}$
Alumina	4.10^{-2}	Dural(Al4%Cu)	$1,5.10^{-2}$	Al	$1,5.10^{-3}$
Zirconia	6.10^{-2}	stainless steel	6.10^{-3}	Ni	9.10^{-4}
Sic	6.10^{-2}	low carbon steel	$1,5.10^{-2}$	Fe	9.10^{-4}
Average	8.10^{-2}	average	1.10^{-2}	Average	$1,5.10^{-3}$

In the design of ceramic parts, it is never necessary to consider the failure by lamination of the part because the sudden rupture = brittle = in the linear area a tensile test; always occurs.

I.9.1.2. Breaking strength of ceramics

It is the plasticity at the crack head that gives the metals their high toughness. The fact that the ceramic still contain cracks and porosity greatly decreases their tenacity:

KIC ceramic = 1 / 50 KIC metals

Mechanical tensile strength depends on the toughness and length of the largest cracks, depending on the relationship:

Rmc= KIC/2am

With 2am = length of the largest crack. Numerically we find for ceramics values in the order of K1c~0.2 - 2MPa.m½, am ~ 10-60 µ m and Rméc~10-300MPa.

This relationship reflects that tensile strength decreases when the length of the larger crack increases, the digital application shows that the characteristic sizes of cracks causing the rupture are very small, in the order of the grain size of a sintered material. There are two ways to improve the mechanical strength of ceramics: [6]

- Decrease the length of the largest crack by checking the the particle size of powders and methods of application.
- Increase KIC using composites or alloys, as in incorporating chopped straw into bricks or fibreglass in cement.

Brittle

Fracture

Stop of crack

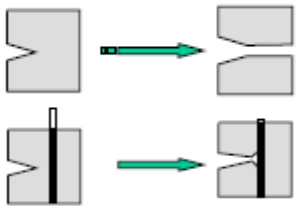

Figure.I.15: Increase in toughness for ceramic matrix composite.

I.10. Defects in ceramics

A defect is an imperfection or irregularity, of the order of the diameter of the atoms in the crystalline structure. Ceramics, as in the case of metals, contain defects since ceramics comprise at least two distinct types of ions [7], it As a result, each of them may present defects.

The defects that often exist in ceramics are:

- Point defects.
- Surface defects.
- Volume defects.

I.10.1. point defects

These are network disturbances at the atomic scale. Among the atomic defects in the ceramics we find:

- Gaps (vacant sites on the network).
- Interstitials (atoms between crystal atoms), atoms of a species Different chemical in substitution solution (in the network) or insertion (interstitial).
- Electronic faults are the electron/hole pairs.

Among the properties influenced by point defects in the behaviour hot mechanical, percolation and transport properties (diffusion of material, heat), as well as electrical conductivity.

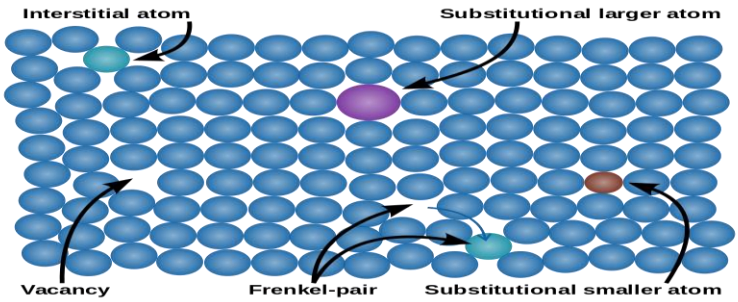

Figure.I.16 **:** point defects**.**

I.10.2. Surface defects

For example, free surfaces (disturbance of the vicinity of surface atoms have lost some of their neighbours) and interfaces between grains or between different phases. They can be consistent, semi-consistent (that is, consistent "almost everywhere" by a network of defects) or inconsistent interfaces and free surfaces (strong disturbance in the vicinity of atoms).
This interface energy plays à considerable role in the formation and evolution of the structure of materials.

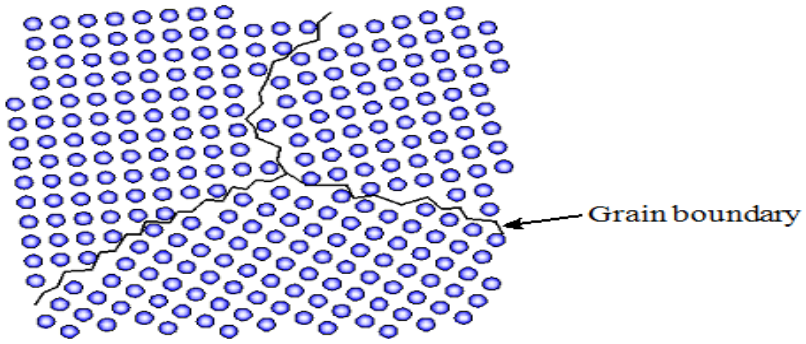

Figure.I.17 **:** Surface defects.

I.10.3. Volume defects

"Volume" defects are essentially cavities, unwanted phases, and inclusions (pieces of foreign material, from the process, for example, particles from a crucible. They come mainly from the development of the material (sintering of ceramics) or damage to it during its use.

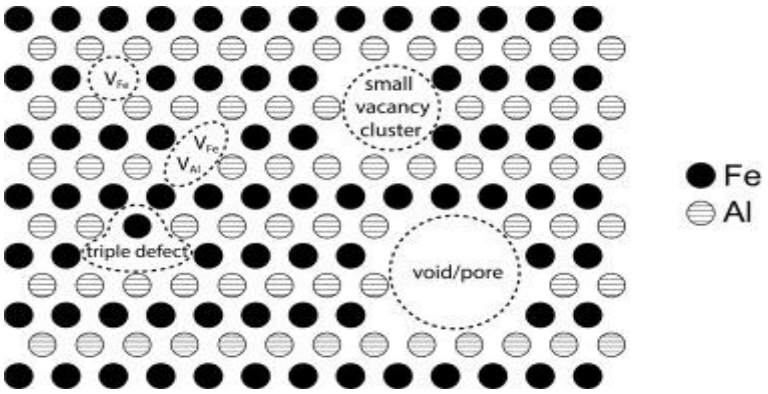

Figure.I.18 : Volume defects.

Chapter II

SPECKLE PHOTOGRAPHY AND DIGITAL IMAGE CORRELATION

II.1 Origin of Speckle

II.1.1.Introuduction

The invention of the laser in 1960 allowed for the availability, as never before, of light sources with a high degree of coherence. Researchers working with this kind of light source noticed that a strange phenomenon was produced: when a rough surface is illuminated with laser light, a high-contrast and finescale granular pattern is observable.This effect was called the "speckle effect," characterized by the random distribution of scattered light. Although the random distribution of the optical field can be deterministically modified by displacement or rotation of the diffuser where the light is reflected or transmitted,this effect was considered as a mere nuisance, especiallyforthefirstholographytechniquesdevelopedatthattime.Inaddition to this property, the distribution is also modified by changes in the illumination and observation geometry, in the wavelength of the laser light, and in the refractive index of the medium through which the laser travels. Thus, speckle distribution can be used to measure features of the surface under investigation, such as (a) out-of-plane and in-plane components of the surface deformation of a rough object, (b) 3D surface shapes (by generating contours of the constant depth of an object), and (c) derivatives of the surface displacements. For these reasons, important research efforts began in the late '60s and early '70s focusing on the development of new methods for high-sensitivity measurements on diffusely reflecting surfaces; these methods can be categorized as speckle interferometry. Photographic films were initially used to produce images, and the information was processed by optical methods. The need for an optical table to process and reveal negative films was the main drawback to overcome for measurements in industrial environments. Consequently, research was directed to substitute holographic film with TV cameras and to electronically process the video signal. The new method was called electronic speckle pattern interferometry (ESPI). The first results were discouraging because of the low detector resolution, low sensitivity, and high SNR. Advances in technology, particularly for high-speed and high-resolution data-acquisition systems, made it possible for engineers to connect a TV camera (later, a CCD or CMOS camera) to a host computer in order to acquire a digital image of the surface illuminated by the laser light. Advances in data transmission enabled a direct link from the cameras to the computer to transmit digital images without needing additional elements to digitize the acquired image (such as frame grabbers). At this point, ESPI was renamed DSPI (the word "electronic" was changed to "digital") due to the use of digital images as well as digital processing techniques. Over the years, the technique has

been thoroughly investigated, theoretically as well as experimentally, and it has been improved. For this reason, speckle methods can now be considered as well-established experimental techniques and important tools for performing measurements in laboratory and industrial environments.[6]

When an optically rough surface is illuminated with light having a high degree of coherence, such as one coming from a laser, the scattered light presents a particular intensity distribution, making the surface appear to be covered with a fine granular structure. This structure, which consists of alternately dark and bright spots of variable shapes, and distributed in a random way, as shown in Figure II.1, has no obvious relation to the macroscopic properties of the surface. Such intensity distribution, which is also observable when coherent light propagates through a medium presenting random variations in its refractive index, is known as a speckle pattern.[7]

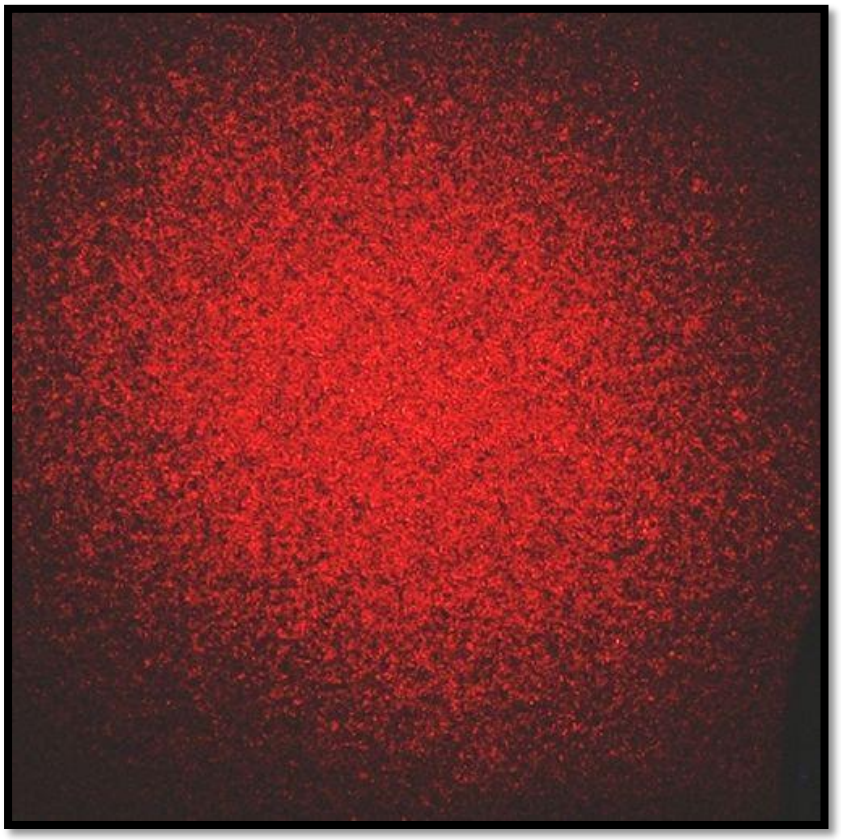

Figure.II.1:A photograph of an objective speckle pattern.

II.2.Speckle principle

Huygens' principle states that "every point on a propagating wavefront serves as the source of spherical secondary wavelets, such that the wavefront at some later time is the envelope of these wavelets". When a surface is illuminated by coherent light from a laser, each point on the surface can be considered as a small source that follows Huygens' principle (shown in Fig. II.2). In addition, the magnitude of the optical field in each point of the space will be determined by the complex coherent addition of all wavelets coming from each scattering point on the surface.

Additionally, if the laser light is incident on an optically rough surface with height variations greater than the wavelength λ of the light or transmitted through an "optically rough" diffuser having thickness variations greater than λ , and because the lateral scale of the surface roughness is smaller than the illuminated spot, the incident laser light will be scattered in all directions. The scattered waves will interfere and form an interference pattern consisting of dark and bright spots that are randomly distributed in the space. This light distribution, called speckle distribution, can be seen in Fig. II.3. Consider a surface located in a plane xy that is illuminated by a coherent source light with a wavelength λ (see Fig. II.4). The light field at a specific point Q(r) in a speckle pattern is the sum of a large number of components that represent the light coming from all points located on the scattering surface.[6]

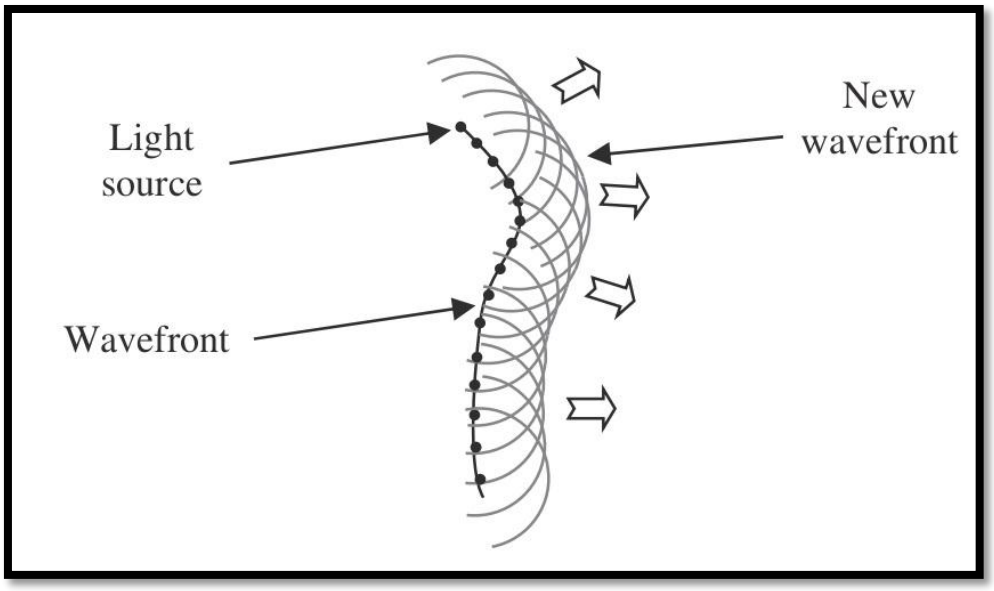

Figure.II.2: Huygens' principle: each point is considered as a light source of the propagating wavelet.

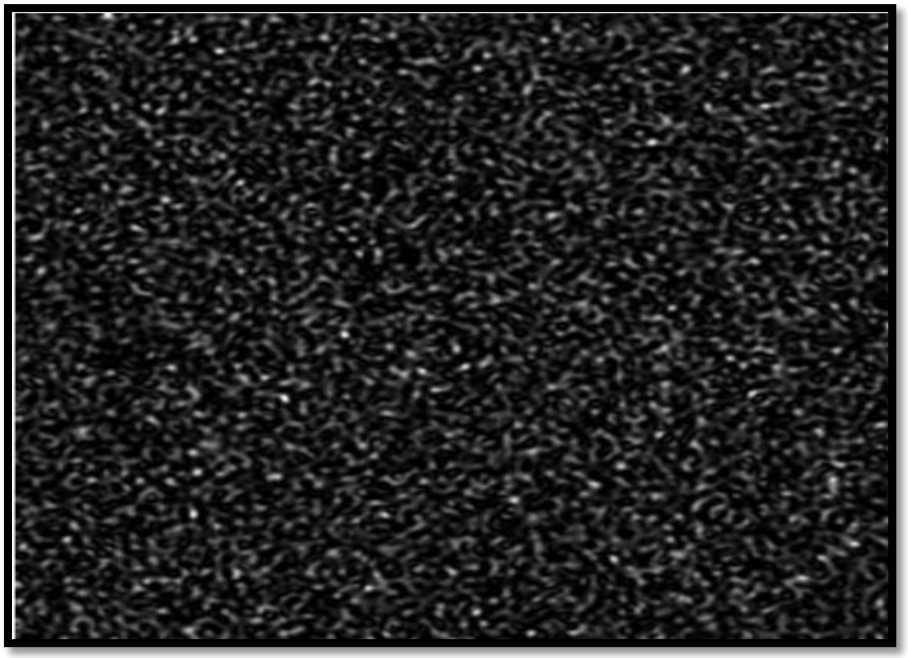

Figure.II.3:Typical simulated speckle distribution.

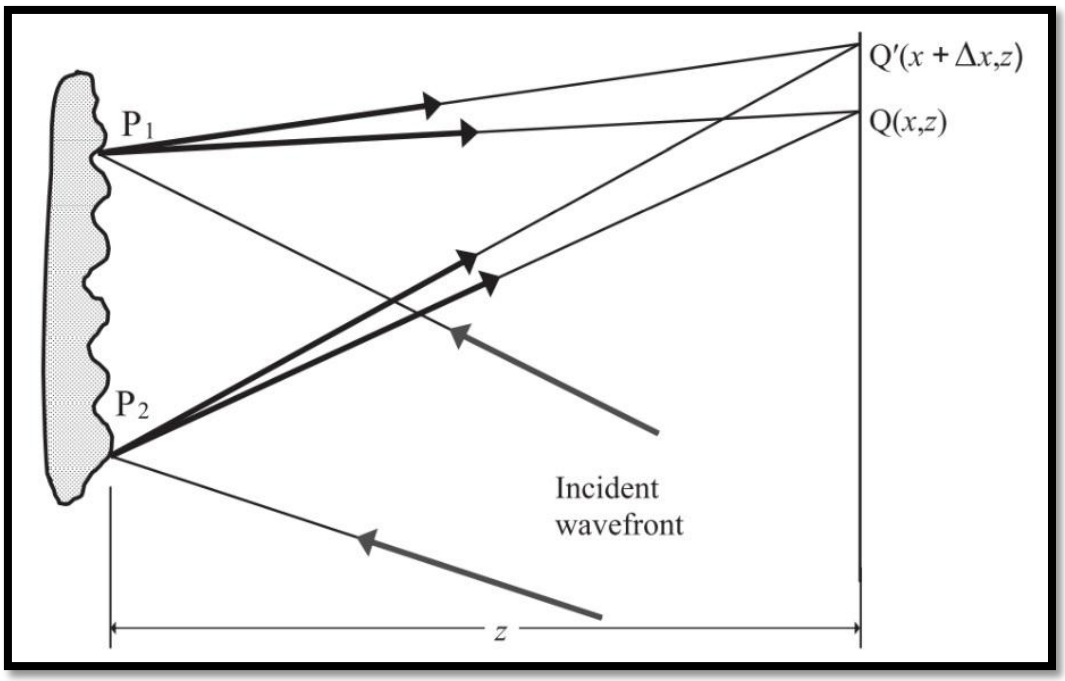

Figure.II.4: Objective speckle.

Therfore, the complex amplitude at each point in a a speckle pattern can be written as:

$$Q(\mathbf{r}) = k_c \iint_S \omega_i(x,y)\exp[2\pi i/\lambda . G_e \xi(x,y)]dxdy, \qquad (\mathbf{II}.1)$$

where **r** is the position vector of the point Q , S is the scattering surface, k_c is a constant, ω_i is the complex amplitude of the incident light in (x, y), ξ (x, y) is the surface height at that point, and G_e is a geometric factor associated with the directions of illumination and observation (this

factor can be considered as a constant value when the point Q is far away from the scattering surface). Because the height of the roughness of the scattering surface varies randomly with a magnitude equal to or larger than the wavelength of the incident light, the phase terms $G_e\xi(x, y)$ will also change randomly with the same magnitude. For this reason, the random amplitude value of the point Q is described by a set of vectors with random phase (which are added), thus generating a resulting vector with random amplitude. This problem is known as "random walk." The amplitude has a value with ranges from zero and the maximum value, which is determined by the magnitude and the phase of the individual amplitudes. As the observation point moves, the resulting amplitude and intensity will have different values.

The vector with the thicker arrow represents the resultant of the complex sum.

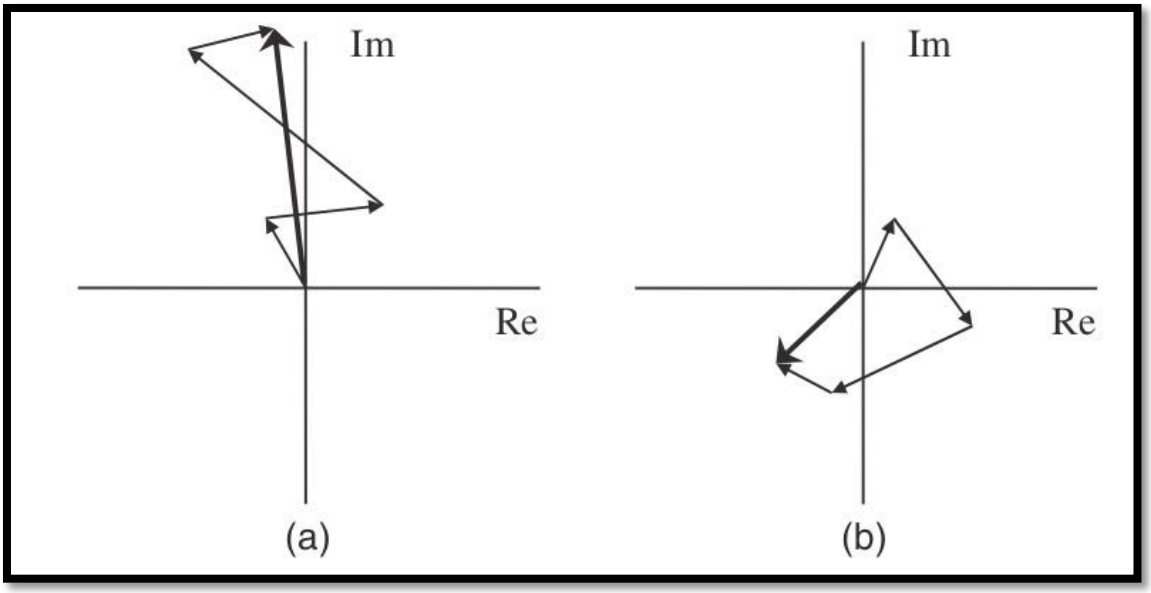

Figure.II.5: Random walks: (a) constructive addition and (b) destructive addition.

shows two random walks that produce (a) a large resultant and (b) a small resultant. In both cases, phasor directions and lengths are random, and no single contribution dominates the sum

II.3.Statistical properties of the Speckle

II.3.1.Statistics of the intensity

Simple observation of a speckle diagram reveals that dark and bright points occur with different frequency. In fact, it can be readily seen that dark spots are much more common than bright ones. Instead of going too deep into mathematics, we outline here the main assumptions and steps to arrive at the description of the intensity statistics of a speckle diagram. We will assume that a collimated coherent field of wavelength L illuminates an optically rough surface; that means the chosen wavelength is much smaller than the surface height variations with

respect to its mean. In practice, this is the case for most materials having optical wavelengths about 0.5 μm. Because the height of the surface varies in a random way, the spherical wavelets reflected by the surface also present a random distribution of phases (Figure II.6 a). All these wavelets interfere at a given point in space, P(x,y,z). A completely analogous situation results from considering a ground glass that is being illuminated from its back by a coherent collimated beam, as shown in (FigureII.6 b). The surface at which light enters the diffuser can be considered flat, and the small local curvatures at the exit surface spread the field into spherical wavelets. Additionally, the random thickness variations of the glass produce the random phases of the secondary waves.[7]

Moreover, if an optical system is used to image the surface, diffraction considerations cannot be avoided. In fact, if speckle is to be observed with such configuration, the optical system must be properly chosen to have a point spread function broad enough to guarantee that many individual regions of the object overlap at the image plane, as sketched in Figure II.6 c.

No matter which picture is assumed, it is easily realized that the light field at a specific point P(x,y,z) in a speckle pattern must be the sum of a large number N of components representing the contribution from all points on the scattering surface. Under illumination by monochromatic and fully polarized light, the contribution to the field at P produced by any surface element, j, is given by

$U_j(p) = |u_j| e^{i\varphi_j} = |u_j| e^{ikr_j}$ (**II**.2)

r_j being the (random varying) distance from the j-th scattering surface element to the point P. The complex amplitude of the scattered field at point P can therefore be written as

$$U(P) = \frac{1}{\sqrt{N}} \sum_{j=1}^{N} u_j(p) = \frac{1}{\sqrt{N}} \sum_{j=1}^{N} |u_j| \, e^{i\phi_j} = \frac{1}{\sqrt{N}} \sum_{j=1}^{N} |u_j| \, e^{ikr_j} \quad (\mathbf{II}.3)$$

The summation in Equation **II**.3 can be considered as a random walk in the complex plane due to the random phases $\varphi_j = kr_j$.this erratic motion of the field components is represented in (Figure II.7) for a few of them. Assuming that:

(1) the amplitude u_j andphase φ_j of each field component are statistically independent of each other and are also independent of the amplitude and phase of all other field components and (2) the phases φ_j are uniformly distributed on the interval $(-\pi, \pi)$ which means that the surface is rough in comparison to the wavelength, and with the additional hypothesis that the number of total scattering centers N is very large, thus ensuring validity of the central limit theorem, Goodman has demonstrated that the real and imaginary parts of the resultant field are asymptotically Gaussian.(7)

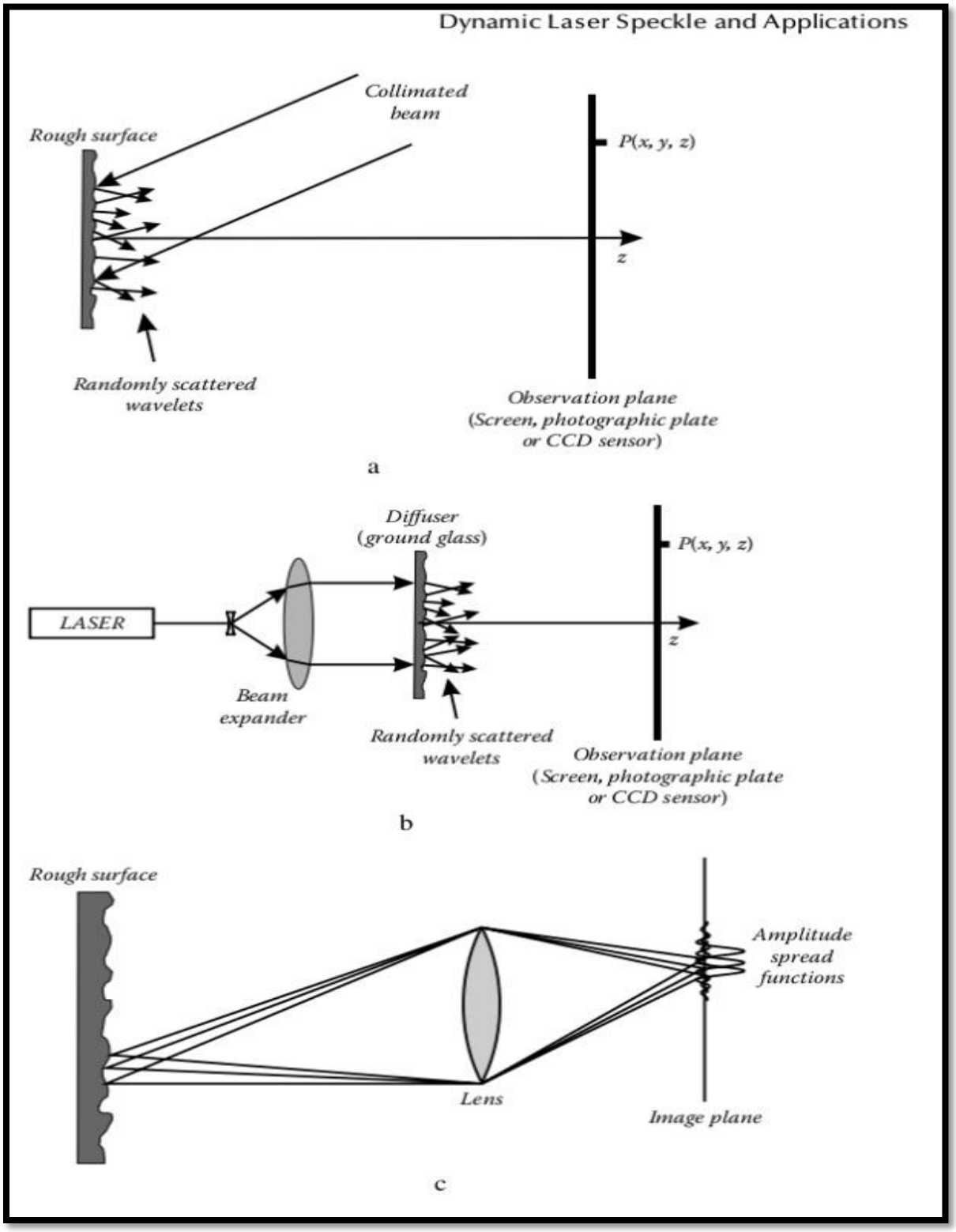

Figure II.6: The physical origin of speckle patterns. (a) Diffuse reflection of coherent light from a rough surface, (b) Transmission of coherent light through a translucent object, and (c) image formation of a rough surface.

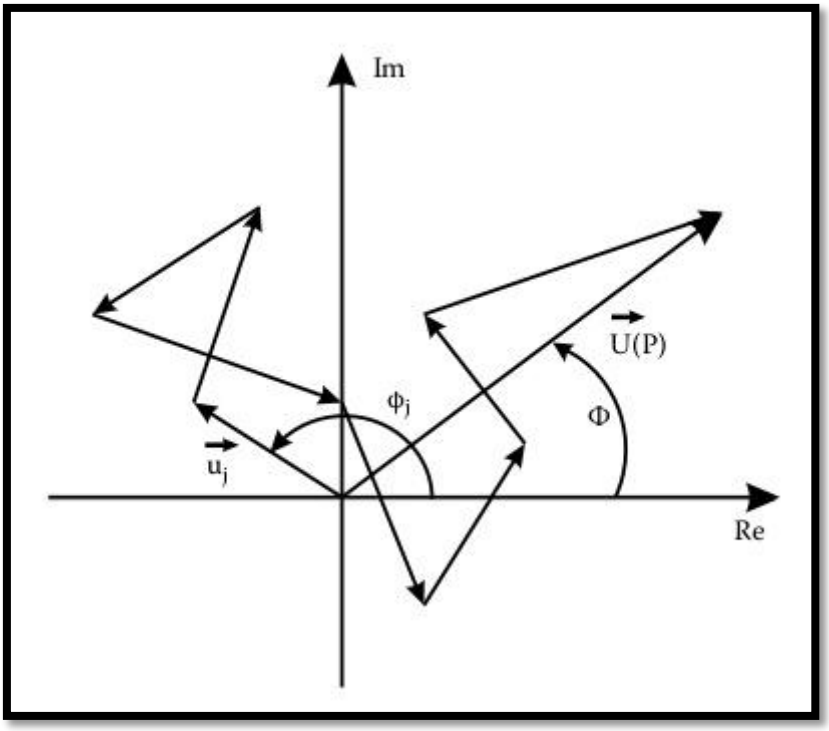

Figure.II.7: Several scattered fields $u_j(P)$, plotted in the complex plane with their respective random phases(φ_j), contributing to the total field at point P, U(P).

The joint probability density function for them is thus given by

$$(U^{(r)}, U^{(i)})=\frac{1}{2\pi\sigma^2}\exp\left[\frac{(U^{(r)})^2+(U^{(i)})^2}{2\sigma^2}\right] \qquad \textbf{(II.4)}$$

known as a circular Gaussian, where

$$\sigma^2 = \lim_{N\to\infty} \sum_{j=1}^{N} \frac{\langle|u_j|\rangle^2}{2} \qquad \textbf{(II.5)}$$

From Equation **II**.4, and taking into account that the intensity *I* and phase φ of the resultant field are related to the real and imaginary parts of the field according to

$$U^{(r)} = \sqrt{I}\cos\Phi, \qquad U^{(i)} = \sqrt{I\ \sin\Phi} \qquad \textbf{(II.6)}$$

it follows that the probability density of the intensity p(*I*) and of the phase P(φ) & are given by

$$P(I) = \frac{1}{\langle I\rangle} e^{\frac{-1}{\langle I\rangle}} \qquad \text{for} \quad I \geq 0 \qquad \textbf{(II.7)}$$

$$P(\Phi)=\frac{1}{2\pi} \qquad \text{for} \quad -\pi \leq \Phi \leq \pi \qquad \textbf{(II.8)}$$

respectively.

In Equation **II**.7,$\langle I \rangle$ stands for the mean value of the intensity in the speckle diagram. Thus, according to the last two equations, the intensity distribution follows a negative exponential law, whereas the phase is uniformly distributed in the interval (-π ,π).

The moments of intensity distribution are defined as

$$\langle I^n \rangle = n!(2\sigma^2)^n = n!\langle I \rangle^n \qquad (\mathbf{II}.9)$$

and of special interest are the second-order moment and the variance:

$$\langle I^2 \rangle = 2\langle I \rangle^2 \; and \; \sigma_I^2 = \langle I^2 \rangle - \langle I \rangle^2 = \langle I \rangle^2 \qquad (\mathbf{II}.10)$$

This equation shows that the standard deviation of a polarized speckle pattern equals the mean value of the intensity. A usual measure of the degree of modulation of a speckle pattern is called the contrast, defined as

$$C=\frac{\sigma_I}{\langle I \rangle} \qquad (\mathbf{II}.11)$$

This definition, together with the result in Equation II.10, means that the contrast of a polarized speckle pattern is always unity, and the speckle pattern is said to be fully developed.

II.3.2.Typical dimensions of speckle grains

Consider the schema shown in Figure **II**.8 in which a point source P_0 is imaged by a lens, assumed to be perfect. We are not making any particular assumption about P_0, thus it can be taken as any individual point on the surface of the diffuser. The geometric image of P_0 is located at $P`_0$; the center of curvature of ∑, the emerging spherical wave, and thus, all the wavelets emerging from this wave front are in phase at $P`_0$. If we now consider another point P located at the same plane as $P`_0$ but laterally displacing a small distance y, the wavelets arriving at P will present some phase difference. The maximum phase difference will occur between points located at opposite extremes of the aperture, and the corresponding path difference can be easily evaluated to be

$$\Delta = d \sin\theta \qquad (\mathbf{II}.12)$$

d being the lens diameter, and $\boldsymbol{\theta}$ the angle defined by the optical axis and the line going from the center of the lens to the point P. If the structure of the diffraction figure at P does not differ significantly from that at $P`_0$, it is necessary that the path difference remain much smaller than the wavelength λ. In symbols**,**

$$d \sin\theta \ll \lambda \qquad (\mathbf{II}.13)$$

Or, because y is very small in comparison to the image distance D,

$$d\frac{y}{D} \ll \lambda \qquad (\mathbf{II}.14)$$

Equation **II**.14 can be now used to define the lateral extension D or diameter of the bright spot at $P`_0$,which can be taken as the "typical" size for a single speckle grain. Thus,

$$\delta = 2y \approx 2\gamma \frac{D}{d} = \frac{\gamma}{\alpha} \quad \text{(II.15)}$$

Being $2\alpha=\frac{d}{D}$ the aperture of the image-forming objective. Clearly, such a result is consistent, apart from having a constant factor for the circular aperture, with diffraction considerations.(7)

To determine the axial extension of the bright spot, let us now consider a similar situation depicted in Figure II.8. Following Françon,[37] let us assume that we axially displace the observation plane from π', where the image P'$_0$ of the source P0 is located by an amount δ_z to a parallel position π''. It is also assumed that δ_z is small in comparison to the distance from the lens to π', shown as D= OP$_0$' in Figure II.8. Again, P'$_0$ being the image of P'$_0$, it is located at the center of curvature of the wave front ∑, and the waves emerging from different points of it are all in phase at P'$_0$. However, they present some phase difference at plane π'', which will give rise to a certain image deterioration. The path difference at P''$_0$ located on the axis at plane π'' can reach, at most, the value (7)

$$\Delta = IP_0'' \quad \text{(II.16)}$$

where *I* is the point at which the wave front ' intercepts the ray emerging from the lens border. Note also that IP'_0= OP$_0$'=D.

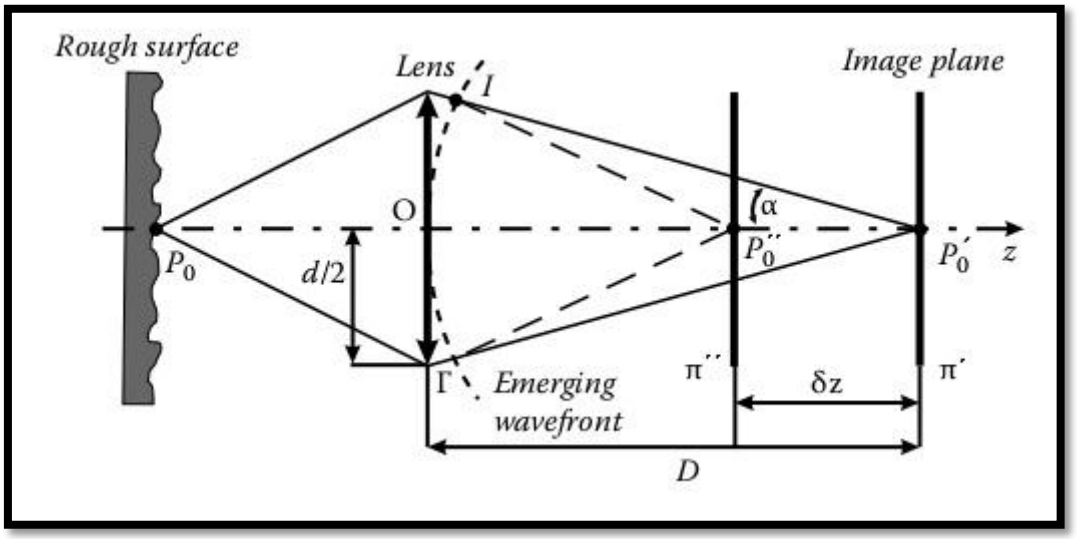

Figure.II.8: Geometrical considerations to determine the axial extension of speckles. The situation is similar to that shown in Figure.II.7, but now the image point P'$_0$ is compared to another point P''$_0$ axially displaced by a small stepδ_Z. Again, the angle α is a measure of the aperture of the imaging lens.

In accordance with the cosine theorem, and with reference to Figure II.8 ,we can write

$$(IP''_0)^2 = D^2 + \delta z^2 - 2D\delta z \cos\alpha \quad (\text{II}.17)$$

And also

$$OP_0'' = D - \delta z \quad (\text{II}.18)$$

Equation II.17 can be also written

$$IP_0'' = D\sqrt{1 + \frac{\delta z^2}{D^2} - 2\frac{\delta z}{D}\cos\alpha} \approx D\left(1 - \frac{\delta z}{D}\cos\alpha\right) = D - \delta z\cos\alpha \quad (\text{II}.19)$$

where it is assumed that $D \gg \delta z$has been used. It follows now from Equations II.15, II.17, and 1.18 that

$$\Delta = D - \delta z\cos\alpha - D + \delta z = \delta z(1 - \cos\alpha) = 2\delta z\sin^2\frac{\alpha}{2} \quad (\text{II}.20)$$

Finally, considering that the aperture A of the system is small, we can write for the maximum path difference:

$$\Delta = \delta z\frac{\alpha^2}{2} \quad (\text{II}.21)$$

Using the preceding analogous arguments, we conclude that, if this path difference is much smaller than the wavelength, the image deterioration will be insignificant. This condition means that

$$\delta z \ll 2\frac{\lambda}{\alpha^2} \quad (\text{II}.22)$$

And thus,

$$\delta z \approx 4\frac{\lambda}{\alpha^2} \quad (\text{II}.23)$$

can be taken as a measure of the axial dimension of the bright spot.

These considerations are based on coherence arguments, and the conclusions are summarized in the results of Equations II.15 and II.23. These two equations give an order of magnitude for the dimensions of single speckle grains. Equivalent argumentslead to the same results in the case of free space propagation. Speckle grains happen to be ellipsoids of revolution (cigar-shaped) of typical dimensions δ and δz, as shown schematically in Figure II.9.

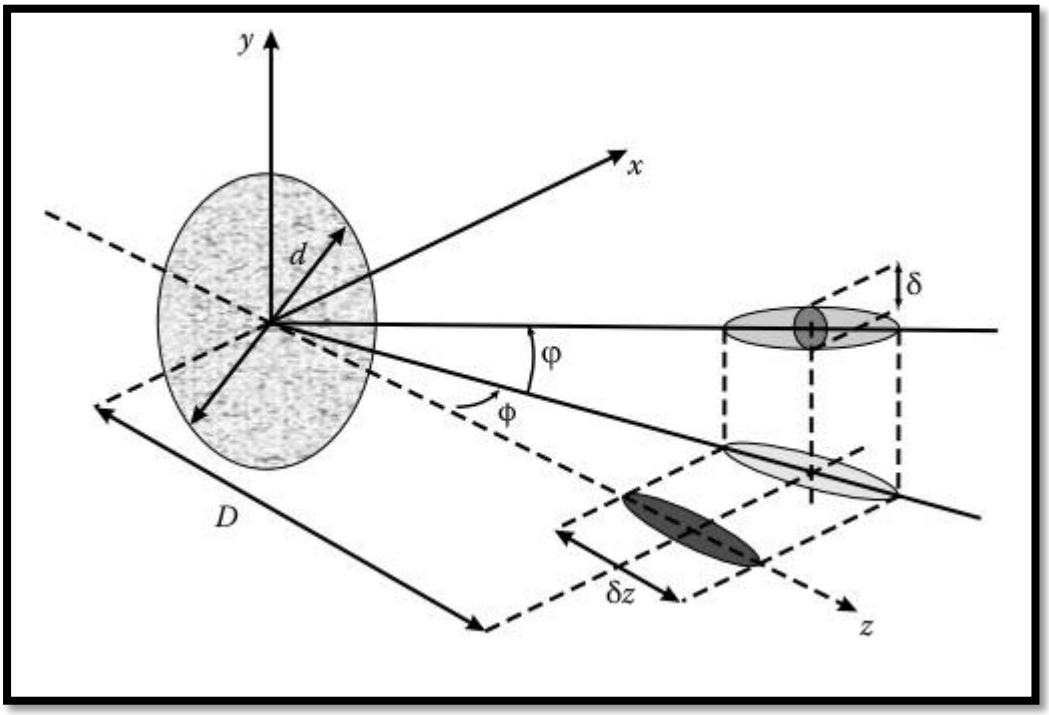

Figure.II.9:A perspective sketch showing the "cigar" structure of speckle grains in space with lateral and axial extents given by $\delta$and δz, respectively.

Thus, independent of the type of optical setup producing a speckle pattern, image formations, or free space, the typical dimensions of the speckles are determined by the wavelength and the aperture of the system, diffraction being the optical phenomenon behind this.

Additionally, when the light source is partially coherent, a somewhat different speckle pattern is obtained. In this situation, as in the coherent case, the average speckle size is determined by the autocorrelation function; but this function is the convolution of the coherent autocorrelation function with the light source autocorrelation function. Therefore, the average speckle size is larger than in the former case.[16] With respect to the speckle contrast, it is obviously less than or equal to 1.(7)

II.4.Objective and subjective speckle

illuminated by a laser, there are two primary geometries where speckles are observed. The first is called an "objective speckle" and corresponds to speckles in a freely propagating field that fills the 3D space in front of the object surface. Conversely, if an image is captured by using an image device, such as a camera or the human eye, speckles will be present in the image plane, and they will be called "subjective speckles."(6)

II.4.1.Objective speckle

In order to find a representative value of the speckle size, a geometric computation can be performed with the help of Fig. II.4. This figure shows a rough surface illuminated by laser light over an area with a cross-section $L_0 \times L_0$. Points P_1 and P_2 belong to the boundaries of this surface. The optical path difference sOPD from points P_1 and P_2 to Q(x,y) can be expressed by

$$S_{OPD} = P_1Q - P_2Q \approx \frac{xl_0}{z} + \left(\frac{1}{2}\right)\frac{{l_0}^2}{z} \text{(II.23)}$$

In the same way, the OPD for an adjacent point Q'(x+Δx,y) will be described by

$$P_1Q' - P_2Q' \approx \frac{xl_0}{z} + \left(\frac{1}{2}\right)\frac{l_0^2}{z} + \frac{\Delta x l_0}{z} \text{(II.24)}$$

Thus, the relative OPD between Q and Q_0 is expressed as

$$\Delta_{S_{OPD}} = \frac{\Delta x l_0}{z} \text{(II.25)}$$

For those points where $Ds_{OPD} < \lambda$, the relative phases of the components will have approximately the same value. On the other hand, if

$$\Delta_{S_{OPD}} = \frac{\Delta x l_0}{z} \approx \lambda, \text{ (II.26)}$$

then the relative phases will be completely different, and the intensity at point Q' will not be correlated with the intensity at point Q. Consequently, the averaged speckle size d_{sp} will be expressed as

$$d_{SP} = \lambda_z / l_0. \qquad \text{(II.27)}$$

According to Eq. (II.27), it can be seen that the speckle size depends on the size of the illuminated area as well as on the distance between the screen where the scattered light is gathered and the object. In addition, the speckle size does not depend on the optical system used to observe it, which is why this kind of speckle is referred to as objective.(6)

II.4.2.Subjective speckle

Figure II.10 shows the same conditions observed in Fig. II.4, but in this case, the scattering surface is imaged by an optical system comprising a lens and a circular aperture.

In accordance with this figure, a point $Pyfhf_1$ that belongs to the illuminated surface is imagined on the imaging plane as an intensity distribution centered at point Q (Airy disc). As shown for objective speckle, the light coming from point P_1 has a random phase related to the roughness of the scattering surface. The point Q receives light contributions from other points placed in the neighborhoods of the point P_1. Thus, a set of Airy distributions with random phase will be superposed in Q. In the same way, a new point P_2 can then be considered (see Fig.

II.10)whose diffraction pattern is centered at point Q'. For this particular point, the first minimum intensity value of the Airy distribution will be coincident with point Q, and thus point P_2 will not illuminate point Q. Additionally, points placed farther from point P_1 will also not contribute to illumination at point Q because the secondary maximum intensity values are quite lower than the central maximum, which has a weak contribution.(6)

As a result, the light intensity at point Q is provided by contributions from a circular area of the illuminated object centered at point P_1 whose radius is the distance between points P_1 and P_2. The averaged speckle size dsp corresponds to the radius of the Airy disc :

$$d_{sp} = 1.22\frac{\lambda z_i}{b}, \qquad (\mathbf{II}.28)$$

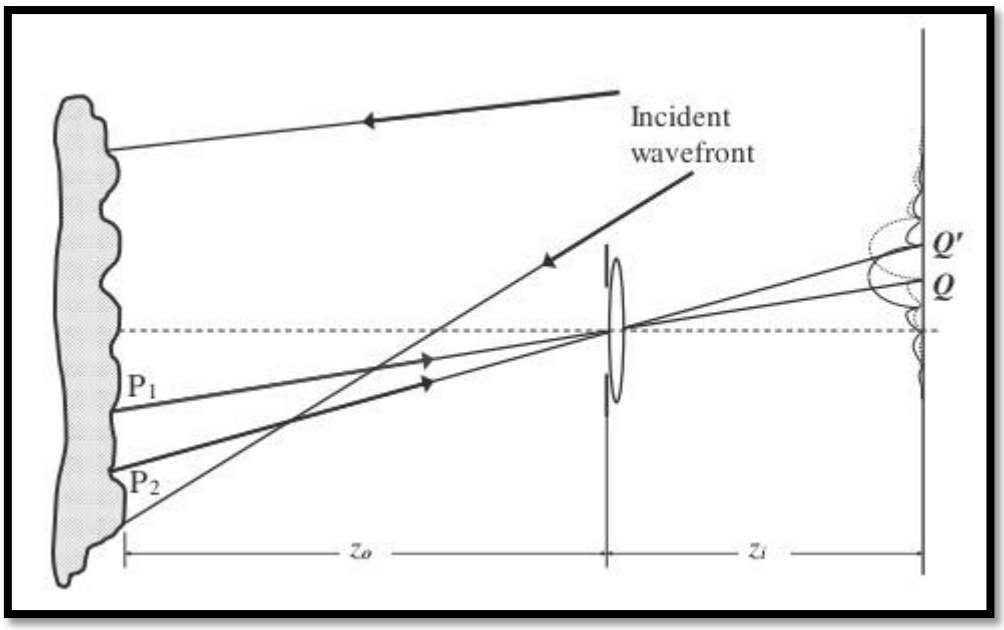

Figure.II.10: Subjective speckle.

where z_i is the distance between the aperture and the imaging plane, and b is the diameter of the aperture. The distance P_1P_2, which is the radius of the scattering element placed on the illuminated surface that scatters the light at point Q , is given by

$$(d_{SP})_{obj} = 1.22\frac{\lambda z_0}{b}, \quad (\text{II}.29)$$

where z_o is the distance from the object to the aperture. This area is known as the resolution cell of the optical system, and it corresponds to the speckle grain on the illuminated object.
If M_g is the magnification of the optical system and f is its focal length, the following relations can be deduced:

$$z_i = (1 + M_g)f, \quad (\text{II}.30)$$

$$z_0 = \frac{z_i}{M_g} = \frac{1+M_g}{M_g}\, f. \quad (\text{II}.31)$$

By considering $F_b = f/b$ as the numerical aperture of the optical system, the speckle size can be written as

$$d_{SP} = 1.22\lambda F_b(1 + M_g). \quad \text{(II.32)}$$

Finally, the size of the speckle on the illuminated object can be expressed as

$$(d_{sp})_{obj} = 1.22\frac{\lambda F_b\ (1+M_g)}{M_g} \text{ (II.33)}$$

Thus, small subjective speckles are related to large lens apertures. In other words, as the lens aperture increases, smaller subjective speckles are obtained. This can be easily verified by stopping down the eye aperture when looking at a speckle pattern.

II.5.Speckle photography (Focused and Unfocused)

II.5.1.Speckle photography

Speckle photography is a technique that makes it easy to measure in-plane displacements using simple optical systems. The general procedure is to illuminate the object with a single laser beam and make a photographic recording on a single photographic plate of the object before and after displacement. The developed plaque is called a double exposure specklogram .

The recording plane of the speckle figures must be located either in the image plane of the object or in the focal plane or in an intermediate plane of the optical system.

Therefore, there are two types of speckle photography depending on the position of the recording plane, focused and unfocused speckle photography. In general, the focused speckle photography technique generates fringes sensitive to in-plane displacements, on the other hand unfocused speckle photography is sensitive to out-of-plane displacements.(9)

II.5.2.Focused speckle photograph

The double exposure focused speckle photography method developed, is the most widely used technique to determine the displacement components in the plane based on the speckle effect. Considering the double exposure specklogram recording procedure illustrated in Figure (II.11). A diffusing surface is illuminated by a diverging laser beam. The lens L with focal length f and numerical aperture F forms in the plane (X, Y) the image of the object surface. The photographic plate is exposed twice, one before and the other after displacement.

Taking into account the principle of geometric optics, the distances d_0 andd_i separating the object and the lens on the one hand and the lens and the recording plane on the other hand, are related to the focal length f of the lens by relation :$\frac{1}{d_0} + \frac{1}{d_j} = \frac{1}{f}$.

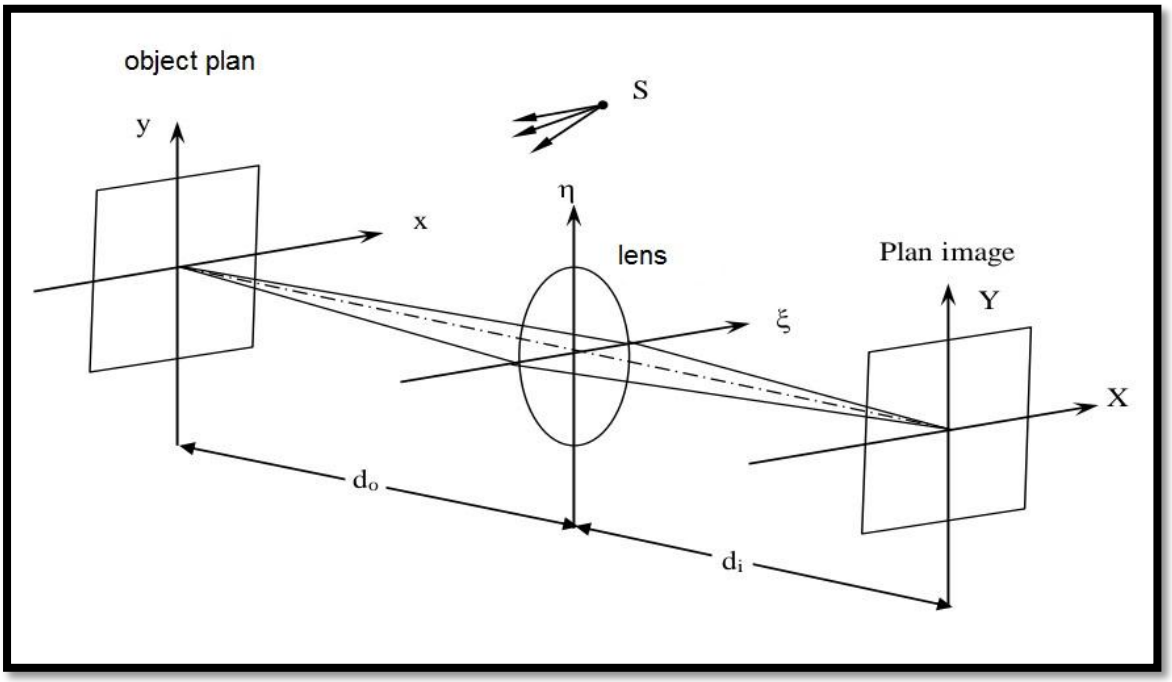

Figure.II.11:Focused Speckle Photography Optical Arrangement.

The amplitude distribution of each point (X, Y) in the image of the object is expressed by [10,11]:

$$U(X,Y) = K \iiint \int U_0(x,y).P_L(\xi,\eta).\exp\left\{\frac{-iK[\xi(X+gx)+\eta(Y+gy)]}{d_i}\right\} dxdyd\xi d\eta \quad \text{(II.34)}$$

K is a complex constant, $U0\ (x, y)$ represents the amplitude distribution just in front of the object surface, $PL\ (\xi, \eta)$ is the pupillary function, and g is the magnification of the optical system.

The intensity distribution recorded on the plate before displacement is proportional to $[U\ (X, Y)\ U*\ (X, Y)] = I\ (X, Y)$.

When the object undergoes a deformation such that the object points move by a value that exceeds the average diameter of a speckle, there will be a change in the amplitude distribution which corresponds to $U\ (X + AX, Y + AY)$; where AX and AY are the displacement components of the speckle grains in the (X, Y) plane with $(AX, AY) = g\ (ux, uy)$.

With (ux, uy) which represent the displacement components of the speckle grains in the (x, y) plane.

The total intensity recorded on the plate after the two exposures is given as follows:

$$I_T\ (X, Y) = U\ (X, Y)\ U*\ (X, Y) + U\ (X + A_X, Y + AY)\ U*\ (X + A_X, Y + AY)$$
$$= I\ (X, Y) + I\ (X + A_X, Y + A_Y) \quad \text{(II.35)}$$

After photographic development of the double exposure specklogram, the latter will have the properties of transparency; hence the amplitude of the transmittance function $h\ (X,\ Y)$ defined by:

$$h(X,Y) = h_0 + \beta\tau[I(X,Y) + I(X + A_X + A_Y) \quad \text{(II.36)}$$

h_0 and β are constants which depend on the photographic emulsion and τ is the exposure time. When the recording medium has sufficient resolution to separate an average size from an individual speckle, two identical speckle figures slightly offset from each other will be recorded on the photographic plate.

Information on the deformation of the object is contained in the correlation properties between the two recorded speckle fields. The optical spatial filtering process is used to transform these correlation properties into visible fringes.(9)

II.5.3.Unfocused speckle photograph

Several methods of speckle photography do not require focusing the object surface on the image plane. That is, the object can be placed forward or backward from its object plane (see Figure **II**.12). This method is widely used to measure the different components of deformations. Consequently, the characteristics of the speckle displacement in the image plane will be modified. The fringe spacing produced by this technique depends on the shape of the illuminating wavefront and the position of the recording plane [6].By proper choice of illumination geometry and recording plane position, we can separate out-of-plane displacements and make speckle grain shifts sensitive only to this type of motion.(9)

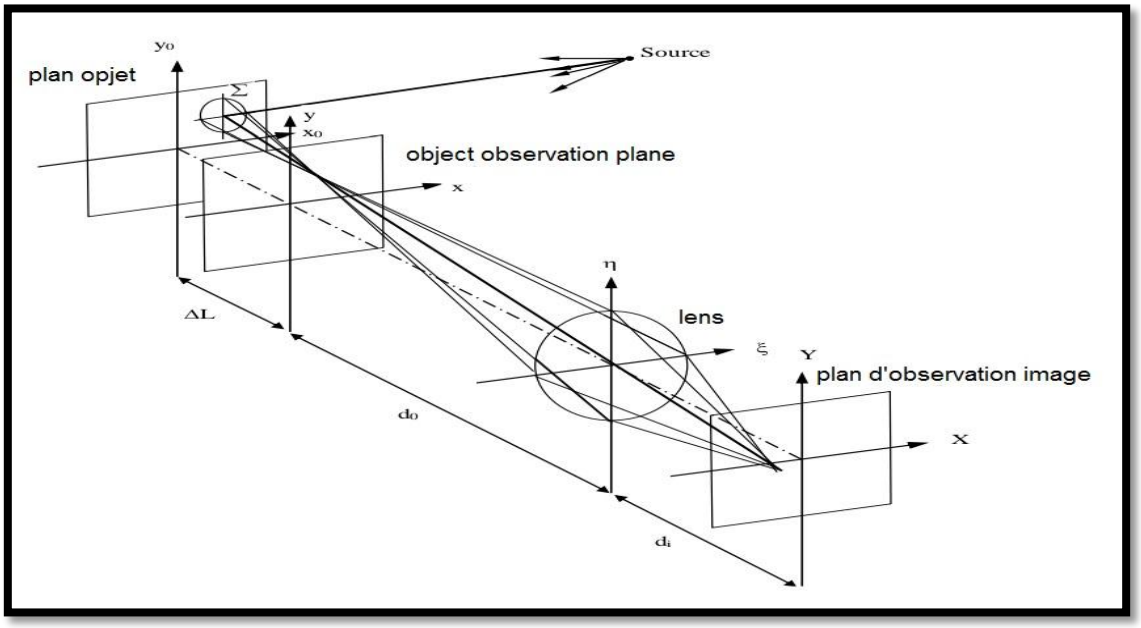

Figure .II.12:Optical arrangement of unfocused speckle photography.

The image observation plane records the speckle figure produced in the object observation plane (x, y) (represented by the surface Σ), homothetic to the pupil of the recording lens. The developed specklogram can be analyzed by one of the spatial filtering techniques.

II.6.Digital speckle correlation

II.6.1.Expermental setup

The expermental setup of a Digital speckle correlation system is schematically depicted in figure **II**-13.the quasi-monochromatic light of wavelength λ and angular frequency $\omega=2\pi c/\lambda$ from a laser source is filtered and expanded so that the object under investigation is illuminated by a collimated beam under an angle Θ. The scatterd light is collected by a lens and imaged onto the target of an electronic camera, usually a high resolustion charge- coupled-device (CCD).instead of a single lens, a more complex imaging system,for example a standard photographic lens, can be used. Yet, the specimen's surface and the camera target are assumed to be in conjugate planes,i.e.,the image of the specimen is focused onto the target. The image taken by the camera are transferred to PC based image processing system where they can be displayed and analysed.

A simple measuring process consists of taking a reference image of specimen in its initial state, subjecting the specimen to a specific load or surface process,and taking another image in the deformed state. Usually a set of images with an appropriate interval is taken during a deformation or surface process. As all data are stored in the image processing system, any two images can be compared to analyse the changes between the associted object states.(8)

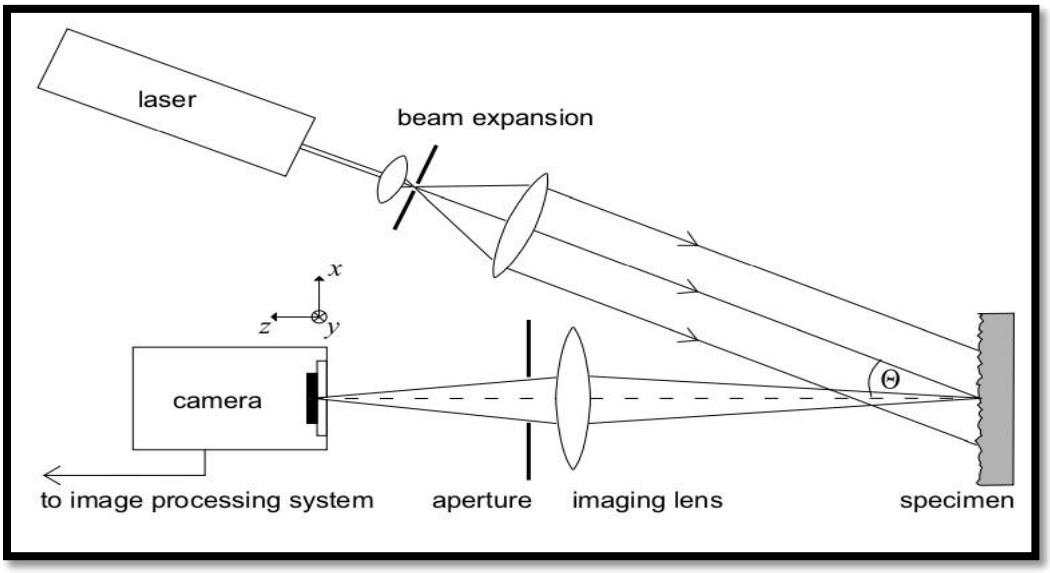

Figure.II.13: the experimental setup for digital speckle correlation..

II.6.2.Simple mathematical model

To describe the optical part of the digital speckle correlation setup in fig II-13 mathematically, we adopt linear system's point of view. The imaging system can then be adequately characterized by its transfer function or –synonymously – by its point spread function .In the following analysis, the system is assumed to be diffraction limited and with a neglible focus error. Let the amplitude of the light field at position (x,y) on the camera target be represented by the scalar function a (x,y). For the case of a lineary polarized wave, this function may be regarded as the electric or magnetic field strengh, where the time dependence exp(-iωt) is omitted. Now, a(x,y) can be expressed as

$$a(x,y) = u(x,y) \times p(x,y) \text{(II.37)}$$

Wher p(x,y) is the coherent point spread function of the imaging system, u(x,y) is the image amplitude that would be obtained in the limiting case of an infinitely large lens aperture (geomtrical optics limit) and * denotes convolution. The intensity i'(x,y) of the light field on the sensor is simply given by $i'=|a|^2$. Yet, if we omit a constant factor of proportionality and a possible offset, the intensity siganal i(x,y), as recorded by the camera, is calculated as

$$i(x,y) = i'(x,y) \times h(x,y) + n(x,y) \qquad \text{(II.38)}$$

Where the characteristics of the camera are taken into consderation through the impluse response function h of the CCD-senso and readout electronics and the electronic noise n. If a digital camera is used there is no further image degradation. Otherwise, in case of an analog camera output,the signal must first be transferredbto the framegrabber of the imaging processing systeme, where it is sampled and converted into a digital signal. Then, the charateristics of the framegrabber need to be incorporated into h and n. The primary image information $i(x_j,y_k)$ of the sensor pixels, is then transferred to and stored in the image processing system. In the analysis to follow, we will often make use of the image spectrum,i.e. the fourier transform of i :

$$I(v_x, v_y) := F[i(x,y)] := \iint_{-\infty}^{\infty} i(x,y) e^{-2\pi i(v_x x + v_y y)} dx dy \text{ (II.39)}$$

Because the image is always of finite size,the integral in eq (II-39) exists and the spectrum can be written in this form. Using the convolution theorem, I is given by :

$$I(v_x, v_y) = F[i']F[h] + F[n] = I'H = N \qquad \text{(II.40)}$$

Where I'is the spectrum of the speckle intensity on the sensor, H is the camera transfer function and N is the noise spectrum. The dependency on the spatial frequencies v_x ,v_y has been omitted

for brevity. The spectrum A=F[a] of the field amplitude on the camera sensor is given from Eq.(II-41)by :

$$A(v_x, v_y) = U(v_x, v_y)P(v_x, v_y) \qquad \text{(II.41)}$$

With the transforms P=F[p] and U=F[u]. For a diffraction limited imaging system, the coherent transfer function P is simply the transmission or pupil function of aperture [Goo68]in the case of single lens, as shown in figure (II.13),P is directly given by the transmission of the physical aperture stop. For a more complex imaging system,the exit pupil, wich can be found by geometrically projecting the smallest physical aperture through the imaging elements onto the exit plane, has to be used instead.(8)

Next we are going to model the alterations of the object surface. To keep things simple, we will initially restrict ourselves to in-plane displacements and microstructure changes only, thus neglecting all out-of-plane deformations. With these restrictions, the amplitude u of the scattered speckle field in the geometric optics limit can be written as

$$u(x, y) = u_0(x, y) + \Delta u(x, y) \qquad \text{(II.41a)}$$

In the intial object state and

$$\tilde{u}(x, y) = u_0(x - \Delta x, y - \Delta y) + \Delta\tilde{u}(x, y) \text{ (II.41b)}$$

in the final object state after deformation. The formal partition of u into a constant part $u_0$and a fluctuating part Δu reflects the primary decorrelation due to microstructure changes. The amplitudes u, Δu and $\Delta\tilde{u}$ are assumed to be mutually uncorrelated. If there is no change in the mean scattered intensity, $\Delta\tilde{u}$ and Δu will have the same variance. The horizontal shift Δx In the image plane is connected to a respective displacement $\Delta x' = \frac{1}{M}\Delta x$ in the object plane,where M is the magnification or demagnification of the imaging system. The vertical shift in the object plane is respectively given by $\Delta y' = \frac{1}{M}\Delta y$.

In case of a non-uniform in-plane displacement, Δx and Δy will depend on the position (x,y).

Using Eqs (**II**-37)and(**II**-38),and similar expression for $\tilde{a}$ and $\tilde{\imath}$, the recorded speckle intensities in the initial and final object states,respectively,yield

$$i(x, y) = i_0(x, y) + \Delta i(x, y) + n(x, y) \text{(II.42a)}$$

$$\tilde{\imath}(x, y) = i_0(x - \Delta x, y - \Delta y) + \Delta\,\tilde{\imath}(x, y) + \tilde{n}(x, y) \text{(II.42b)}$$

where the constant and fluctuating part of the image intensity are given by $i_0 = |a_0|^2 \times h$ and $\Delta i = [|\Delta a|^2 + 2Re(a_0^*\Delta a)] \times h$.Here,$a_0$ and Δa are the constant and flucating part of the speckle amplitude, Re denotes the real part and * denotes the complex conjugate.

The random nature of a speckle pattern requires to describe the underlying amplitudes and intensities as statistic processes. Generally, meaningful information can only be extracted

through an averaging process, usually the ensemble average,denoted by $<.>$. If the roughness of the surface under examination is in the order of or larger than the wavelength of the illuminatimg light, the speckle amplitude follows a circular Gaussian statistic. The speckle pattern is then said to be fully developed and the moments of the intensity field are given by $< i^n >/< i >^n = n!$.The standard deviation $\sigma_i = \sqrt{< i^2 > - < i >^2}$ equals the mean intensity$< i >$ and hence the contrast is unity. For a rough surface we can also assume that slight deformations and alterations in the microtopography of the surface do not cause a change in the mean scattered intensity,thus <ĩ>=<i>. For a fully developed speckle pattern this implies that all moments remain unchanged,especially $\sigma_{\tilde{\imath}} = \sigma_i$.

The most important quantity for our purpose is the cross-correlation $C_{\tilde{\imath}\,i}$ of the recorded intensities i and ĩ, which is defined as

$$C_{i\tilde{\imath}}(x, y; x', y') := < i(x, y)\tilde{\imath}(x', y') > \text{(II.43)}$$

Often,a slightly different from will be used, viz the cross-covariance normalized to the geometric mean of the variances:

$$C_{i\tilde{\imath}}(x, y; x', y') := \frac{<(x,y)\tilde{\imath}(x',y')> - <i(x,y)><\tilde{\imath}(x',y')>}{[(<i^2(x,y)> - <i(x,y)>^2)(<\tilde{\imath}^2(x',y')> - <\tilde{\imath}(x',y')>^2)^{1/2}} \text{(II.44)}$$

Usually, a confusion is not cirtical and $C_{i\tilde{\imath}}$ will simply be called the 'correlation function' of the recorded intensities. If a precise differntiation is necessary, will refer to $C_{i\tilde{\imath}}$ as the simple cross-correlation and to $C_{i\tilde{\imath}}$ as the normalized cross-covariance.

$$\mathrm{Ci\tilde{\imath}}(\mathrm{x}', \mathrm{y}') = \frac{<i(\mathrm{x,y})\tilde{\imath}(\mathrm{x}+\mathrm{x}', \mathrm{y}+\mathrm{y}')> - <i><\tilde{\imath}>}{\sigma_{\mathrm{i}}\sigma_{\tilde{\imath}}} \text{(II.45)}$$

Inserting (**II**-42)and using the fact that $i_0, \Delta i, \Delta\tilde{\imath}, n$ and ñ are mutually uncorrelated, we obtain

$$\mathrm{Ci\tilde{\imath}}(\mathrm{x}', \mathrm{y}') = \frac{<\mathrm{i_0(x,y)i_0}(\mathrm{x}-\Delta\mathrm{x}+\mathrm{x}', \mathrm{y}-\Delta\mathrm{y}+\mathrm{y}')> - <\mathrm{i_0}>^2}{\sigma_{\mathrm{i}}^2} \quad \text{(II.46)}$$

$C_{i\tilde{\imath}}$ as well as $c_{i\tilde{\imath}}$ always have their maxima at position (x',y')=(Δx, Δy). The in –plane displacement can thus be determined from the peak position of the correlation. In the case of no electronic noise and no primary decorrelation ,Eq.(II.11) states that the cross-correlation function is just a shifted version of the autocorrelation function c_{ii}. The maximum value of $c_{i\tilde{\imath}}$, which is called the correlation coefficient $cc_{i\tilde{\imath}}$ of i and ĩ,is given by

$$cc_{i\tilde{\imath}} := c_{i\tilde{\imath}}(\Delta x, \Delta y) = \frac{\sigma_{i_0}^2}{\sigma_{i_0}^2 + \sigma_{\Delta i}^2 + \sigma_n^2} \text{ (II.47)}$$

Where $\sigma_{i_0}^2, \sigma_{\Delta i}^2 \; and \; \sigma_n^2$ are the variances of the constant and fluctuating part of the intensity field and the electronic noise, respectively. Thus, the correlation coefficient $c_{i\tilde{\imath}}$ is the ratio of the power in the constant part of the signal to the total power. Thed noise power $\sigma_n^2 = < n^2 >$

Is usually quit small, i,e. $\sigma_n^2 \ll \sigma_i^2$,so that Eqs (II-47)can be rewritten as

$$cc_{i\tilde{i}} = cc_\mu cc_n := \frac{\sigma_{i_0}^2}{\sigma_{i_0}^2+\sigma_{\Delta i}^2}\frac{1}{1+\frac{\sigma_n^2}{\sigma_i^2}} \qquad \text{(II.48)}$$

cc_μ is the primary (de-) correlation factor where the index μ refers to origin from changes in the microstructure of the surface and cc_n is the correlation factor due electronic noise.(8)

II.6.3.The basic correlation algorithm

The objective of the correlation algorithm is to determine the deformation and the degree ofprimary decorrelation between two states of the object from a pair of associated digital imagedata. Again, the analysis will initially be restricted to the determination of in-plane displacements and the degree of decorrelation.

In the last section it was shown that in-plane displacements cause a respective shift of therecorded speckle patterns. The estimation of bulk motions within an image or of parts of it .is a general task in digital image processing, which is often solved with correlation techniques.

Due to the random nature of the speckle patterns, the displacement cannot be inferredfrom a single image point or single speckle. In the theoretical description, this problem hasbeen solved by using ensemble averages. In a real experiment, however, we have to deal witha single realization of the surface and its deformation. Therefore, spatial averages within acorrelation window are used to calculate the quantities of interest. The correlation functions,obtained from ensemble and infinite spatial averaging, respectively, are mathematically identical, if the speckle patterns are wide-sense stationary processes and ergodic with regard to mean, variance and covariance . In a real experiment, the displacement usually depends on position, i.e., it is not stationary, and images of finite size have to be used. This leads to additional decorrelation and only the average displacement within the correlation window can be determined.(8)

The principle of a displacement field measurement is illustrated schematically in Figure II-15.The two images, acquired before and after deformation, are usually subdivided into a set ofsubimages. The correlation function is calculated for each pair of corresponding subimages and the respective displacement is derived from the position of the maximum. The deformation field is therefore sampled at the center positions of the subimages. The size of the subimages, which is often chosen to be 32x32 or 64x64 pixels, determines both the spatial resolution and the accuracy of the measurement. The finite width B of the correlation window limits the spatial resolution and thus the spectral contents in the deformation field to frequencies of less than 1/B.

Therefore, according to the Nyquist theorem, the deformation field is sufficiently sampled if the pitch between adjacent subimages is B/2.

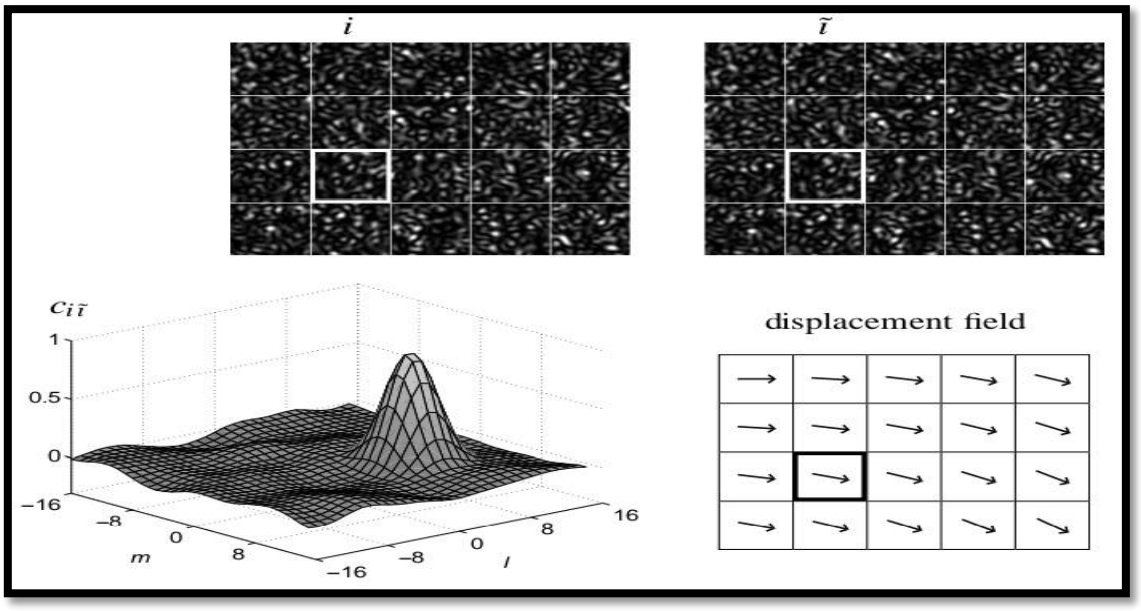

Figure.II.14: Principle of displacement field measurement.

Corresponding subimages i and ĩ are extracted from the reference and deformed speckle images as indicated by the bold whitesquares. The mutual correlation function $c_{i\tilde{i}}$ is calculated and shown here in a pseudo-3Dplot.The position of the maximum of $c_{i\tilde{i}}$ yields the average displacement between the twosubimages, which is pictured by an corresponding arrow. Repeating the procedure gives the whole displacement field,wich is usually visualized in an arrow plot.

Let the subimages, extracted from the reference and deformed speckle images by a rectangular correlation window, be represented by the intensity values i(j,k) and ĩ(j,k),respectively,which have been sampled by the camera sensor at the pixel positions (x_j,y_k),j,k=0...N-1. The width and height of the correlation window are given by $B=Nd_p$,where d_P is the pixel pitch of the sensor. For simplicity, a uniform pixel pitch in horizontal and vertical direction and square subimages are assumed. The extension to a non-uniform pixel pitch and rectangular subimages is straightforward. The discrete cross-correlation between subimages i and ı̃ is defined as:

$$(l,m) = \frac{1}{N^2}\sum_{j,k=0}^{N-1} i(j,k)\tilde{\imath}(j+l,k+m) \quad \text{(II.49)}$$

In analogy to (**II**-44)the discrete normalized cross-covariance is defined as

$$(l,m) = \frac{C_{i\tilde{i}}(l,m)-\bar{\imath}\,\bar{\tilde{\imath}}}{\sigma_i\sigma_{\tilde{\imath}}} \quad \text{(II.50)}$$

where the mean and variance of the reference image i are now given by $\bar{\imath} = \frac{1}{N^2}\sum_{j,k=0}^{N-1} i(j,k)$ and $\sigma_i^2 = \sum_{j,k=0}^{N-1} i^2(j,k) - \overline{i^2}$,and similarly for the deformed image ĩ. Again, to simplify

terminology, both $c_{i\tilde{\imath}}$ and$C_{i\tilde{\imath}}$ will be called correlation functions of i and ĩ and the displacement can be determined from the maximum of either function.

If only single values of the correlation function are needed – for example $ci\tilde{\imath}(0,0)$when the displacement is a-priori known to vanish in case of a pure surface process – the calculation from the definition is straightforward. Usually, the complete cross-correlation function is required and the direct calculation by Eq. (II. 49) is rather time consuming. It is much more efficient to perform the cross-correlation in the Fourier domain by using a fast Fourier transform (FFT) algorithm. In virtue of the Wiener-Khintchine theorem, the cross-correlation is the Fourier transform of the cross-power-spectrum I*Ĩ and can be calculated as

$$C_{i\tilde{\imath}}(l,m) = F^{-1}[I^*\tilde{I}] \qquad \text{(II,51)}$$

F^{-1} is the inverse Fourier transform operation, *denotes the complex conjugate and I is the discrete Fourier transform of subimage i, defined as :

$$I(l,m) = F[i] = \frac{1}{N^2}\sum_{j,k=0}^{N-1} i(j,k)e^{-\frac{2\pi i}{N}(jl+km)} \text{(II, 52)}$$

and similarly for Ĩ=F[ĩ]. The procedure is illustrated in Fig. **II**.15.

As stated in the last section, the correlation coefficient $cc_{i\tilde{\imath}}$ of subimages i and ĩ is defined as the maximum value of the normalized cross-covariance $c_{i\,\tilde{\imath}}$ and the displacement is given by the position of the maximum. The calculation of Eq. (**II**.51) yields a discrete representation of $c_{i\tilde{\imath}}$. Thus, the selection of the highest value in $c_{i\tilde{\imath}}$ (l,m) gives the peak position with a precision of half a pixel.

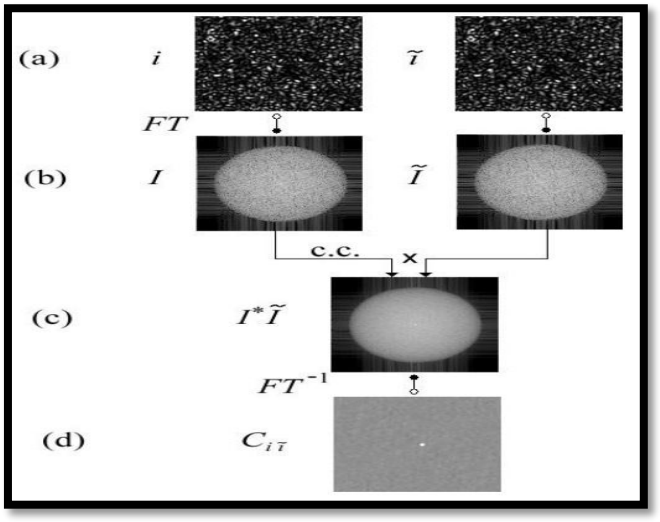

Figure.II.15:Flow chart of the correlation algorithm.(a) subimages from recorded data, (b) spectra,(c) cross-power spectrum, (d) cross-correlationfunction. FT indicates a Fourier transform, c.c.
denotes the complex conjugate and × denotes a multiplication.

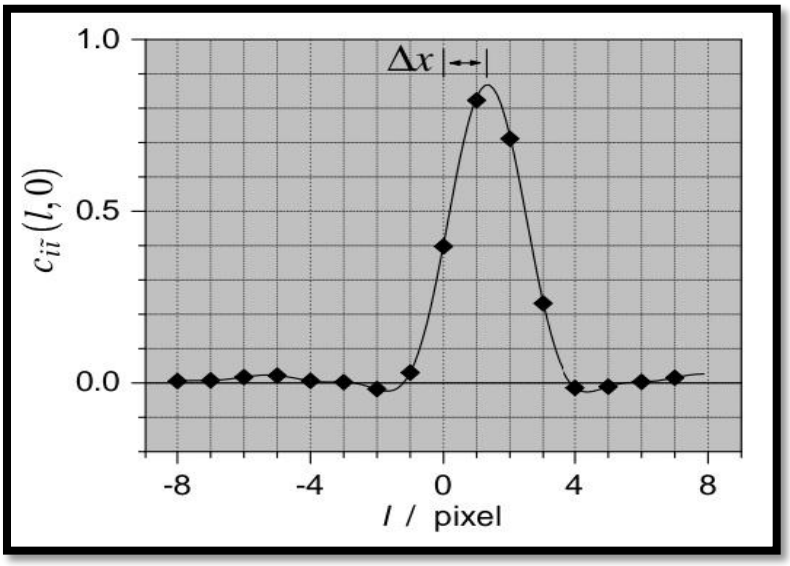

Figure.II.16: Horizontal profile through theCentral region of the cross-correlationFunction; discrete data (◆) with interpolation by a Fourier series expansion (—).

A considerably higher precision can be obtained with central point estimation or by data interpolation, as depicted in Fig. **II**.16. Possible methods are, for instance, parabolic fitting or Fourier series expansion.

At this point, a discussion of the influence of the correlation window, which is used to extract the subimages from the full-size camera frames, is necessary. Mathematically, the correlation function in Eq. (**II**.49) becomes twice as wide as the original sub images.Thus, if the calculation is carried out in the Fourier domain, the input images into the correlation algorithm should be twice as large as the correlation window. To this purpose they must be appropriately padded with zeros, or preferably, with their mean values, to avoid a bias to zero displacement. However, if Eq. (**II**.49) is used without doubling the width of the subimages, the correlation algorithm implies that i and ĩ are cyclically repeated: i(j,k)=i(j mod N,k mod N). Usually, the size of the correlation window is large compared to the speckle size and this wraparound error is negligible, especially if the window for the deformed subimage is iteratively selected as described below.Another option to avoid edge effects is, to use a smooth correlation window which gently falls off from the center to the edges, for example a Gaussian or Hamming window, instead of a rectangular window as hitherto assumed. But then the intensity information close to the edges of the sub images is suppressed, which lead to less accurate estimates of correlation coefficient and displacement values.

If the subimages are selected at identical positions within the original camera frames, and in case of an appreciable in-plane displacement, two different regions of the speckle patterns will be compared. This leads to an additional decorrelation. The situation can be

improved in a new calculation, where the correlation window for the deformed image is shifted according tothe first displacement estimate. Since the image data are discrete samples and the displacement generally corresponds to a non-integral pixel value, it is better to use a shifted replica ĩ shift of the deformed image. With a Fourier transform method it is possible to achieve a non-integral shift by:

$$\tilde{\imath}_{shift} = F^{-1}[\tilde{I}(l,m)e^{\frac{-2\pi i}{M}(\delta x l+\delta y m)}] \text{(II .53)}$$

Where δx and δy are the last estimated displacement values in horizontal and vertical direction, respectively. Note that the width Md_P of the window for the shift operation has to be larger than the final correlation window due to the cyclic nature of the Fourier transform now, the cross-correlation function of i and $\tilde{\imath}_{shift}$ is calculated and a better estimate of the correlation coefficient and displacement can be obtained. The process may be repeated until the correlation peak has reached the origin, to give the best possible match of the subimages. In practical applications one or two iterations are often sufficient. In case of a non-uniform displacement field, there is some remaining mismatch due to rotation and strain. However, the corresponding degradation of the correlation function is usually negligible compared to the initial decorrelation of the recorded speckle images

The experimental determination of the mean intensities and variances is usually straightforward. A complication arises, if there is a non-uniform irradiance of the object within the subimage, which can be caused, for example, by the beam profile of the illuminating laser. The situation may also be viewed as a smoothly varying correlation window. In case of a uniform illumination, the value of the correlation function outside the central correlation peak is equal to the square of the mean intensity and constant except from statistical fluctuations, compare Fig. **II**.14(d). For a non-uniform illumination, the correlation function also decreases on a large scale. The effect is illustrated for a Gaussian beam profile in Fig. **II**.17, where a central crosssection through the correlation function is depicted. In this case, the correlation coefficient will be overestimated if the mean intensity is directly calculated by $\bar{\imath} = \frac{1}{N^2}\sum_{j,k=0}^{N-1} i(j,k)$.

Even if there is zero correlation, $C_{i\tilde{\imath}}$ (0, 0) will have a finite positive value. A similar problem arises in the determination of the width of the correlation peak. A much better estimate for the correlation coefficient can be obtained if the product of the mean intensities ī and $\bar{\tilde{\imath}}$ is calculated

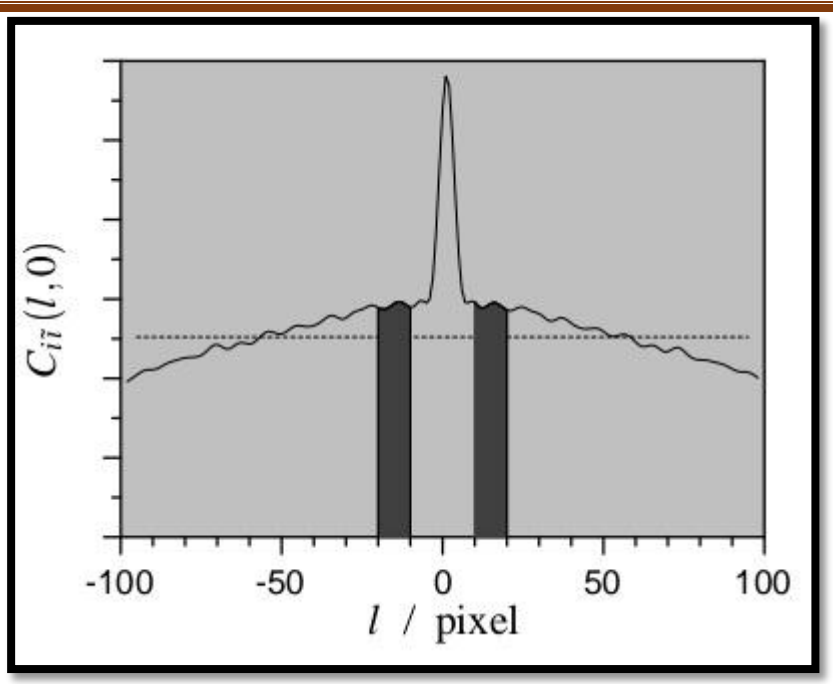

Figure.II.17**:**Profile through cross-correlation function in case of a non-uniform illumination. The dashed line indicates the square of the true mean intensity,and the shaded area marks the region, from where it is estimated to avoid a bias the calculation coefficient.

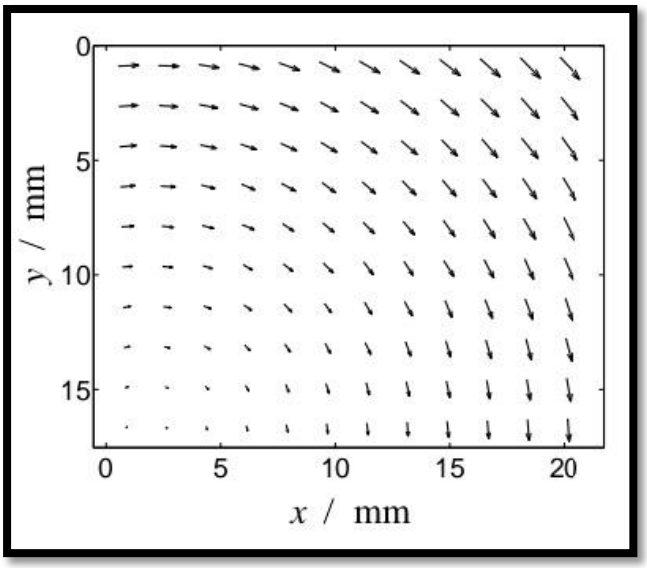

Figure.II.18**:**in-plane deformation field foran object rotation. The position (x,y)refersto the object surface**.**

from an annulus around the peak of the simple cross-correlation function (see Fig.II.17):

$$\overline{i\tilde{i}} \approx \frac{1}{M}\sum_{r_i^2 \le l^2+m^2<r_0^2} C_{i\tilde{i}}(l,m) \text{(II. 54)}$$

The size of the inner diameter $2r_i$ must be large enough to exclude all pixels inside the correlation peak and the outer diameter $2r_o$ must be chosen large enough to enable a reliable statistical average. M is the number of pixels inside the annulus. Similarly, the squared mean

intensities $\bar{i}^2$and $\tilde{i}^2$ can be calculated from an annulus in the simple autocorrelation functionsC_{ii} and $C_{\bar{i}\tilde{i}}$, respectively.

We will conclude this section with an illustration of the typical results of the correlation algorithm. Fig. **II**.18 shows the in-plane deformation field, where the object has been rotated about an axis that is close to the lower left corner of the images. The displacement vectors have been calculated from the peak position of the interpolated correlation function $c_{\bar{i}\tilde{i}}$ for subimages of size 64x64 pixels. The maximum displacement in the upper right corner is found to be ~1.5 pixels or 40 µm.(8)

Chaptre III

EXPRESS RELEASE

Introduction

This chapter is devoted to the presentation of the experimental results of the application of the speckle photography technique for the measurement of deformations and compressive stresses in ceramic parts. We study the effect of the compressive forces exerted during the application of parts by uniaxial pressing on the behaviour of these parts during compression tests.

III.1. Kaolin of Tamazert (Kaolin T)

Located in the El-Milia region (eastern Algeria), the Tamazert kaolin deposit, discovered Located in the El-Milia region (eastern Algeria), Tamazert kaolin deposit, discovered 1925, has been exploited since 1932. The size of the deposit is considerable, but the raw rock is so poor in kaolinite that some do not hesitate to call it sand of Tamazert, precisely cause of the very high quartz concentration. In 1925, has been exploited since 1932. The size of the deposit is considerable, but the raw rock is so poor in kaolinite that some do not hesitate to call it sand of Tamazert, precisely to cause of very high quartz concentration.

The primary rock, from the orthosesorthoses feldspar, decomposed giving different minerals, mainly free silica, mica, kaolinite and oxide impurities metal, with a significant proportion of iron oxide, which thwarts its use by local industry. The quality of this kaolin, in the raw state, is therefore very poor.

III.1.1 Kaolin T crude

Raw kaolin is a mixture of several minerals. In the diffraction spectra of the following minerals appear in order of decrease in line intensity:

First, the SiO_2 quartz (50% by weight), whose lines are by far the most intense, then the Muscovite $K_2O_3Al_2O_3.6SiO_22H_2O$ (28% by weight), of the Micas family, then the Kaolinite $Al_2O_3.2SiO_2$. $2H_2O$ (18% weight), with wide but not very intense lines, finally the Feldspar or those (some percentage quite variable) with lines of low intensity. Chemical analysis also reveals the concentration of oxide impurities which varies from 3% to 5% by weight, and whose main impurity is an iron oxide which may exceed 2% by weight (Table.III.1). [10]

Table.III.1: Chemical compositions of crude Tamazert kaolin (%by weight).

P.F	$S1O_2$	$A1_2O_3$	Fe_20_3	TiO_2	CaO	MgO	K_2O	Na_2O
5.32	71,57	18,48	0,58	0,15	0,22	0,26	3,15	0,10
5,09	70,72	18,66	0,86	0,32	0,27	0,19	3,83	0,21
4,45	71,5	18,19	1,03	0,34	0,29	0,36	0,36	0,23
4,00	70,22	19,10	1,50	-	0,40	0,33	3,10	-
4,90	70,90	18,70	0,88	0,32	0,01	0,34	3,44	0,12

P.F: fire loss at 1000°C

III.1.2 The Different Phases of Kaolin T Crude

Raw Tamazert kaolin can not be analysed in the same state as the diffractograms of the RX then include all the lines of the different phases present which result in overlaps and interferences between the different lines.

It is possible to use simple raw mineral processing methods, which provide more enriched phases with main minerals and more exploitable RX diffraction spectra.

The methods used are mechanical screening and levitation. These methods with limited efficiency, do not result in à complete separation of the phase but rather to enrichment which is an intermediate step. Total separation requires physical flotation methods using a heavy liquid of the desired density, sorting electrolytic or electromagnetic sorting.

The levitation method, used on a fairly large quantity of plain kaolin (= 100 kg) gave the following results after drying at 100°C (loss of mixing water): enriched phase (in kaolinite): 29.6% Residue: 70.4%

The second method used is a simple sieve (0.5mm) applied to the residue and which has produced the following results:

- Large materials (> 0.5 mm): 45%.
- Fine materials (< 0.5 mm): 25.4%.

The predominant mineral is quartz which is mainly present in the residue in the form Muscovite mica and kaolinite are the most common fine material.

The A.S.T.M file allows us to compare the spectrum of each mineral with that recorded.

Kaolinite is of type It (fileASTM14-164) of the crude formula: $Al_2.(OH)_4.Si_2O_5$.

Mica is à muscovite type with the crude formula $K.Al_2.Si_3.Al.O_{10}.(OH)_2$.

We are in the presence of two micas of the muscovite family.

The first is a solid solution where the atoms of Fe or Mg are substituted for 1'Al, while Na substitutes K: the formula would then be: (K.Na) (Al, Mg, Fe) (Si_3.Al 0.9). O_{10}. $(OH)_2$: (muscovite 3T ASTM file: 7-042).

The second is pure muscovite with however some OH radicals replaced by F: K.A12. (Si_3. Al). O_{10}. $(OH, F)_2$ (muscovite 2M1 AMS file: 6-0263a).

It seems very easy to enrich, relatively, the kaolin of tamazert, by extracting a large part of the quartz, which is the largest fractions of the material 0.5mm aperture sieve. Separation of mica, which seems to contain in solutions solids the harmful elements (mainly iron oxide) to the quality of the ceramics, would require more sophisticated techniques. [10]

III.1.3.Chemical and mineralogical compositions

In their natural state, kaolinitic clays consist mainly of kaolinite, The latter is associated with other minerals, in addition to various impurities contained in small quantities (different oxides). The chemical composition of enriched kaolin (KT2) given by the petrochemical and geochemical research centre in the service analysis of rock and minerals are shown in Table.III.2: [2]

Tableau.III.2: Chemical composition of enriched kaolin (KT2).

Elements	**SiO_2**	**Al_2O_3**	**FeO_3**	**K_2O**	**Na_2O**	**TiO_2**	**CaO**	**MgO**	**P. à. F**
I.C.P.M.S (C.R.P.G)	48.85	33.07	2.53	2.92	0.07	0.28	0.06	0.38	11.57
A.A.L.E.M	50.7	32.92	2.38	2.96	0.10	0.27	0.06	0.41	10.14
L.E.M Corrected	51.09	33.18	2.40	2.98	0.10	0.27	0.06	0.41	10.22

I.C.P: Plasma Coupling Induction.

L.E.M:

P.F:Loss of Fire at 1000°C

Analysis results expressed in mineralogical reconstitution of the same kaolin (KT2)

Table.III.3: Mineralogical Analysis of Enriched Kaolin (KT2).)

Kaolin	Illite	Quartz	geothite	other	P to F.C	P to F.M
61.43	25.07	11.10	2.23	0.18	10.17	-0.03

III.2.The characteristics of kaolin KT2

III.2.1.Differential thermal analysis of kaolin KT2

In kaolin, an endothermic drift, caused by the departure of water, can be observed below approximately 200°C. This is water absorbed from the outer surface of the particles.

The departure of this water varies according to the type and nature of the minerals. Kaolinite undergoes several thermal phenomena during observable heating on differential thermal analysis curves.

In the case of Tamazert kaolin, kaolinite, muscovite and quartz are simply absorbed water whose departure does not alter the structure of the minerals. Its elimination therefore not constituting a characteristic thermal transformation of kaolin KT2. [10]

The curve representative of the behaviour of kaolin KT2 for a 20°C/min heater is shown in Figure III-1.

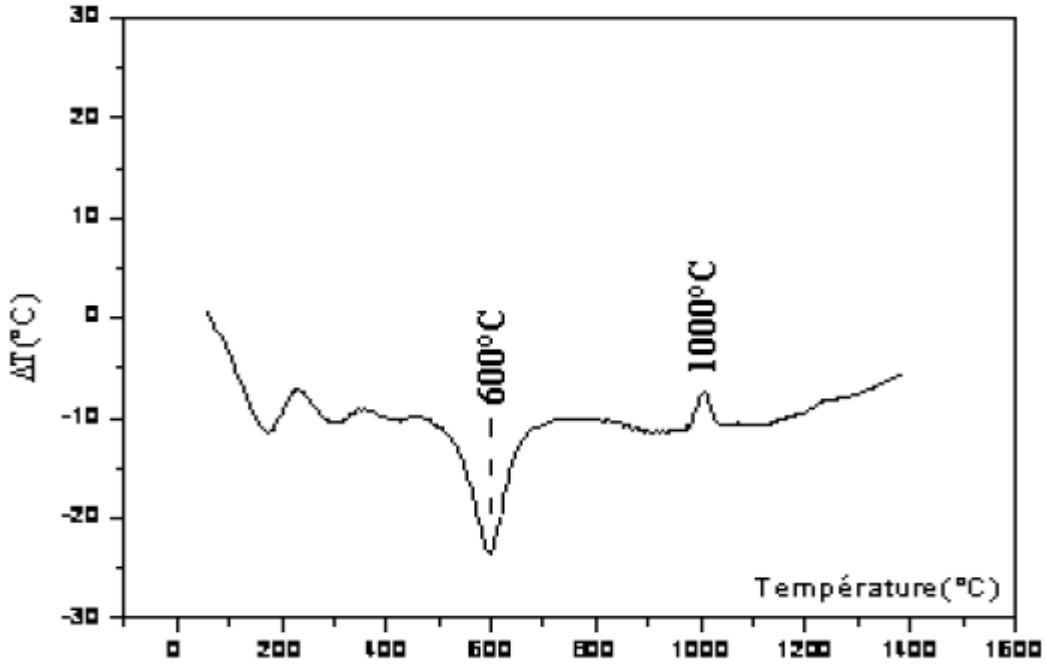

Figure.III.1: ATD curve of kaolin KT2 treated at 20°C/min under air.

According to the figure above, the following phenomena can be observed:

- The endothermic derivative peak, observed between 100°C and 200°C, is caused by the intake of water.
- The endothermic peak observed between 490°C and 650°C is characteristic of the dehydroxylation of clay minerals and the decomposition of metakaolin. It is the departure of structural water.

- The exothermic peak observed between 950°C and 1025°C corresponds to the structural reorganization of clay minerals is generally attributed to the formation of mullite.

The temperature characteristics of the peaks observed are indicated on the differential thermal analysis. [3]

III.2.2.Kaolinite platelet morphology KT2

Scanning electron microscopy (SEM) was used to observe the morphology and size of kaolinite platelets present within kaolin KT2. The resulting image is shown in Figure (III.2).

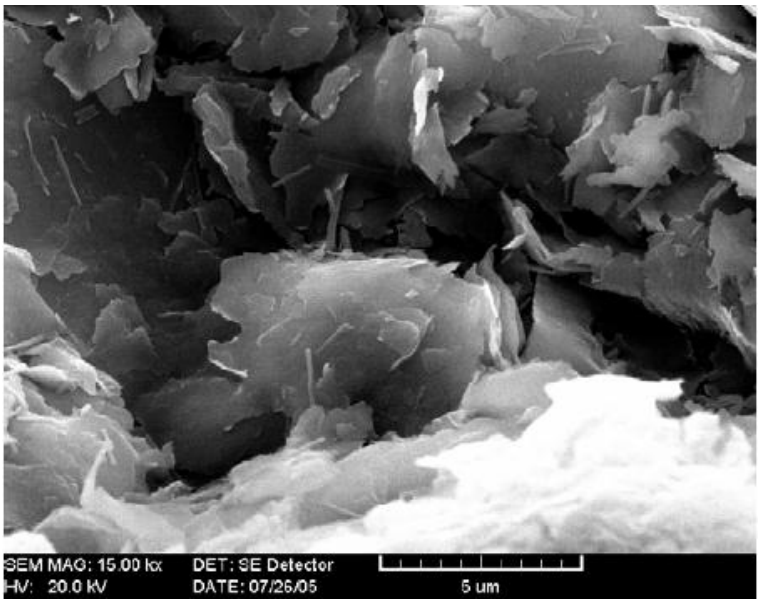

Figure.III.2: The morphology of a kaolinite contained in the raw kaolin KT2.

(Figure III.2) shows kaolinite grains contained in kaolin KT2 which are relatively decided in a plane shape that is sometimes circular and often very irregular when compared with well-crystallised kaolinite (figure III.3). [11]

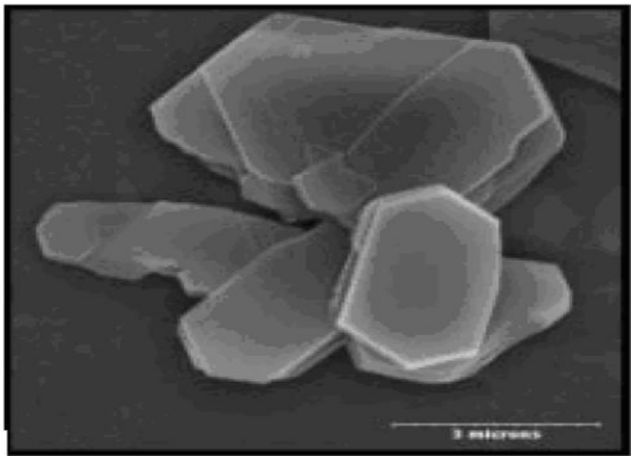

Figure.III.3: The morphology of a well crystallized kaolinite.

III.3. Treatment of kaolin

Taking into account the sensitivity of the kaolinization process to changes in levels hydrothermal circulation, temperature variations in the granitic mass and heterogeneities of granite composition, kaolin generally has different characteristics in the same deposit.To have à marketable product, constant properties, it must therefore be subjected after extraction to a whole series of treatments.

Marketed kaolin generally meets the following conditions:

- remain white after cooking at 1400°C;
- have a maximum grain diameter (usually 20 µm), which does not exceed 50-63 µm;
- contain at least 80% by weight of kaolinite.

Several studies have been done on kaolin behaviour during treatment thermal, the first step in this transformation series is the reaction within the range of 450-600°C in the majority of it is due to the release of all the structural water included in the kaolinite contained in kaolin with the formation of dehydroxylated kaolinite defines as metakaolinite (Al2O3 2SiO2). For the exothermic reaction located in the 980°C limit, represents an inflexion point in the different researchers, the first the group assumes this reaction is due to the formation of alumina spinel phase (Al2O3γ), but others assume the nucleation of mullite and spinel at the same time ,the second group assumes only the nucleation of mullite but the assumption of the first group is predominant. So the transformation between 1100-1200°C is due to the formation of mullite ($3Al_2O_3$ $2SiO_2$), which does not translate that the formation of mullite begins from 1100°C but may be at temperatures below 1100°C. [11]

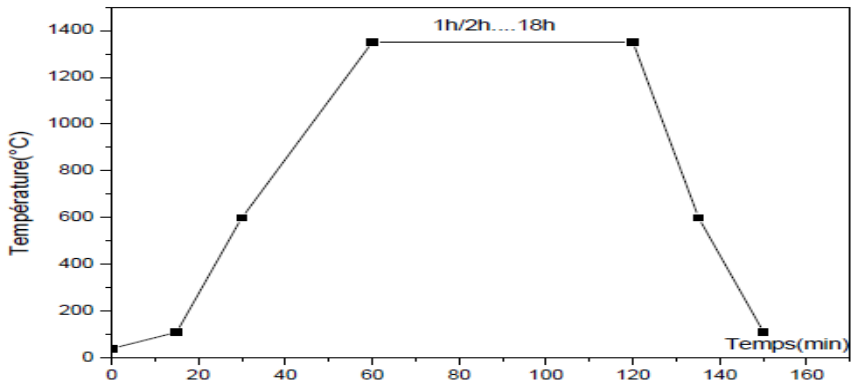

Figure.III.4: The thermal cycle of sintering.

III.4. Specimen Manufacturing Steps

III.4.1. Crushing

Crushing is an operation consisting of dividing a solid, to increase its specific surface (developed surface of the powder per unit of mass) and thus its reactivity. Grinding is done up to the release mesh.

The release mesh of a mineral is the size below which an ore particle is perfectly released, that is to say, consisting only of the mineral species to be valued [12].

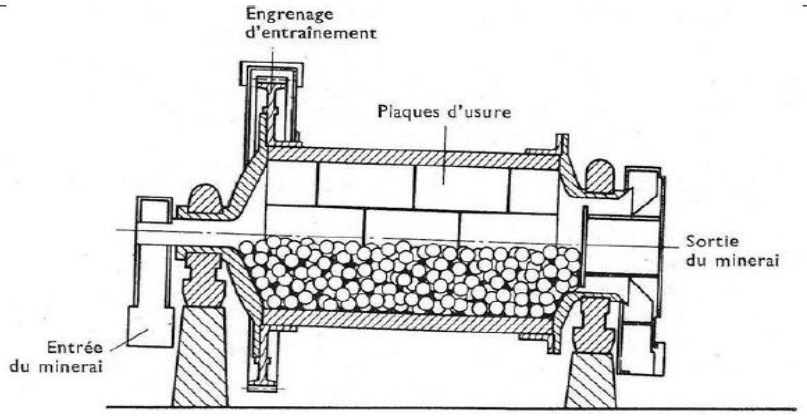

Figure.III.5: Ball mill (longitudinal cut).

The ball mill is a key equipment for crushing after the crushing process, and it is widely used in manufacturing industries, such as cement, silicate, new construction material, refractory material, fertilizers, ferrous ores, non-ferrous ores and ceramics. [12]

III.4.2. Sieving

The samples were sieved by a series of sieves with different mesh, see the series of sieves below:

- **80 µm,**
- **100 µm,**
- **160 µm,**
- **200 µm,**

The choice of the mass of the sample must verify several constraints such as the capacity of the sieves, sieves, etc. Indeed, it is necessary that the sample analyzed is in sufficient quantity to be measurable and not be too large, to avoid saturating or overflowing the sieves.

Particle size analysis must allow the grain to be separated from an ore and graded by diameter. The mesh diameter of the Sieves defines the size classes.

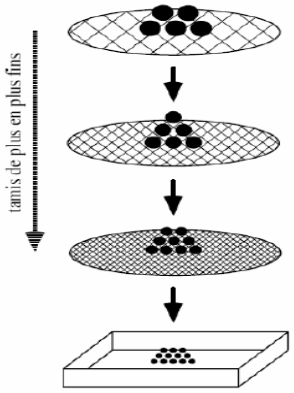

Figure .III.6: b Simplified dry sieving procedure

III.5. Shaping

a. Uniaxial pressing

It is generally accepted that the sequence of steps involved in pressing an atomized powder is the following

Stage I: Rearrangement of granules;

Stage II: Deformation or fragmentation, granules, lead to the elimination of the macroporosity between granules, which we will also refer to as intergranular porosity. The deformation of the granules, one against the other, forms flat interfaces, which can be displayed on the surfaces of the pressed samples.

Stage III: Under higher pressures, microporosity is eliminated initially present inside the granules, by rearrangement or fragmentation of the particles. This microporosity will also be called intragranular porosity. In this stage, the only rearrangement of the particles inside the granules, and possibly their rupture under very high pressure, may explain the decrease in intragranular porosity These steps are illustrated in Figures (III.7 and III.8). [13]

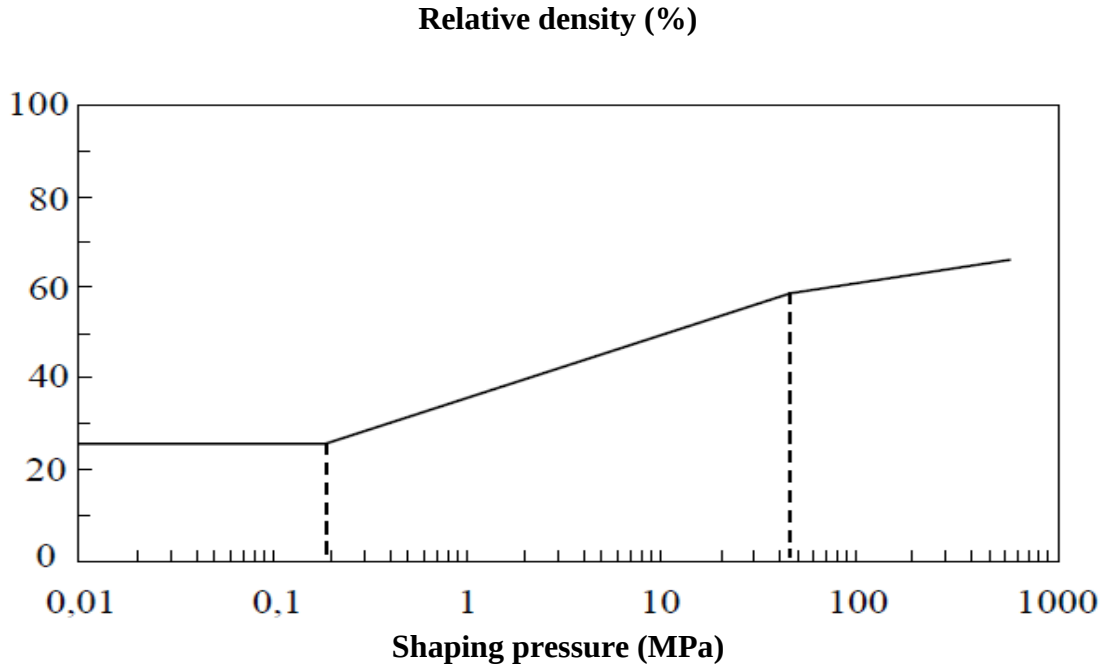

Figure. III.7: The three stages in pressing according to Reed [REE 95].

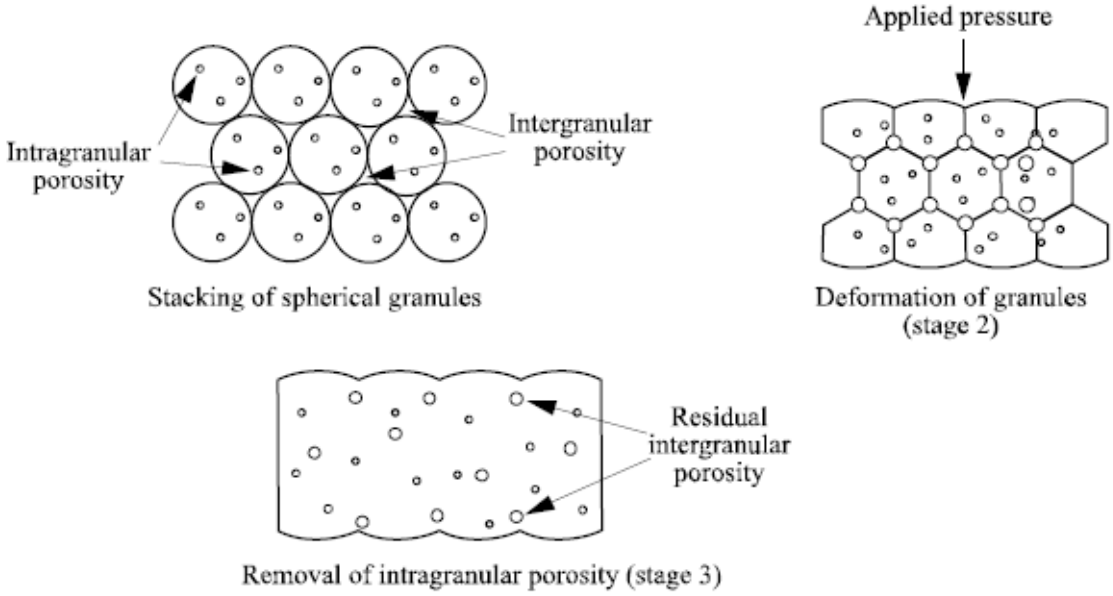

Figure .III.8: Evolution of intergranular and intragranular porosity during the pressing of a spray-dried powder.

In this experiment we carry out a series of samples of 10 g of mass and with a powder of diameters between 80 µm and 100 µm. We therefore develop disks with a diameter of 27.5 mm with different compression forces (15 KN, 25KN, 35 KN, 45 KN and 55 KN).

b. Polishing

Many studies on ceramic materials require clean and well-defined surfaces. In this case, it is essential to polish them. The polishing is done only on pellets already sintered using the Macapol P120 apparatus, the diagram of which is given in (figure II.14). The pellets are glued to à metal cylinder using adhesive tape. The metal cylinder topped with the pellets is then placed on a sample holder so that the faces of the pellets are in contact with the polishing disc. A compressor applies low pressure to the pellets to ensure good contact with the polishing disc. It rotates in the opposite direction to the rotation of the sample holder. It is regularly impregnated with lubricant to avoid excessive heating of the surface. This set ensures homogeneous and good quality polishing. [13]

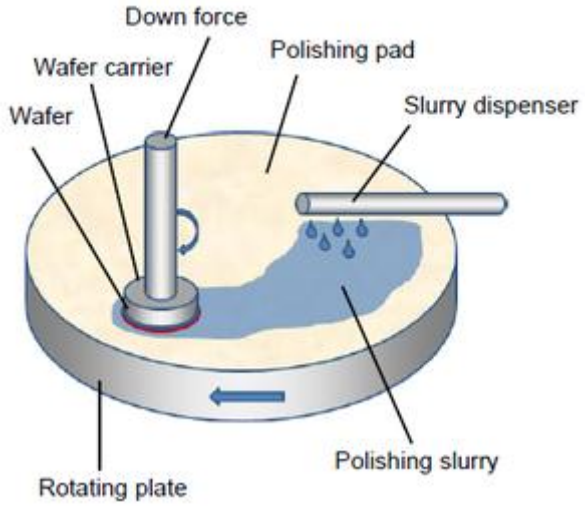

Figure.III.9: Representative diagram of the operation of the Macapol P120 polisher.

III.6. Sintering

The test pieces undergo debinding at 600 °C and sintering at maximum temperatures of 1100°C, for a maintenance of 2h in a programmable oven. When the test pieces reach the maximum cooking temperature, they are cooled in the oven.

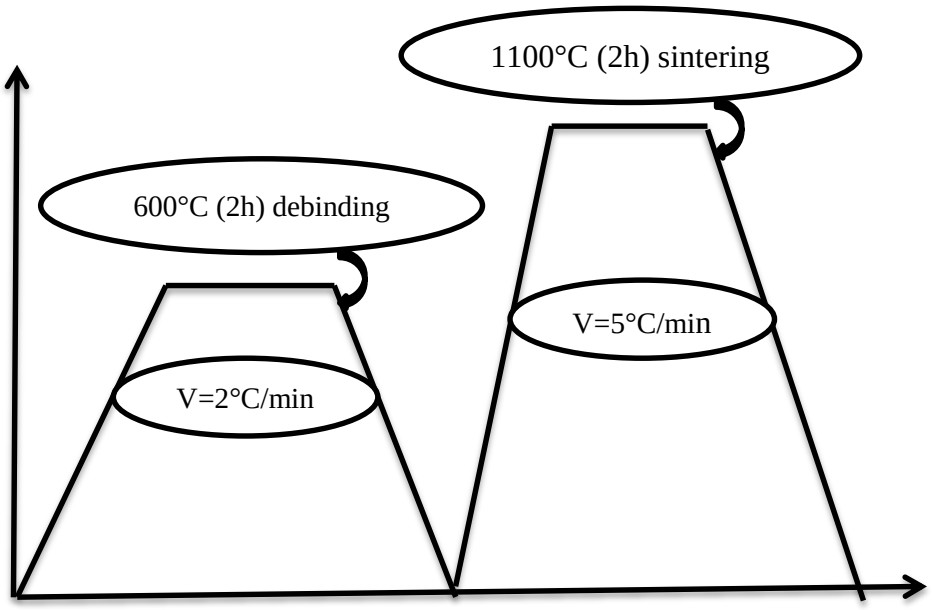

Figure.III.10: Thermal cycle of sintering of kaolin KT2.

III.7. Experimental setup

DSP techniques use simple optical assemblies as shown in figure III.11. The light emitted by a green laser diode with à wavelength of 532 nm. A 27.5 mm diameter ceramic piece mounted on a traction machine, is illuminated by the extended beam. A photographic lens (OP) makes it possible to form the image of the piece on the CCD camera (600 x 800 pixel). The CCD camera is connected to a computer with a video acquisition card for recording images that are scanned on 8 bits. After the acquisition of the different images corresponding to the two deformation states, the displacement is calculated by an algorithm developed with Matlab. Measurements are made by analysing the displacements of this speckle figure. Generally, this analysis is done from two images of the speckle. We take the first while the system is in its initial state. This image is the reference image. Then, the object is subjected to a deformation, which causes the speckle grains to shift in the image plane. A succession of images is then recorded which can be compared to the reference. The samples were mechanically characterised by the Brazilian tensile test.

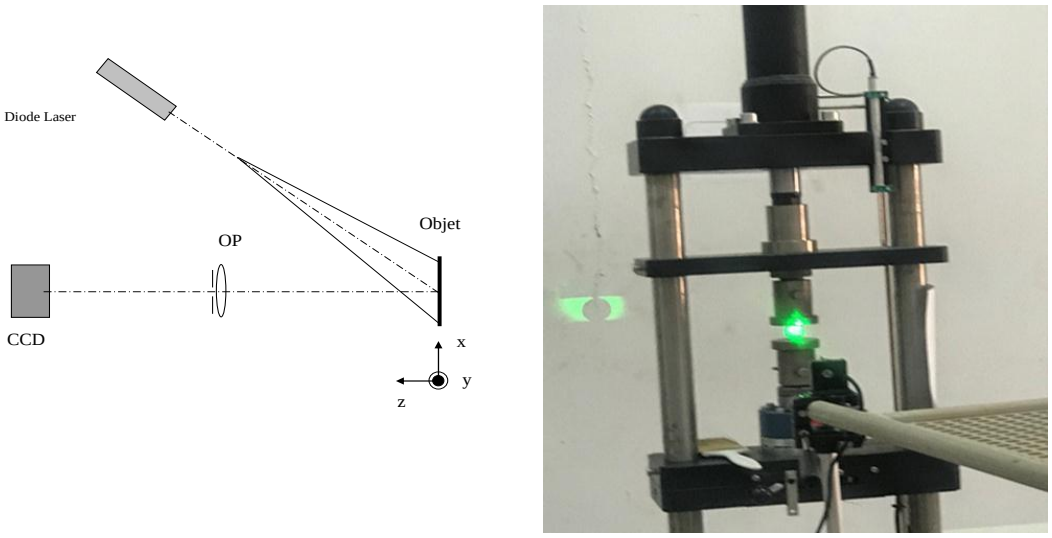

FigureIII.11: Experimental setup.

III.8.Experimental results

III.8.1. Representation of speckle figures and corresponding deformation fields

Below are speckle figures obtained during the compression tests on an elaborated sample with a powder of diameters between 80 µm and 100 µm (80 µm ϕ 100 µm) under a pressure 55 KN.

The figures are for example for different deformation states up to the break, as well as the deformation fields between a reference speckle figure and the other deformation states computed by a speckle correlation algorithm. (Figure.III.18) and (Figure.III.19)

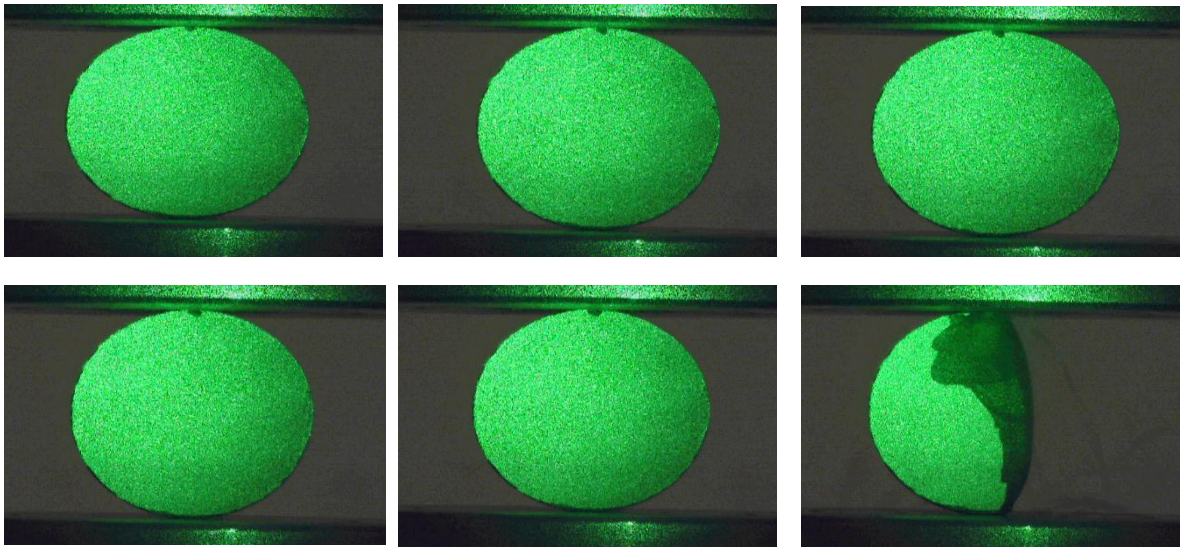

Figure.III.12:Speckle figures for different deformation states.

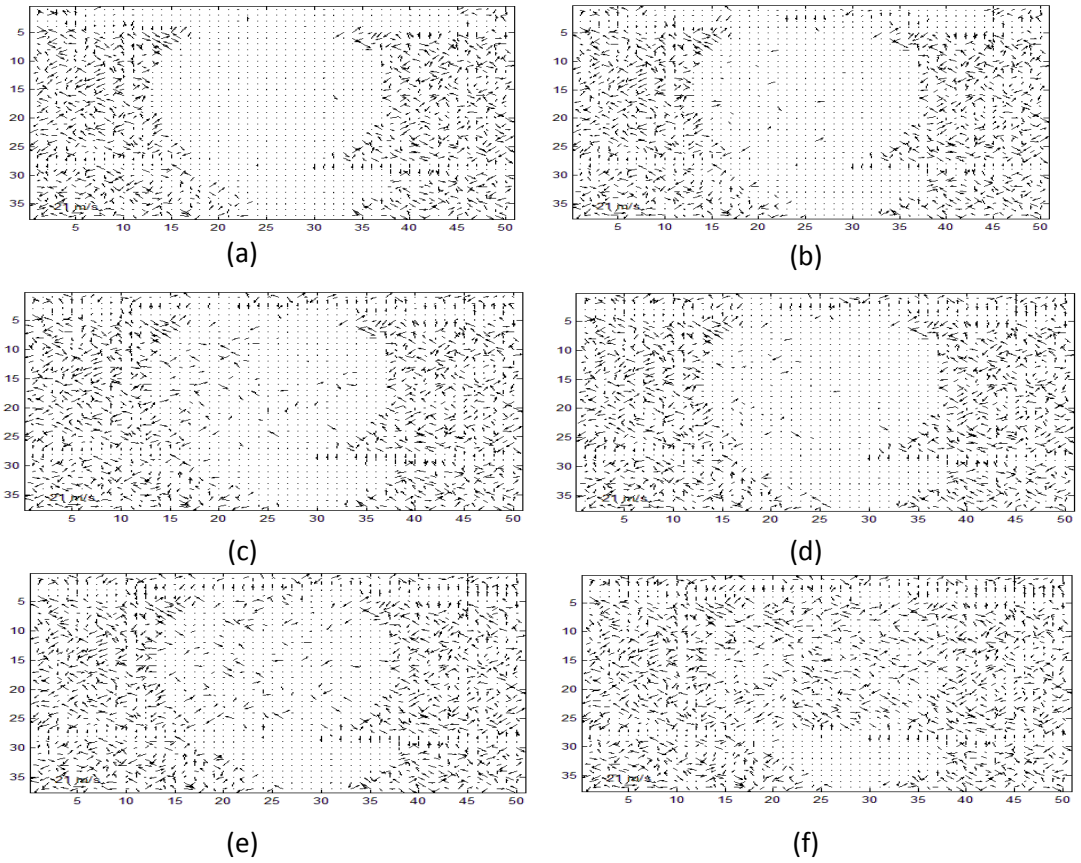

Figure.III.13: Deformation fields resulting from compression of the sample in figure III.11

III.8.2.Deformation fields of the first sample

The first sample is made from a powder with diameters between 80 µm and 100 µm (80 µm ϕ 100 µm) under a pressure of the order of 15 KN.

The deformation fields obtained during the compression test are presented below:

:

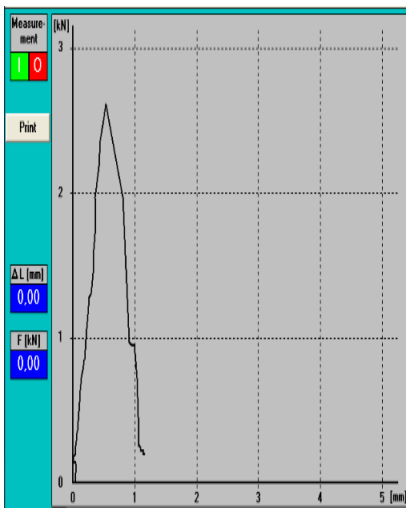

L (mm)	0.0452	F (kN)	0.24
0	0.0448	0	0.26
0.02	0.0542	0	0.29
0.0398	0.0638	0.01	0.31
0.0392	0.063	0.04	0.35
0.0386	0.0824	0.07	0.38
0.048	0.0814	0.1	0.43
0.0476	0.0902	0.12	0.49
0.0372	0.1088	0.14	0.56
-0.003	0.1172	0.15	0.64
0.0066	0.1354	0.17	0.73
0.0062	0.1544	0.19	0.78
0.0262	0.173	0.19	0.85
0.0458	0.193	0.21	0.85

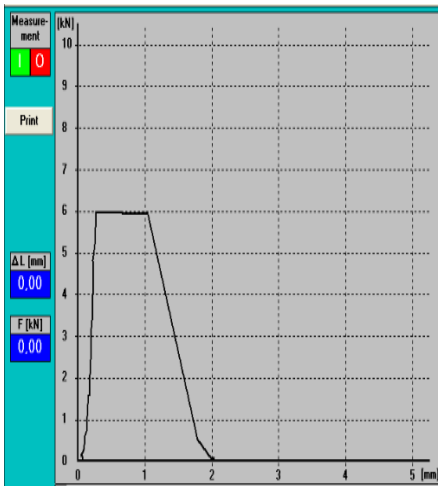

L (mm)	0.0848	F (kN)	0.26
0	0.0842	0	0.29
0.02	0.0936	0	0.32
0.05	0.0932	0	0.34
0.0694	0.0924	0.03	0.38
0.0788	0.1012	0.06	0.44
0.0784	0.1098	0.08	0.51
0.0778	0.1078	0.11	0.61
0.0674	0.1258	0.13	0.71
0.047	0.1334	0.15	0.83
0.0468	0.1304	0.16	0.98
0.0662	0.1468	0.19	1.16
0.0658	0.1428	0.21	1.36
0.0756	0.1584	0.22	1.58

F (kN)	0.21	0.85	σ (N/mm^2)	0.88	3.56
0	0.24	0.85	0	1	3.56
0	0.26	1.06	0	1.09	4.44
0.01	0.29	1.16	0.41	1.21	4.86
0.04	0.31	1.28	0.16	1.3	5.37
0.07	0.35	1.31	0.29	1.46	5.49
0.1	0.38	1.45	0.41	1.59	6.08
0.12	0.43	1.61	0.5	1.8	6.75
0.14	0.49	1.77	0.58	2.05	7.42
0.15	0.56	1.97	0.62	2.34	8.26
0.17	0.64	2.18	0.71	2.68	9.14
0.19	0.73	2.36	0.79	3.06	9.9
0.19	0.78	2.61	0.79	3.27	10.95

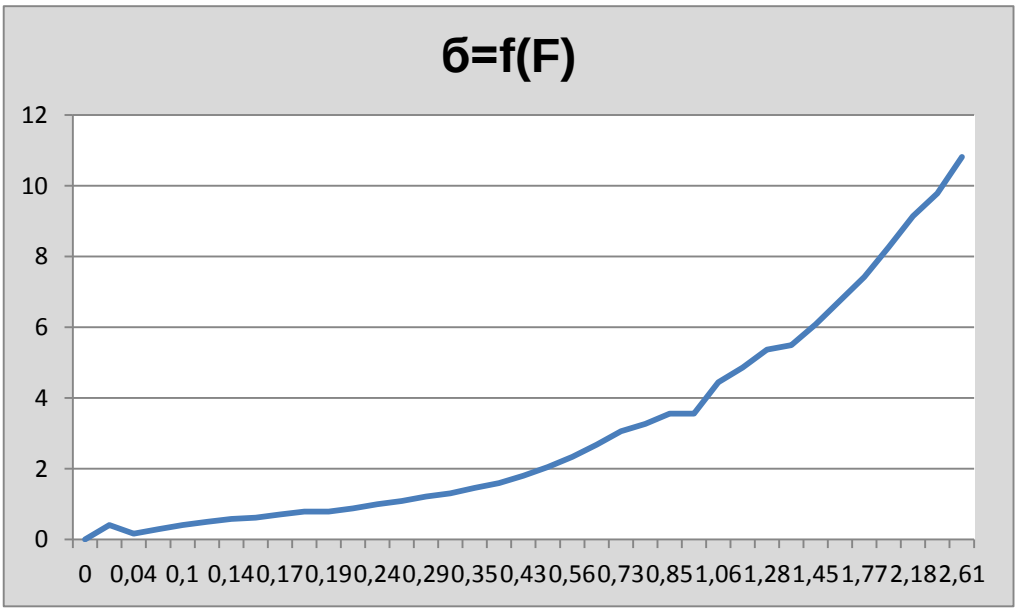

Qualitative analysis

Through the curves obtained through the pressure experiment performed on samples of the same pressure force, we observed a difference in results, due to errors during the experiment and the presence of vacuum on the surface of the sample causing collapse.

We note that the breaking stressбmax = 10.81 N/mm2, which is the highest point the sample has reached in the resistance before the fracture, and we extracted it from the next relationship:

$$б = \frac{F}{\pi Rh}$$

R=(27.5/2)=13.75mm. h=5.65mm.
F: Represents pressure force (N).
R: Represents sample radius (mm).
H: Represents the thickness of the sample (mm).

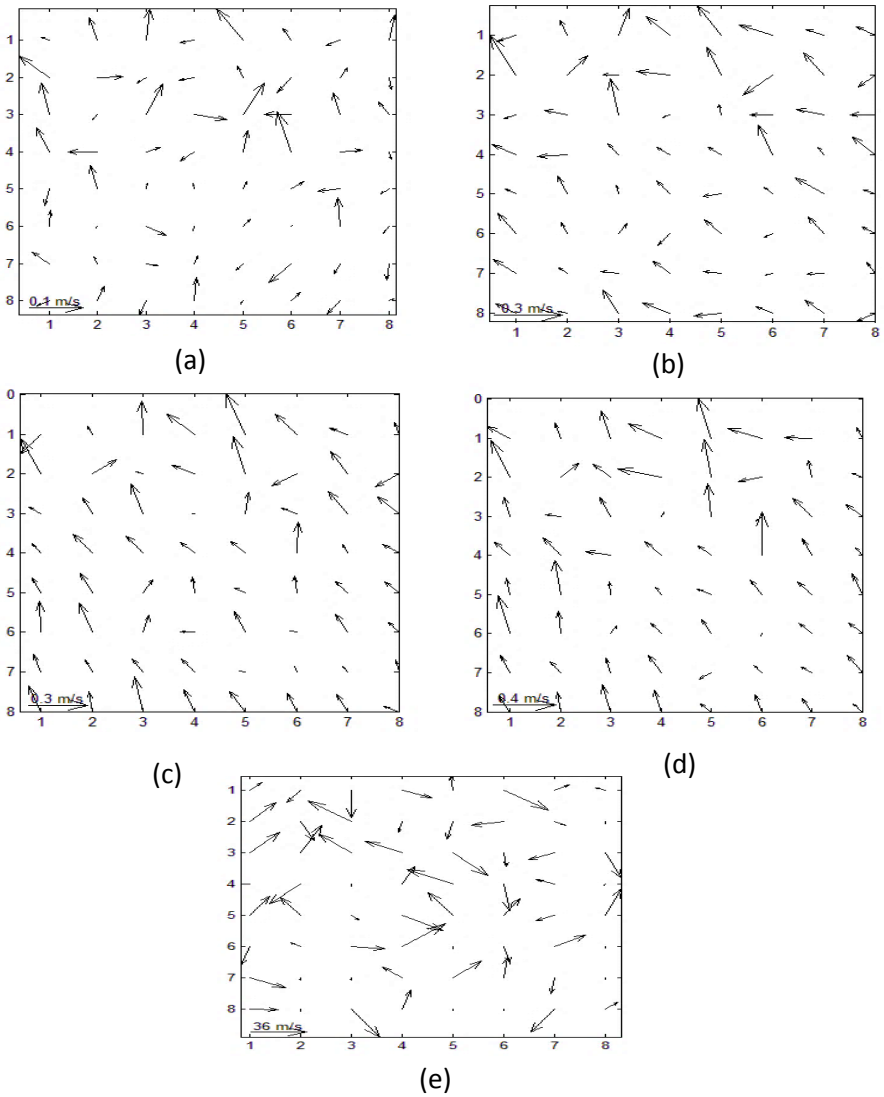

Figure.III.14:Deformation fields of the first sample.

Notice2 : We notice in the deformation fields of the first sample from (a to e) that the traction and the pressure apper togther and then the pressure dominates, and in the last picture (e) there is chaos because the piece has reached the breaking point.

III.8.3.Second sample deformation fields

The second sample is made from a powder with diameters between 80 µm and 100 µm (80 µm ϕ 100 µm) under a pressure of the order of 25 KN.

The deformation fields obtained at the beginning of the compression test

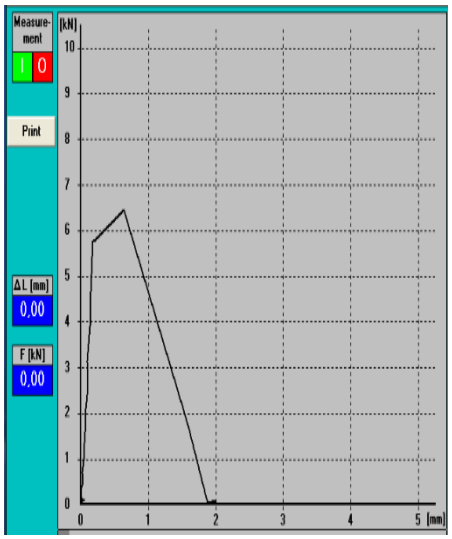

L (mm)	0.0502	F (kN)	0.26
0	0.053	0	0.29
-0.001	0.0584	0.05	0.33
0	0.0734	0	0.38
0.0096	0.078	0.02	0.43
0.0092	0.092	0.04	0.51
0.0086	0.1048	0.07	0.61
0.0182	0.0974	0.09	0.71
0.048	0.1198	0.1	0.84
0.0278	0.1322	0.11	0.99
0.0074	0.1446	0.13	0.99
-0.0034	0.147	0.17	1.35
0.006	0.1592	0.2	1.58
0.0154	0.0502	0.23	1.83

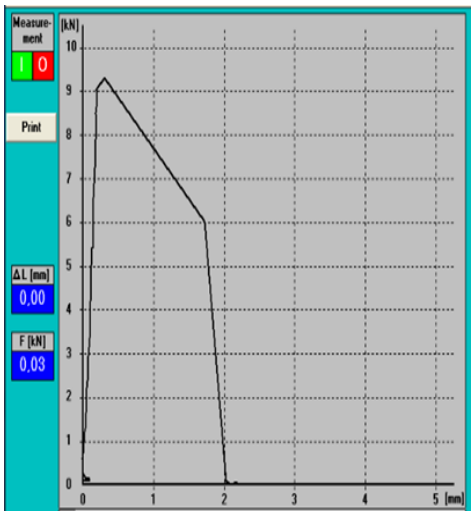

L (mm)	0.0042	F (kN)	0.29
0	0.0036	0	0.32
-0.0004	0.003	0.02	0.35
0	0.0022	0	0.39
-0.0008	0.0012	0.04	0.44
-0.0014	-4.00000000000001E-04	0.07	0.52
-0.002	-0.0124	0.1	0.62
0.058	-0.0046	0.1	0.73
0.0974	0.01	0.13	1
0.0868	0.026	0.16	1.2
0.0366	0.0418	0.17	1.41
0.026	0.0372	0.2	1.64
0.0154	0.0518	0.23	1.91
0.0046	0.0558	0.27	2.21

F (kN)	0.27	1.91	Σ	1.12	7.91
0	0.29	2.21	0	1.2	9.16
0.02	0.32	2.56	0.082	1.33	10.66
0	0.35	2.95	0	1.45	12.28
0.04	0.39	3.36	0.16	1.62	13.99
0.07	0.44	3.77	0.29	1.83	15.62
0.1	0.52	4.19	0.41	2.16	17.36
0.1	0.62	4.6	0.41	2.58	19.06
0.13	0.73	5.01	0.54	3.04	20.76
0.16	1	5.41	0.66	4.14	22.42
0.17	1.2	5.41	0.7	4.97	22.42
0.2	1.41	6.14	0.83	5.84	25.44
0.23	1.64	6.55	0.95	6.79	27.28

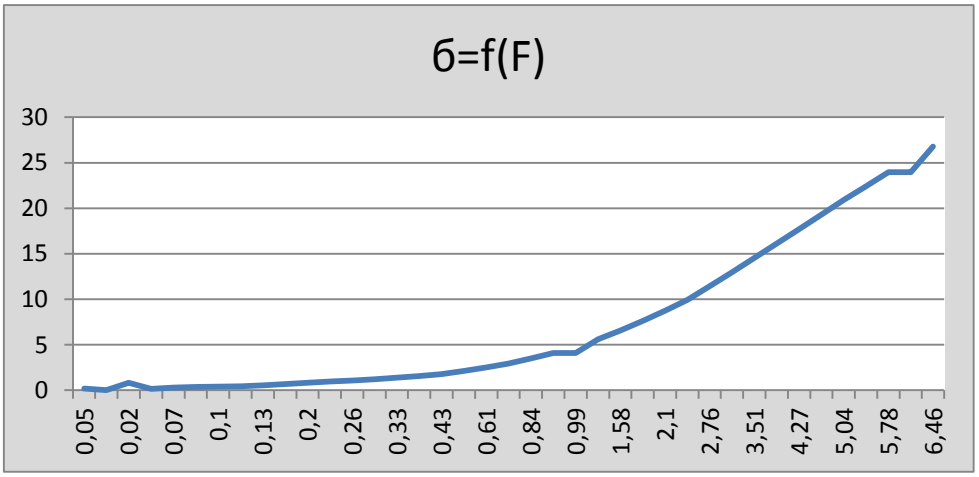

Qualitative analysis

Through the curves obtained through the pressure experiment of samples of the same pressure force, we noticed a difference in results, which is due to errors during the experiment and the presence of a vacuum on the surface of the sample causing a breakdown.

We note that the breaking stress $б_{max}$ =26.77 N/mm^2 which is the highest point the sample has reached in the resistance before the fracture, and we extracted it from the next relationship:

$$б = \frac{F}{\pi \mathrm{Rh}}$$

R=(27.5/2)=13.75mm. h=5.65mm.

F: Represents pressure force (N).

R: Represents sample radius (mm).

H: Represents the thickness of the sample (mm).

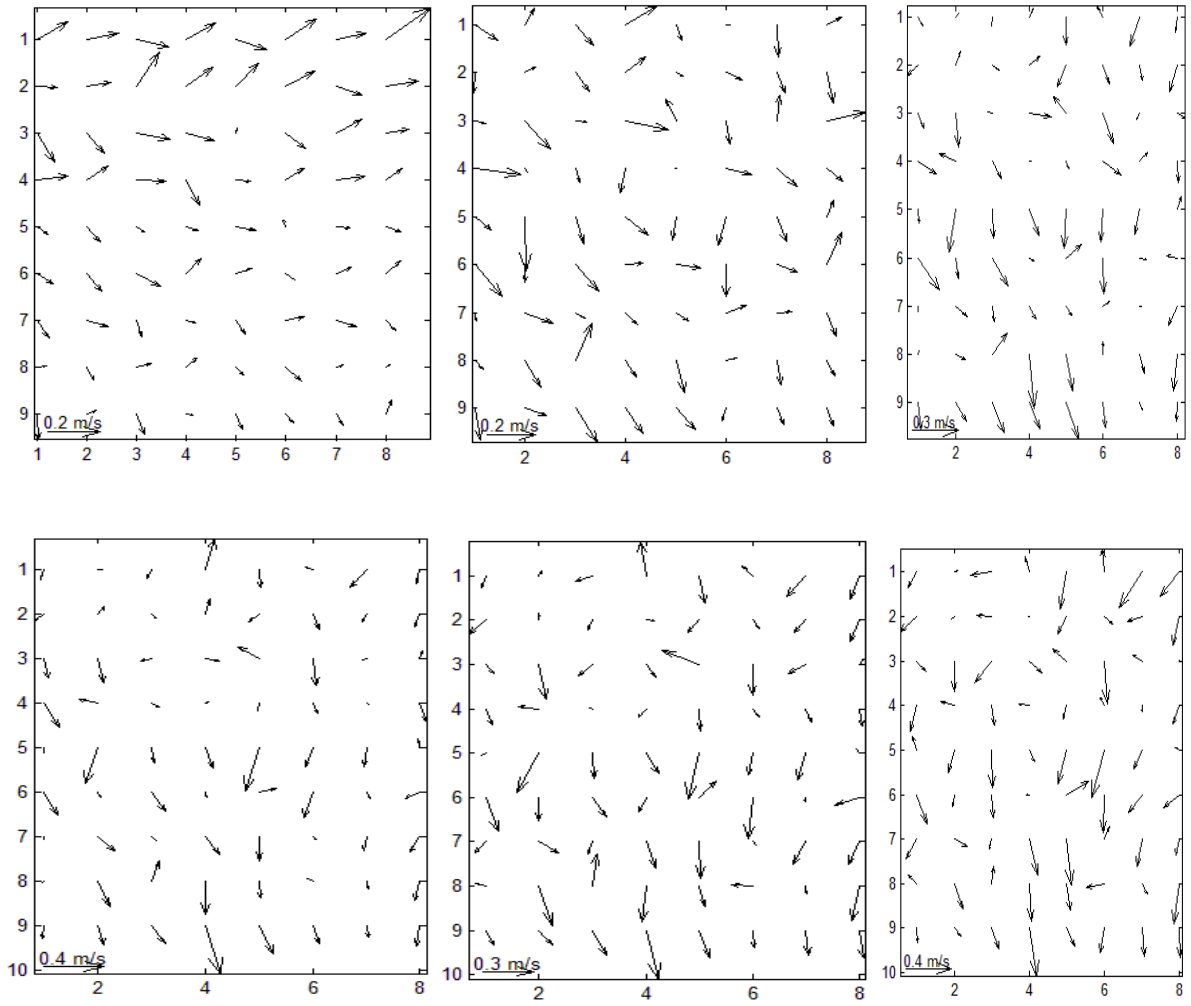

Figure.III.15:The deformation fields obtained at the end of the compression test.

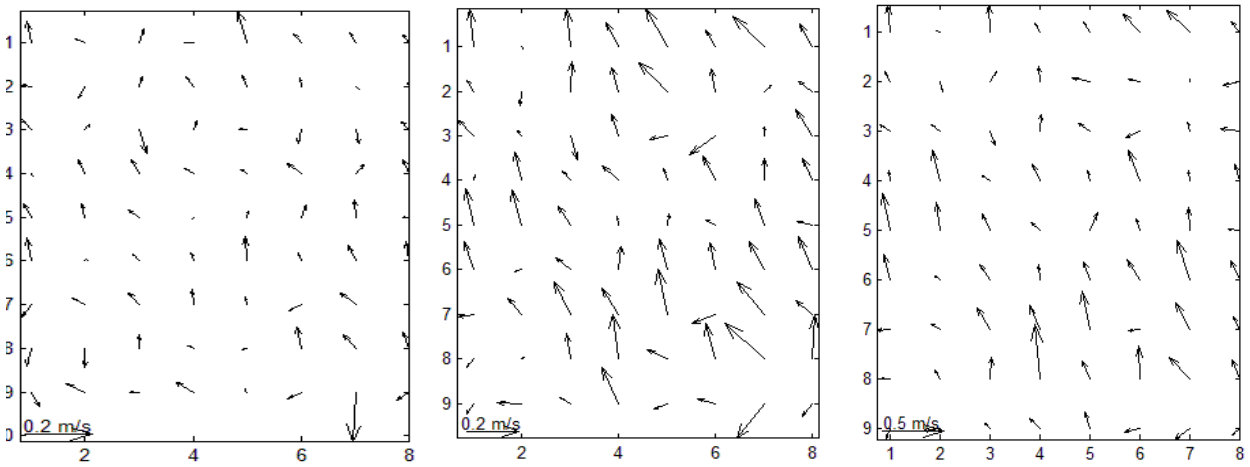

Figure.III.16: The deformation fields obtained at the end of the compression test.

Notice 3 : In the field of deformation we notice that the forces of pressure and attraction appear at the beginning, then the pressure dominates, as the movement of the arrows becomes parallel to the direction of the applied force**.**

III.8.4.Third Sample Deformation Fields

The third sample is made from a powder with diameters between 80 µm and 100 µm (80 µm ϕ 100 µm) under a pressure of the order of 35 KN.

The deformation fields obtained at the beginning of the compression test

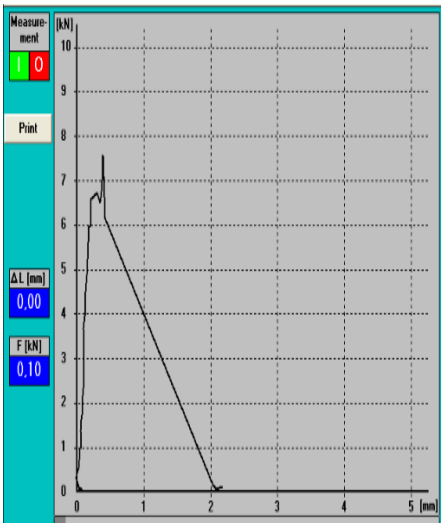

L (mm)	0.0016	F (kN)	0.42
0	0.0196	0	0.52
-0.0004	0.0278	0.02	0.61
0.0192	0.0358	0.04	0.71
0.0788	0.0434	0.06	0.83
0.0588	0.0404	0.06	0.98
0.0282	0.0604	0.09	0.98
0.0174	0.0528	0.13	1.36
0.0168	0.0678	0.16	1.61
0.0062	0.0826	0.19	1.87
0.0056	0.0866	0.22	2.17
0.0048	0.0998	0.26	2.51
-0.006	0.1022	0.3	2.89
-0.007	0.0016	0.35	3.29

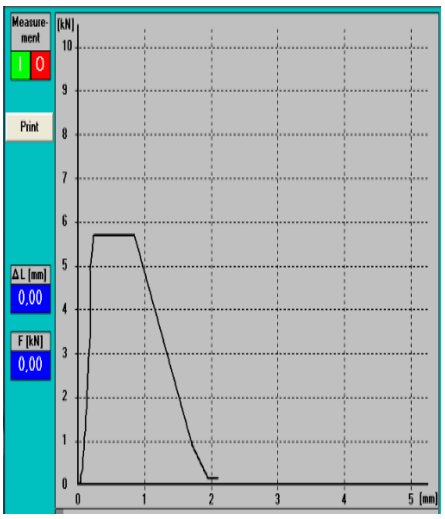

L (mm)	0.0772	F (kN)	0.64
0	0.0846	0	0.77
-0.0004	0.098	0.02	1.1
0.0192	0.1132	0.04	1.34
0.0288	0.1184	0.06	1.58
0.038	0.133	0.1	1.85
0.0372	0.1368	0.14	2.16
0.0366	0.1494	0.17	2.53
0.046	0.1616	0.2	2.92
0.0454	0.1736	0.23	3.32
0.0546	0.1854	0.27	3.73
0.0634	0.1872	0.33	4.14
0.0714	0.1892	0.43	4.54
0.0694	0.1812	0.53	4.94

F (kN)	**0.53**	**4.54**	б (N/mm^2)	**2.2**	**22.96**
0	0.64	4.94	0	2.66	20.47
0.02	0.77	5.32	0.082	3.2	22.05
0.04	1.1	5.69	0.16	4.55	23.58
0.06	1.34	5.69	0.24	5.55	23.58
0.1	1.58	-	0.41	6.54	22.96
0.14	1.85	-	0.58	7.66	20.47
0.17	2.16	-	0.7	8.99	22.05
0.2	2.53	-	0.88	10.53	-
0.23	2.92	-	0.95	12.16	-
0.27	3.32	-	1.12	13.83	-
0.33	3.73	-	1.37	15.46	-
0.43	4.14	-	1.79	17.15	-

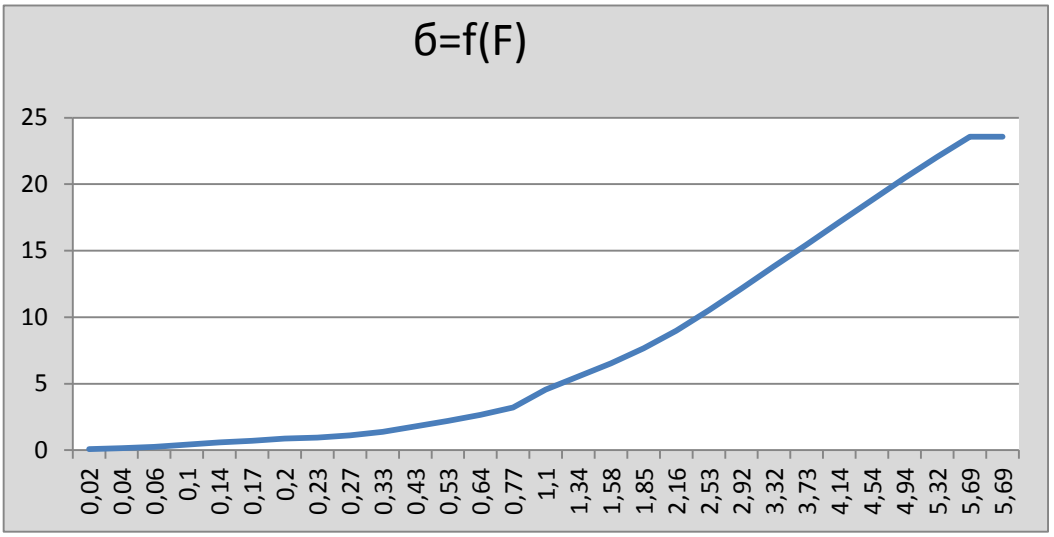

Qualitative analysis

Through the curves obtained through the pressure experiment of samples of the same pressure force, we noticed a difference in results, which is due to errors during the experiment and the presence of a vacuum on the surface of the sample causing a breakdown.

We note that the breaking stress $б_{max}$ =22.05 N/mm^2 which is the highest point the sample has reached in the resistance before the fracture, and we extracted it from the next relationship:

$$б = \frac{F}{\pi Rh}$$

R=(27.5/2)=13.75mm. h=5.65mm.

F: Represents pressure force (N).

R: Represents sample radius (mm).

H: Represents the thickness of the sample (mm).

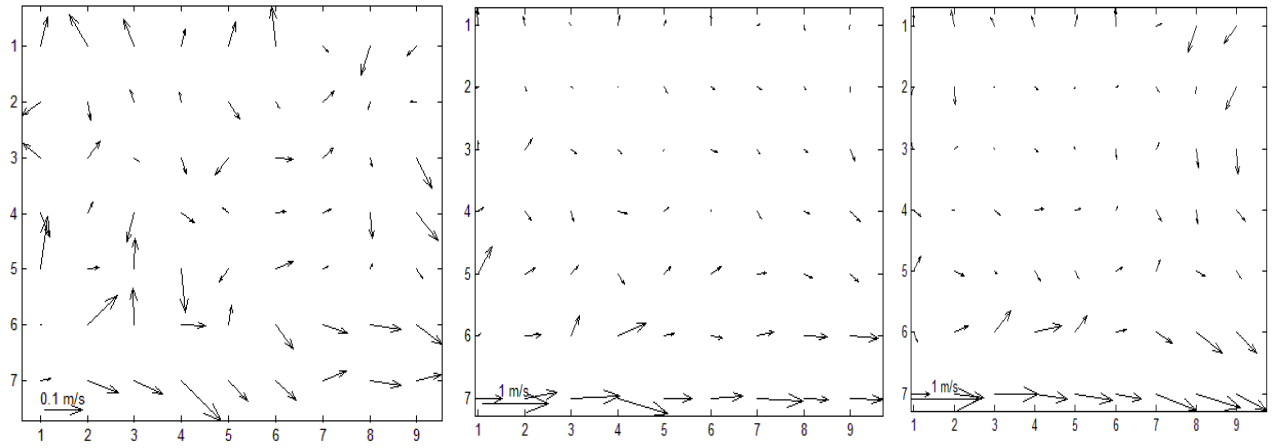

Figure.III.17:The deformation fields obtained in the middle of the compression test.

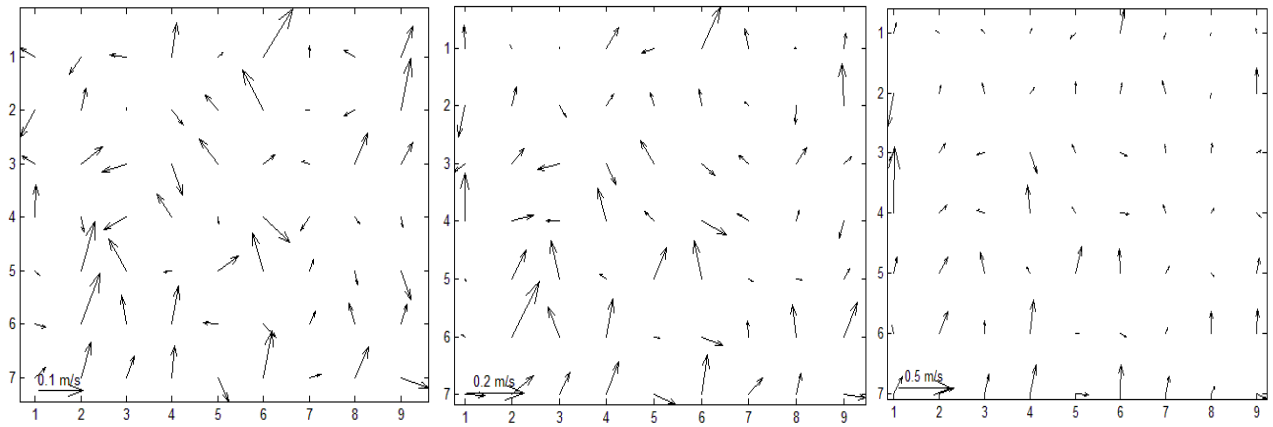

Figure.III.18: The deformation fields obtained in the middle of the compression test.

The deformation fields obtained at the end of the compression test

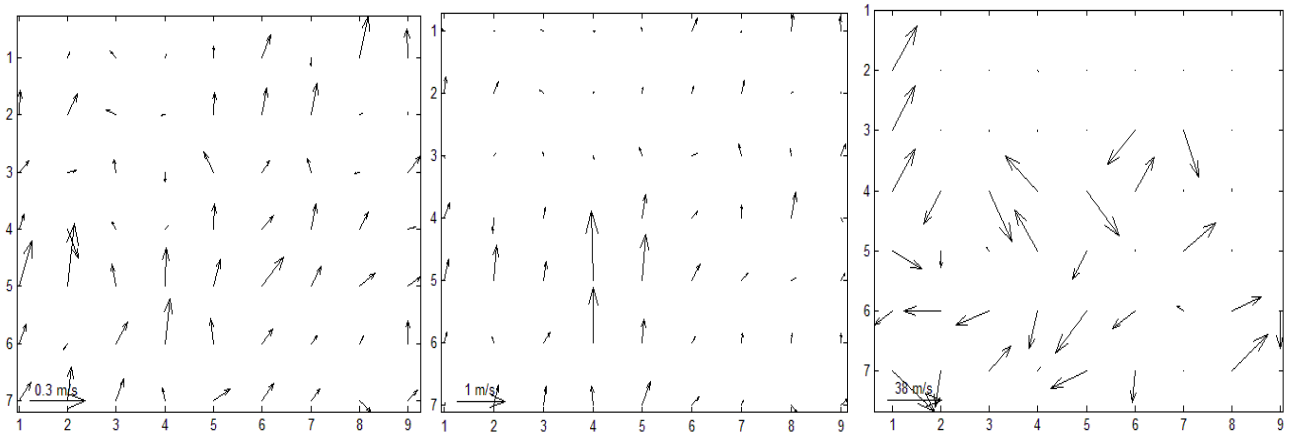

Figure.III.19: The deformation fields obtained at the end of the compression test.

Notice 4 : We notice from the (figuresIII.17 and III.18) in the deformation fields obtained at the beginning and middle of the pressure and attraction appear after that the compressive force dominates completely after observing the direction of change of the arows from the horizontal direction to their parallel to the direction of the vertically applied pressure forces.

At the end of the pressure test (Figure.III.19) the direction of the arrows is reversed explaining that the piece started in resist the pressure forces applied to it, and in the last picture wich represents a states of chaos at the moment of breaking and is impossible to read from it

III.8.5. Deformation fields of the fourth sample

The fourth sample is made from a powder with diameters between 80 µm and 100 µm (80 µm ϕ 100 µm) under a pressure of the order of 45 KN.

The deformation fields obtained at the beginning of the compression test

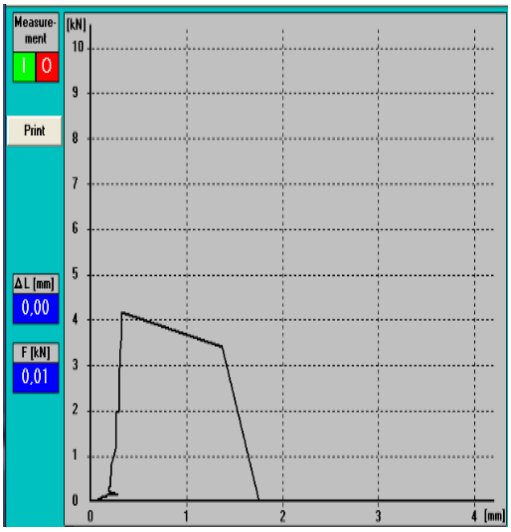

L (mm)	0.1946	F (kN)	0.27
0	0.1936	0	0.32
0.02	0.2128	0	0.36
0.0498	0.2116	0.01	0.42
0.0792	0.2102	0.04	0.49
0.0986	0.2088	0.07	0.56
0.118	0.2168	0.1	0.66
0.1674	0.2154	0.13	0.73
0.167	0.2134	0.15	0.83
0.287	0.2314	0.15	0.93
0.2566	0.2486	0.17	1.07
0.2164	0.2648	0.18	1.26
0.2058	0.2708	0.21	1.46
0.1952	0.2662	0.24	1.69

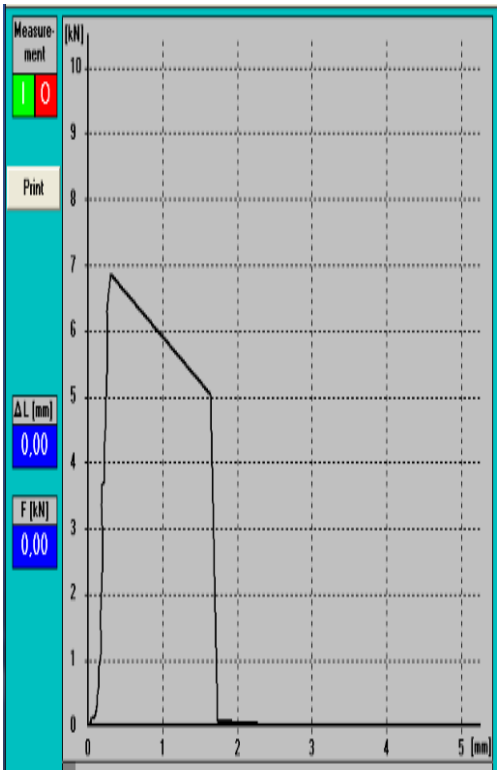

L (mm)	0.1218	F (kN)	0.41
0	0.1304	0	0.48
-0.0004	0.1466	0.02	0.67
0.019	0.1444	0.05	0.78
0.0382	0.1518	0.09	0.91
0.0376	0.1684	0.12	1.08
0.0574	0.1744	0.13	1.28
0.0868	0.1702	0.16	1.49
0.106	0.1652	0.2	1.74
0.1054	0.1798	0.23	2.01
0.1148	0.1838	0.26	2.31
0.1142	0.1966	0.29	2.67
0.1136	0.1888	0.32	3.06
0.123	0.1882	0.35	3.09

F (kN)	0.35	3.06	б (N/mm^2)	1.45	12.68
0	0.41	3.09	0	1.7	12.8
0.02	0.48	3.36	0.083	1.98	13.92
0.05	0.67	3.68	0. 2	2.77	15.25
0.09	0.78	3.68	0.37	3.23	15.25
0.12	0.91	4.31	0.49	3.77	17.86
0.13	1.08	4.68	0.54	4.47	19.39
0.16	1.28	5	0.66	5.33	20.72
0.2	1.49	3.06	0.83	6.17	-
0.23	1.74	3.09	0.95	7.21	-
0.26	2.01	3.36	1.08	8.33	-
0.29	2.31	3.68	1.2	9.57	-
0.32	2.67	3.68	1.33	11.06	-

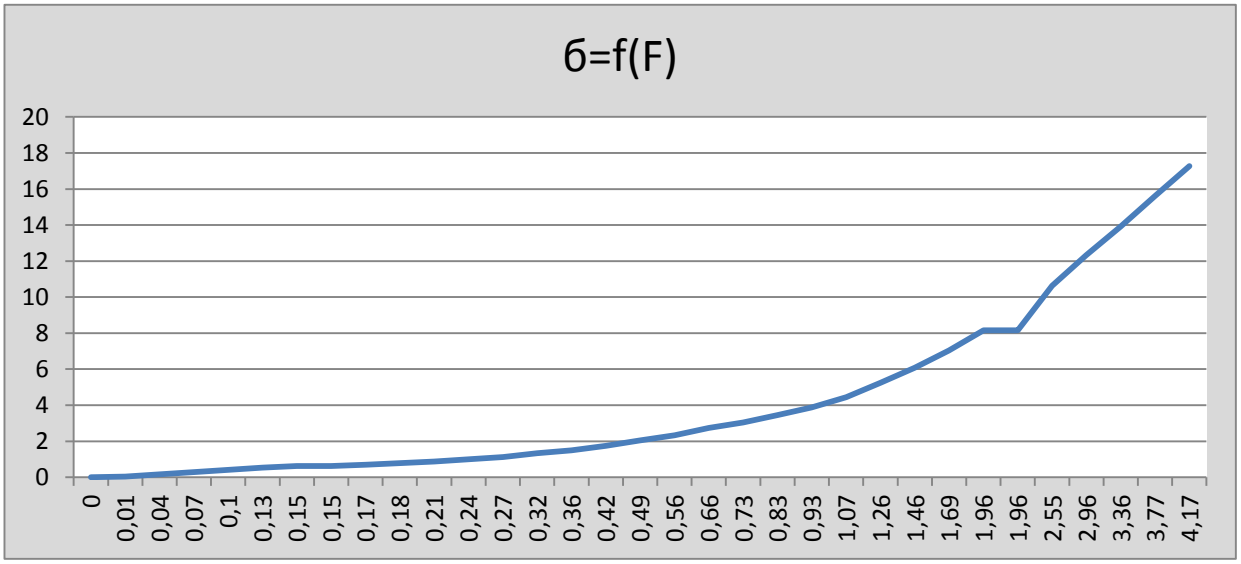

Qualitative analysis

Through the curves obtained through the pressure experiment of samples of the same pressure force, we noticed a difference in results, which is due to errors during the experiment and the presence of a vacuum on the surface of the sample causing a breakdown.

We note that the breaking stress $б_{max}$ =17.28 N/mm^2 .which is the highest point the sample has reached in the resistance before the fracture, and we extracted it from the next relationship:

$$б = \frac{F}{\pi Rh}$$

R=(27.5/2)=13.75mm. h=5.65mm.

F: Represents pressure force (N).

R: Represents sample radius (mm).

H: Represents the thickness of the sample (mm).

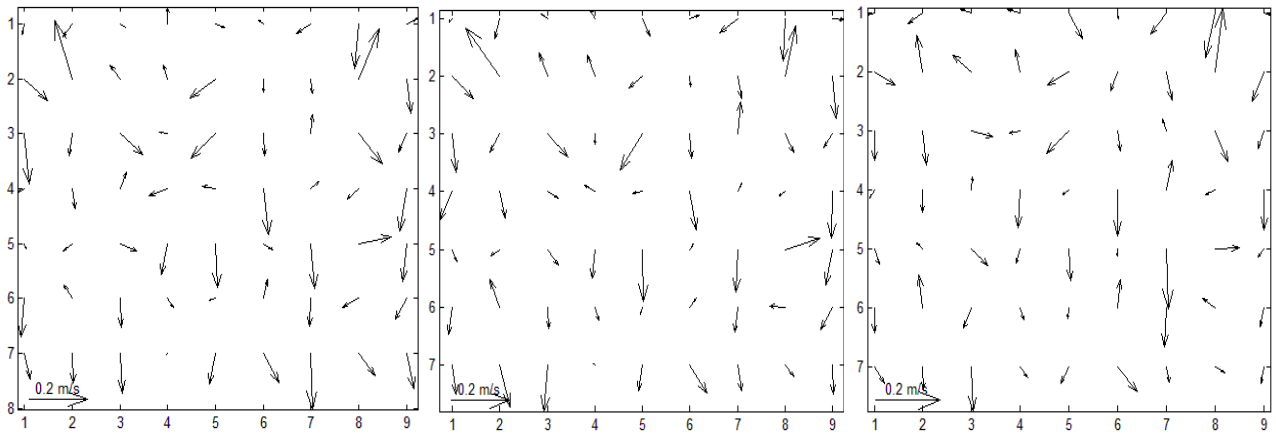

Figure.III.20: The deformation fields obtained at the beginning of the compression test

The deformation fields obtained in the middle of the compression test

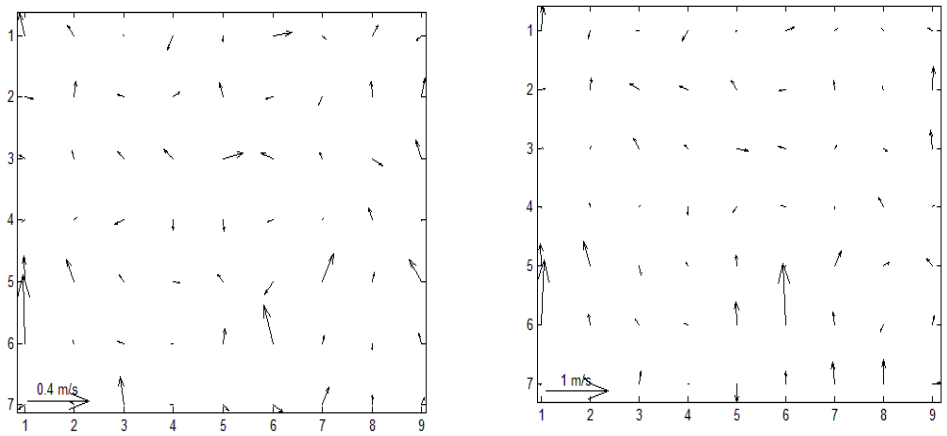

Figure.III.21: The deformation fields obtained at the beginning of the compression test
The deformation fields obtained at the end of the compression test

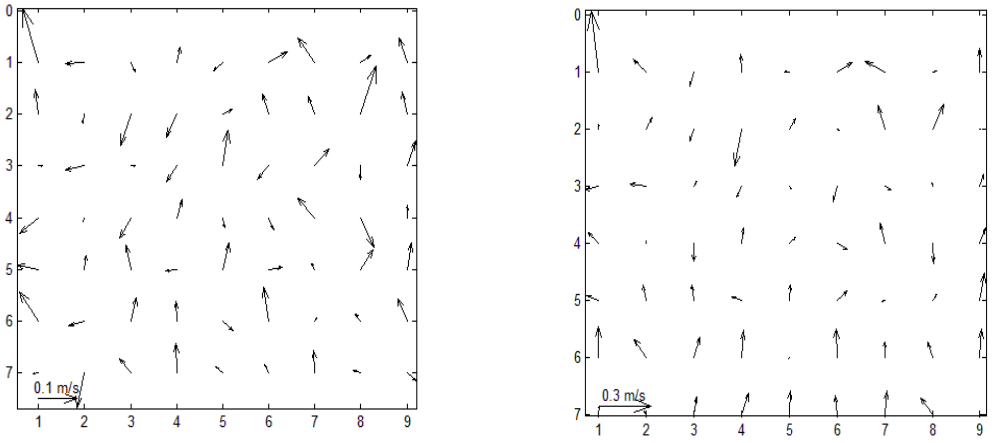

Figure.III.22: The deformation fields obtained at the end of the compression test

Notce5 :in the fields of deformation that were obtained at the beginning and end of test depending on the arrows in the pictures and from the direction of their Movement we noticed the appearance of the forces of attraction and pressure at the beginning befor the predominance of the pressure force completely which led to the beginning of the resistance of the piece wich was manifested in the reflection of the movement of the arows before it fell into state of chaos as a result of a moment sample fracture

III.8.6.Deformation fields of the fifth sample

The fifth sample is made from a powder with diameters between 80 µm and 100 µm (80 µm ϕ 100 µm) under a pressure of the order of 55 KN.

The deformation fields obtained at the beginning of the compression test

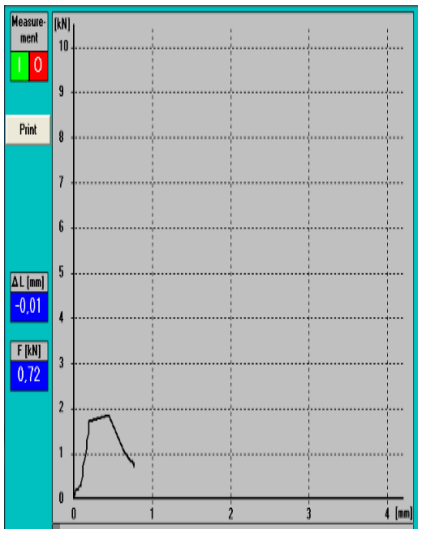

L (mm)	-	F (kN)	-
0	,0646	0	,27
,0894	,0842	,03	,29
0	,0938	0	,31
,0092	,0934	,04	,33
,0088	,0926	,06	,37
-,0014	,1104	,07	,48
-,0018	,1188	,09	,56
,0174	,1172	,13	,64
,0168	,1152	,16	,74
,0262	,1328	,19	,86
,0258	,15	,21	1
,0552	,167	,24	1,15
0	,0646	0	,27

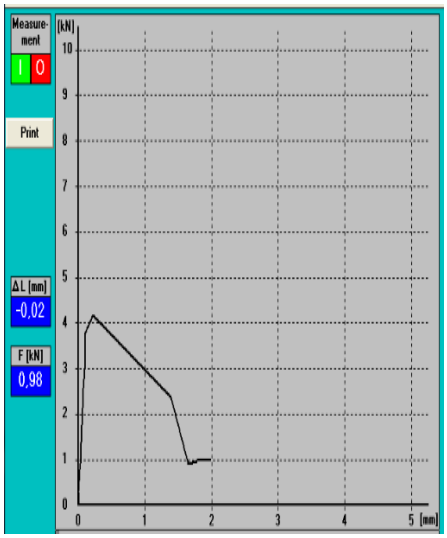

L (mm)	-	F (kN)	-
0	1,3922	0	2,39
,008	1,6516	,1	,92
,004	1,7706	,3	,97
,0096	1,7704	,52	,98
,0244	1,9304	,78	,98
,0388	1,9604	1,06	,98
,0424	1,9704	1,38	,98
,0676	1,9804	2,12	,98
,0788	1,3922	2,56	2,39
,0906	1,6516	2,97	,92
,1024	1,7706	3,38	,97
,1044	1,7704	3,78	,98
,2164	1,9304	4,18	,98

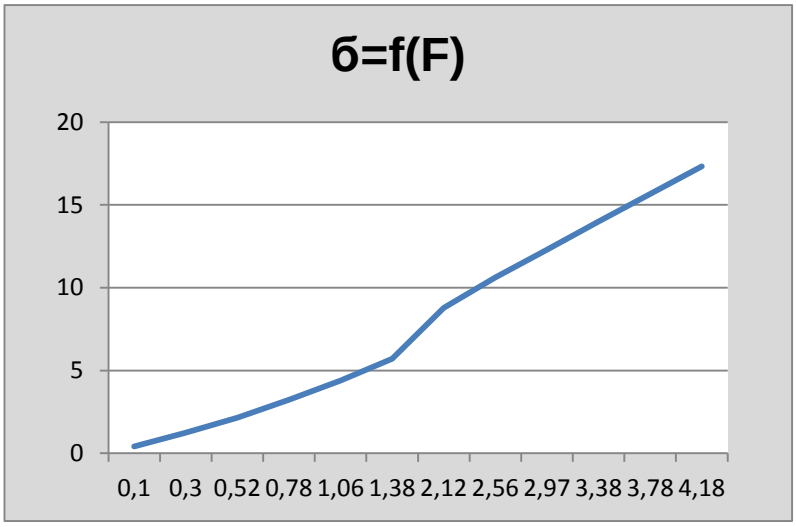

F (kN)	б (N/mm^2)
0	0
0.1	0.41
0.3	1.24
0.52	2.15
0.78	3.23
1.06	4.39
1.38	5.71
2.12	8.78
2.56	10.61
2.97	12.31
3.38	14
3.78	15.66

Qualitative analysis

Through the curves obtained through the pressure experiment of samples of the same pressure force, we noticed a difference in results, which is due to errors during the experiment and the presence of a vacuum on the surface of the sample causing a breakdown.

We note that the breaking stress $б_{max}$ =15.65N/mm^2. Which is the highest point the sample has reached in the resistance before the ne fracture, and we extracted it from the next relationship:

$$б = \frac{F}{\pi Rh}$$

R=(27.5/2)=13.75mm. h=5.65mm.

F: Represents pressure force (N).

R: Represents sample radius (mm).

H: Represents the thickness of the sample (mm).

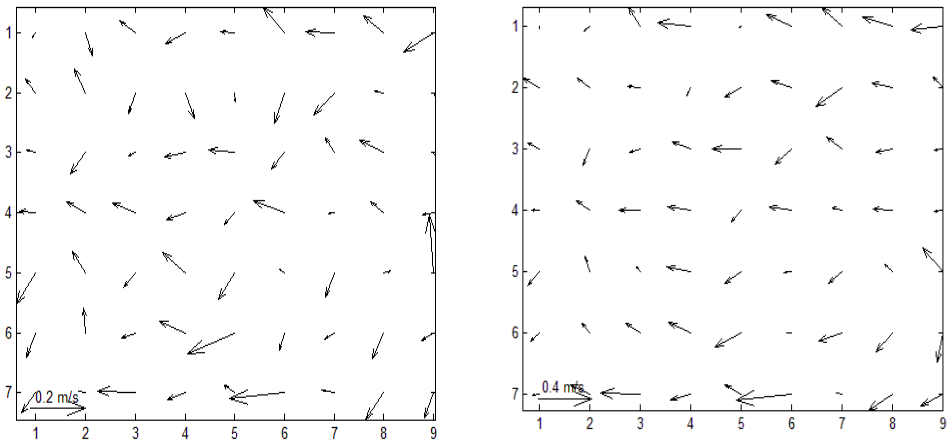

Figure.III.23: The deformation fields obtained at the beginning of the compression test

The deformation fields obtained in the middle of the compression test

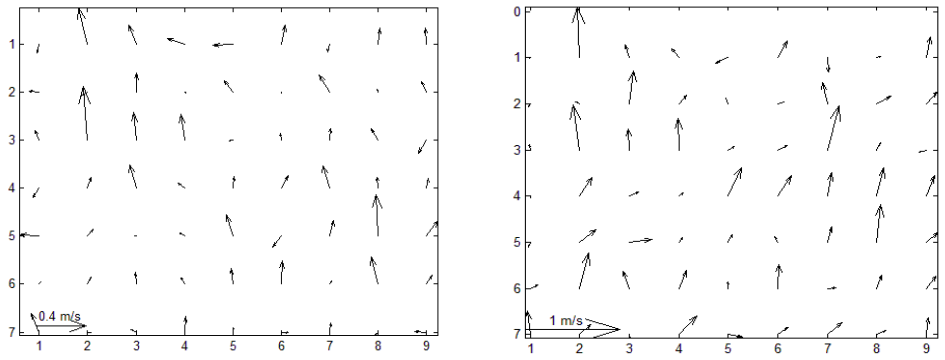

Figure.III.24: The deformation fields obtained in the middle of the compression test

The deformation fields obtained at the end of the compression test

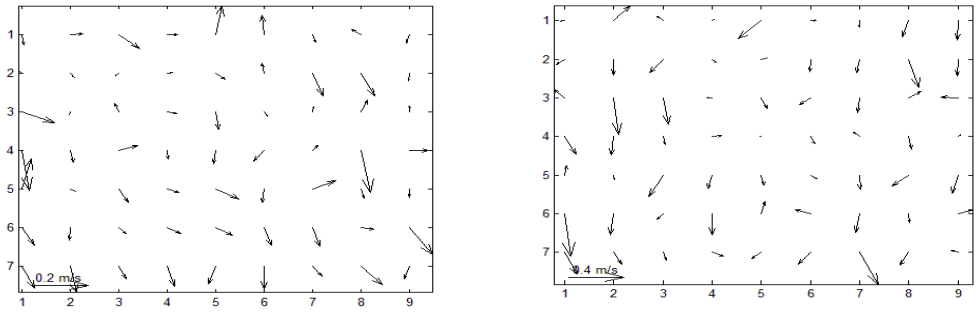

Figure.III.23: The deformation fields obtained at the end of the compression test.

Notce6 : Like all previous observations, we first notice the appearance of traction and pressure forces, after which the compressive force completely prevails in (Figures III.29, III.28) and then the resistance of the sample appears before it breaks in(FigureIII.30)

GENERALE CONCLUSION

Conclusion :

The most important results that we get from this study are the preparation of kaolin samples, which were made by grinding these samples and cutting them under different continents. (80 μm, 100 μm, 160 μm, 200 μm). They were then made under the pressure of various forces, which were (15KN.25KN.35KN.45KN.55KN), and we cooked them below 1100 ° C in 2h.

This research is aimed at studying the mechanical properties of ceramics, especially kaolin, where we used one of the techniques called speckle photography, which in turn enables us to learn about errors in the whole piece internally and to study them well and carefully.

We conclude from our work and research that the lower the pressure during the production of the piece, the greater the distortion when information is lost, the faster the piece breaks down. While the greater the pressure during the making of pieces, the less the distortion is worth, and we do not lose information quickly. We also note that the higher the pressure during manufacturing, the greater the resistance of the piece to fracture, by changing the direction of distortion from the horizontal to the vertical direction, from top to bottom, and by changing the direction from bottom to top.

The search remains open in the context of changing additions to improve mechanical properties

Bibliographic references

Bibliographic references :

Bibliographic references

[1] M.F.Ashby, D.R.H.Jone, « matériaux microstructure et mise en oeuvre » Pergamon Presse, Oxford, 1980. Dunod, Paris 1991.

[1](REZZAG, Hadda. Synthèse ET Caractérisation des mélanges de poudres céramiques à base de TiC-Al2O3, destinés à la compaction à chaud.Diss.Université Badji Mokhtar de Annaba, 2010.) structure céramique.

[2]Gilbert Fantozzi ; Les céramiques industrielles ; Edition Dunod 2013 (code GC/F438)

[3]Meziani hakima, elaboration d'un composite WC/ CU par infiltration, université mouloud mammeri de tizi- ouzou de 2013.

[4] S. Zouai, Thèse doctorat en sciences, Université de Constantine, Algérie, (2013).

[5] REZZAG, Hadda. Synthèse ET Caractérisation des mélanges de poudres céramiques à base de TiC-Al2O3, destinés à la compaction à chaud.Diss.Université Badji Mokhtar de Annaba, 2010.) structure céramique.

[6] MATIAS .R VIOTTI [Albertazzi,_Armando] ROBUST.SPECKLE METROLOGY Techniques for stress Analysis and NDT.

[7] Hector_J._Rabal,_Roberto_A._Braga_Jr.]_Dynamic_La(BookZZ.org)] Dynamic laser speckle and applications .

[8] TOMAS Fricke-begmann ge boren am 20. August 1966 in bielefeld ,optical measiurement of deformation field and surface processes with digital speckle correlation.

[9] Redouane ZEMMAMOUCHE,Analyse desfigures de speckle pour la mesure de Déformations par corrélation d'image Numériques, UNIVERSITÉ FERHAT ABBAS - SÉTIF1 INSTITUT D'OPTIQUE ET DE MÉCANIQUE DE PRÉCISION. 20/09/2016.

[10] lalmi khier, etude par diffraction des Rx de materiaux à base de kaolin de kt2 ET dd, université mentouri – Constantine.

[11] hellal radia, etude et caracterisation d'un refractaire à base de k.t. (kaolin de tamazert), universite mentouri-constantine de 2006.

[12] Belamri Zehira, Elaboration ET caractérisation des matériaux polycristallins à base de kaolin DD ET KT2, Université mentouri-constantine de 2008.

[13] Chouafa Mohamed, Comportement du Kaolin à l'enrichissement par flottation. CAS de la mines de Tamazert – Jijel, universite badji mokhtar Annaba de 2016.

[14] belhouchet hocine, elboration et caracterisation d'un composite a dispersoides a base d'alumine et de zircon, universite ferhat abbas-setif de 2008.

[15]Philippe boch jean-claude niepce, ceramic materials processes, properties and applications.